

**Conversion Efficiency Enhancement of
Millimeter-wave Optoelectronic Mixers for
Fiber-fed Wireless System**

Jae-Young Kim

THE GRADUATE SCHOOL

YONSEI UNIVERSITY

Department of Electrical and Electronic Engineering

**Conversion Efficiency Enhancement of
Millimeter-wave Optoelectronic Mixers for
Fiber-fed Wireless system**

A Dissertation

Submitted to the Department of Electrical and Electronic Engineering
and the Graduate School of Yonsei University

in partial fulfillment of the requirements for the degree of

Doctor of Philosophy

Jae-Young Kim

January 2011

This certifies that the dissertation of Jae-Young Kim is approved.

Thesis Supervisor: Woo-Young Choi

Sang-Kook Han

Hideki Kamitsuna

Tae-Wook Kim

Hyuk-Kee Sung

THE GRADUATE SCHOOL

YONSEI UNIVERSITY

January 2011

Table of Contents

Abstract	xi
1. Introduction	1
1-1. Fiber-fed wireless system for millimeter-wave broadband wireless applications	1
1-2. Considerations for fiber-fed wireless schemes	6
1-3. Optoelectronic mixers for antenna base station	11
1-3-1. InP-based O/E mixer for long-wavelength (1.3 or 1.55 μm) optical link	12
1-3-2. CMOS-based O/E mixer for short-wavelength (850 nm) optical link	15
1-4. Objective of dissertation	17
1-5. Outline of dissertation	20
2. InP HBT-based self-oscillating O/E mixers	22
2-1. Introduction	22
2-2. Characteristics of self-oscillating O/E mixer	25
2-2-1. Conversion efficiency of self-oscillating O/E mixer	26
2-2-2. Spurious-free dynamic range of self-oscillating O/E mixer ..	31
2-3. 30-GHz-band Bi-directional fiber-fed wireless link demonstration ..	36
2-3-1. Bi-directional fiber-fed wireless system	36
2-3-2. Experimental setup and results for 30-GHz downlink	37
2-3-3. Experimental setup and results for 30-GHz uplink	45
2-4. 60GHz-band fiber-fed downlink demonstration	51
2-4-1. 60-GHz sub-harmonic O/E frequency up-converter	51
2-4-2. Experimental setup and results for 60-GHz downlink	57
2-5. Summary	60

3. CMOS-based APD optoelectronic mixers	62
3-1. Introduction	62
3-2. Large-signal equivalent circuit modeling of CMOS-based APD	63
3-2-1. CMOS-based APD used in the modeling.....	63
3-2-2. Equivalent circuit model for the CMOS-based APD	65
3-2-3. Parameter extraction process and fitting results.....	66
3-3. Optimization of CMOS-based APD for 60-GHz O/E mixer	73
3-3-1. Considerations for RF loss of APD O/E mixer	73
3-3-2. Design optimization and experimental verification	76
3-4. 60-GHz-band sub-harmonic balanced O/E mixer	82
3-4-1. Operation principle of balanced sub-harmonic O/E mixer	82
3-4-2. Design of balanced APD O/E mixers.....	85
3-4-3. Measurement results	87
3-5. Summary.....	93
4. Conclusion.....	94
Appendix	97
A-1. Optical injection-locking of MMIC HBT oscillator	97
Bibliography	101
Publication Lists	112

List of Figures and Tables

Fig. 1-1. Examples of millimeter-wave broadband wireless applications.....	4
Fig. 1-2. Applications of fiber-fed wireless systems consisting of separated closed areas in buildings and houses	4
Fig. 1-3. A comparison of system configurations between (a) a conventional baseband-feeder wireless network, and (b) a fiber-fed wireless system.	5
Fig. 1-4. Simplified configurations of millimeter-wave fiber-fed wireless systems based on (a) optical millimeter-wave transmission scheme, and (b) remote frequency conversion scheme.	7
Fig. 1-5. Operation principle of an O/E mixer based on photo-transistor with electrical LO supply.	10
Fig. 1-6. Fiber-fed wireless configuration utilizing optical LO distribution.	10
Fig. 1-7. A low cost fiber-fed wireless configuration utilizing short-wavelength (850 nm) lightwave, multi-mode fiber and CMOS-based OEIC antenna base station including O/E mixer.	12
Fig. 1-8. Bi-directional operation of InP HBT O/E mixer with optical LO supply.	14
Fig. 1-9. Simplified cross-section of a CMOS-based APD using P+/N-well junction and DC avalanche multiplication characteristics of APD.	16
Fig. 1-10. Operation principle of CMOS-based APD O/E mixer.	17
Fig. 1-11. Power budget for antenna base station based on O/E mixer or conventional cascaded photo-detector, IF amp. and mixer topology.	18
Fig. 2-1. The operation principle of optically injection-locked self-oscillating O/E mixer based on InP HBT.	22
Fig. 2-2. Cross-sectional layer structure of the undoped-emitter InP/In _{0.53} Ga _{0.47} As HBT used in this work.	23
Fig. 2-3. Circuit diagram of 10-GHz InP HBT MMIC oscillator.	25
Fig. 2-4. Experimental setup for measurement and comparison of O/E mixing efficiencies. (a) O/E frequency up-conversion (b) frequency down-	

conversion.....	28
Fig. 2-5. O/E frequency up-conversion efficiencies of OIL-SOM and discrete HBT O/E mixer with change of optical LO power. Spectrum is RF signal of OIL-SOM when optical LO power is -6 dBm.....	29
Fig. 2-6. Frequency down-conversion efficiencies of OIL-SOM and discrete HBT O/E mixer with change of optical LO power. Spectrum is output IF signals of OIL-SOM when optical LO power is -6 dBm.....	30
Fig. 2-7. Experimental setup for measurement of SFDR of O/E frequency up-conversion in MMIC OIL-SOM.....	34
Fig. 2-8. Measurement of SFDR of O/E frequency up-conversion in MMIC OIL-SOM.....	34
Fig. 2-9. Experimental setup for measurement of SFDR of frequency down-conversion in MMIC OIL-SOM.....	35
Fig. 2-10. Measurement of SFDR of O/E frequency up-conversion in MMIC OIL-SOM.....	35
Fig. 2-11. Schematic diagram of 30GHz bi-directional fiber-fed wireless system utilizing 3 rd harmonic operation of 10GHz MMIC OIL-SOM.	37
Fig. 2-12. Experimental setup for 30-GHz downlink data transmission.....	39
Fig. 2-13. (a) Spectrum of optically injection-locked 32.4-GHz 3 rd harmonic LO (b) Measured phase noise of 32.4-GHz 3 rd harmonic LO in free-running and optically injection-locked conditions.....	40
Fig. 2-14. 3 rd harmonic LO and harmonically frequency up-converted RF signal power with change of optical LO power and measured spectrum when optical LO power is 0 dBm.	41
Fig. 2-15. Spectrum of (a) 3 rd harmonically frequency up-converted downlink RF signal (b) frequency down-converted downlink IF and data signal.	43
Fig. 2-16. Measured error vector magnitudes (EVMs) as a function of optical LO power when the optical IF power is 0 dBm. Inset is constellation of 32-QAM data demodulated by vector signal analyzer.....	44
Fig. 2-17. Experimental setup for 30-GHz uplink data transmission.....	47
Fig. 2-18. Harmonically frequency down-converted IF signal power with change of optical LO power. Inset is measured IF spectrum when optical	

LO power is 0 dBm.....	48
Fig. 2-19. Spectrum of (a) 30.2-GHz input uplink RF signal (b) harmonically frequency down-converted uplink IF signal.	49
Fig. 2-20. Measured error vector magnitudes (EVMs) as a function of optical LO power when the uplink RF power is -2 dBm. Inset is constellation of 32-QAM data demodulated by vector signal analyzer.....	50
Fig. 2-21. Schematic diagram of 30-GHz hybrid OIL-SOM and spectrum of optically injection locked 60-GHz sub-harmonic LO.....	53
Fig. 2-22. Measured phase noise of 60-GHz injection-locked LO at 10-kHz and 100-kHz frequency offset with change of incident optical LO power. Inset is measured phase noise in free-running and injection-locked conditions.....	54
Fig. 2-23. Measured locking range of hybrid HBT oscillator with change of incident optical LO power.....	55
Fig. 2-24. Internal conversion gain of 60-GHz harmonic O/E frequency up-conversion with change of optical LO power. Spectrum was measured with 0-dBm optical LO and -6 dBm optical IF powers.	56
Fig. 2-25. Experimental setup for 60-GHz downlink data transmission.....	58
Fig. 2-26. Spectrum of 60-GHz downlink signal.....	59
Fig. 2-27. Measured EVM as a function of optical LO power when the optical IF power is -6 dBm. Inset is constellation of 16-QAM data.....	59
Fig. 3-1. Schematic cross-section and layout of CMOS-based APD using P+/N-well junction surrounded by swallow trench isolation (STI).	64
Fig. 3-2. Measured I-V characteristics of CMOS-based APD in dark and 0-dBm optical illumination.	65
Fig. 3-3. Large-signal equivalent circuit model of CMOS-based APD.	66
Fig. 3-4. Measured DC characteristics of CMOS-based APD with 0-dBm optical illumination in linear scale.....	68
Fig. 3-5. Measured DC characteristics and simulation results with 0-dBm optical illumination in log and linear scale.....	70
Fig. 3-6. Measured S-parameters and simulation results with 0-dBm optical illumination and 9.9 V reverse bias voltage.....	71

Fig. 3-7. Measured S-parameters and simulation results with 0-dBm optical illumination and 10.0 V reverse bias voltage.....	71
Fig. 3-8. Measured S-parameters and simulation results with 0-dBm optical illumination and 10.1 V reverse bias voltage.....	72
Fig. 3-9. Measured S-parameters and simulation results with 0-dBm optical illumination and 10.2 V reverse bias voltage.....	72
Fig. 3-10. 60-GHz sub-harmonic O/E mixer operation described with equivalent circuit model.....	74
Fig. 3-11. 60-GHz sub-harmonic O/E mixer simulation results with a plot of the 61-GHz RF power as a function of reverse bias voltage with change of junction capacitance.	75
Fig. 3-12. Measured DC optical response of APDs with different device size.	77
Fig. 3-13. Measured AC photo-response of APDs with different device size under 0-dBm optical illumination.....	78
Fig. 3-14. Measured 60-GHz LO and 60.1-GHz RF signal powers with 0-dBm optical IF power and APDs with different size.	78
Fig. 3-15. Measured 60.1-GHz RF signal powers with different bias configurations.	81
Fig. 3-16. Measured 60-GHz LO and 60.1-GHz RF signal powers with and without silicide layer under P+ model contact.....	81
Fig. 3-17. Operation principles of (a) electrical sub-harmonic mixer using anti-parallel diode pair (b) balanced APD O/E mixer in anti-podal APD pair structure.	84
Fig. 3-18. Simulated 60-GHz sub-harmonic O/E mixing efficiencies based on balanced and single-ended structures.....	85
Fig. 3-19. (a) cross-section and (b) top-view schematic diagram of fabricated balanced APD pair.	86
Fig. 3-20. Measured DC and IF photo-detection characteristics of a single CMOS-based APD with lateral dimension of $10 \times 10 \mu\text{m}^2$ as a function of reverse bias voltage.....	89
Fig. 3-21. Measurement setup for 60-GHz band sub-harmonic O/E mixing	

characteristics using the fabricated balanced APD O/E mixer.....	90
Fig. 3-22. Measured 60-GHz-band sub-harmonic LO and 60.1-GHz RF power from the balanced APD O/E mixer and single APD O/E mixer with 0-dBm optical IF and 19-dBm LO powers.....	91
Fig. 3-23. Measured 60.1-GHz harmonic RF power from the balanced APD O/E mixer and single APD O/E mixer as a function of LO power in reverse bias voltage of 11 V.....	92
Fig. A-1. Experimental setup for optical injection-locking of MMIC oscillator.....	98
Fig. A-2. Measured output spectrum of oscillator in (a) free-running and (b) optically injection-locked by optical LO of 0-dBm power.....	99
Fig. A-3. Measured locking range of MMIC oscillator with change of incident optical LO power.....	100
Fig. A-4. Free-running oscillation frequency of MMIC oscillator with change of operating temperature.....	100
Table 1-1. Summarized performances of conventional O/E mixers.....	19
Table 2-1. Performance comparison of InP HBT-based conventional O/E mixers and OIL-SOMs.....	61
Table 3-1. Extracted circuit parameters.....	69
Table 3-2. Performance comparison of CMOS-based APD O/E mixers.....	93

Abstract

Millimeter-wave optoelectronic mixers (O/E mixers) for fiber-fed wireless system are investigated based on integration-compatible electrical devices of InP heterojunction bipolar transistors (HBTs) and CMOS-based avalanche photodiodes (APDs). The O/E mixers simultaneously perform photo-detection and frequency conversion and simplify the antenna base stations. The conversion efficiency enhancement techniques for O/E mixers with optical LO or electrical LO are presented to create a high performance O/E mixers.

The InP HBT-based optical injection-locked self-oscillating O/E mixer (OIL-SOM) scheme that uses optical LO is proposed for the enhancement of conversion efficiency in long wavelength (1.55 μm) fiber-fed wireless system. For evaluation, the optoelectronic frequency conversion efficiency and spurious-free dynamic range of OIL-SOM that uses the MMIC HBT oscillator are experimentally investigated. Also, the characteristics of OIL-SOM are directly compared with a discrete HBT optoelectronic mixer.

Utilizing the HBT-based OIL-SOM in harmonic operation, fiber-fed 30-GHz-band bi-directional link data transmission of 25-Mbps 32-QAM data and 60-GHz downlink data transmission of 20-Mbps 16-QAM are successfully demonstrated.

For an inexpensive and highly integrated antenna base station in short wavelength (850nm) fiber-fed wireless system, CMOS-based APD O/E mixer is designed for sub-harmonic operation at the device and structural level. For characterization of the high frequency operation in detail, the equivalent circuit model of APD is established. Based on the circuit model and O/E mixing simulation, the APD devices are down-scaled and optimized for 60-GHz O/E mixing operation.

The sub-harmonic balanced APD pair O/E mixer is proposed for the enhancement of conversion efficiency. The prototype balanced APD O/E mixer is implemented with down-scaled APD pair and measured with a differential LO supply. The maximum conversion gain of the 60-GHz balanced O/E mixer is 7 dB, which is about 30-dB higher than that of the previous O/E mixer.

Keywords: InP, heterojunction bipolar transistor, CMOS, avalanche photodiode, fiber-fed wireless system, self-oscillating mixer, optical injection-locking, 60 GHz, millimeter-wave, balanced sub-harmonic mixer

1. Introduction

1-1. Fiber-fed wireless system for millimeter-wave broadband wireless applications

After mobile communication services were commercialized, wireless communication technologies have been rapidly evolved and have become ubiquitous throughout our daily lives. Presently, we can use voice, broadband data and video streaming services through many types of wireless networks such as cellular and Wi-Fi in many places. Consequently, the rapid growth of our network usage has created the demand for higher data rate wireless systems beyond those operating at gigabit per second throughput.

In general, the future wireless communication system will require a high frequency carrier with a wide bandwidth that can handle high data rate signals. Thus, the millimeter-wave band is very attractive for this application. The 60-GHz band is a particularly promising candidate, as the 7-GHz-wide license-free band has opened in many countries [1-2]. For the utilization of the 60-GHz band, active research has been conducted on devices, circuit technologies, and system architecture [3-8]. Also, the 60-GHz wireless personal area network (WPAN) and wireless local area network (WLAN) are under discussion at IEEE

802.15.3c and 802.11ad working groups [9-10]. Fig 1-1 shows the millimeter-wave broadband wireless applications.

There are some problems associated implementing a low cost wireless network using millimeter-wave band. Firstly, due to the high transmission loss of millimeter-wave in air [11] and requiring a high-sensitivity receiver for gigabit per second data detection, the wireless coverage of a transceiver is limited [4]. Thus, the millimeter-wave wireless systems that use picocell network topology, which require a large number of antenna base stations, are expected. Second, the millimeter-wave band circuit implementation is still challenging and it is therefore hard to increase the transmission power for coverage extension. Accordingly, networks with simple antenna base station architecture must be designed carefully for overall cost reduction.

Fiber-fed wireless systems have received much attention as a solution to these problems [12-18]. Fig. 1-2 shows the application example of the fiber-fed wireless systems on the wireless environment consisting of many closed areas in buildings and houses. In this system, the optical fibers connect the numerous number of antenna base stations to a central station. The optical fiber provides low loss and large bandwidth for effective linkage of network units. It also offers easy incorporation ability to the pre-deployed fiber-optic networks.

Fig. 1-3 shows comparison of a conventional baseband-feeder wireless network and the fiber-fed wireless system. In a conventional baseband feeder network, control functions such as channel allocation, modulation/demodulation and channel coding selections are included in base station, as shown in Fig. 1-3 (a). In fiber-fed wireless system, however, these functionalities are consolidated in central station as shown in Fig. 1-3 (b). The modulated RF signals are optically transmitted via an optical fiber and the antenna base station acts as a simple optical-to-electrical signal converter. The antenna base station architecture is therefore greatly simplified resulting in overall cost reduction. As the optical link from the central station to the antenna base station is an analog system, the key parameters are overall link gain, nonlinearity and noise figure.

Millimeter-wave Broadband wireless application



Fig. 1-1. Examples of millimeter-wave broadband wireless applications

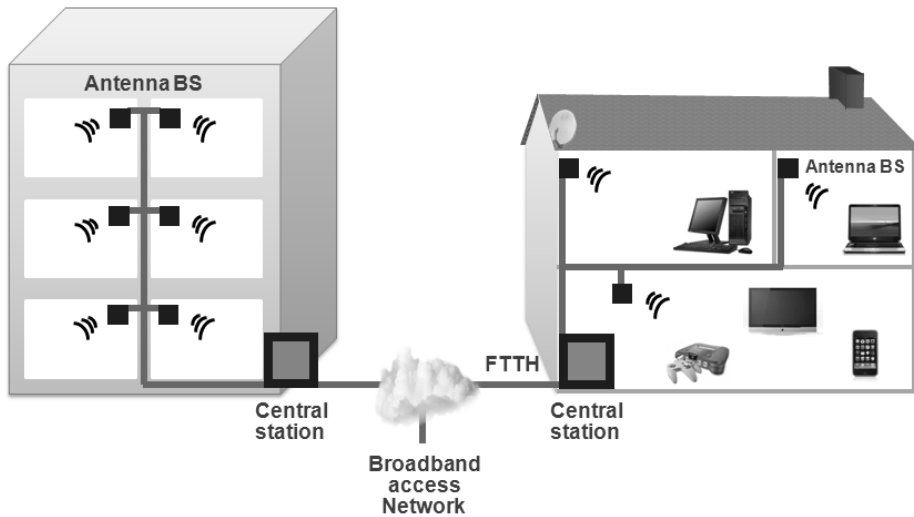


Fig. 1-2. Applications of fiber-fed wireless systems consisting of separated closed areas in buildings and houses

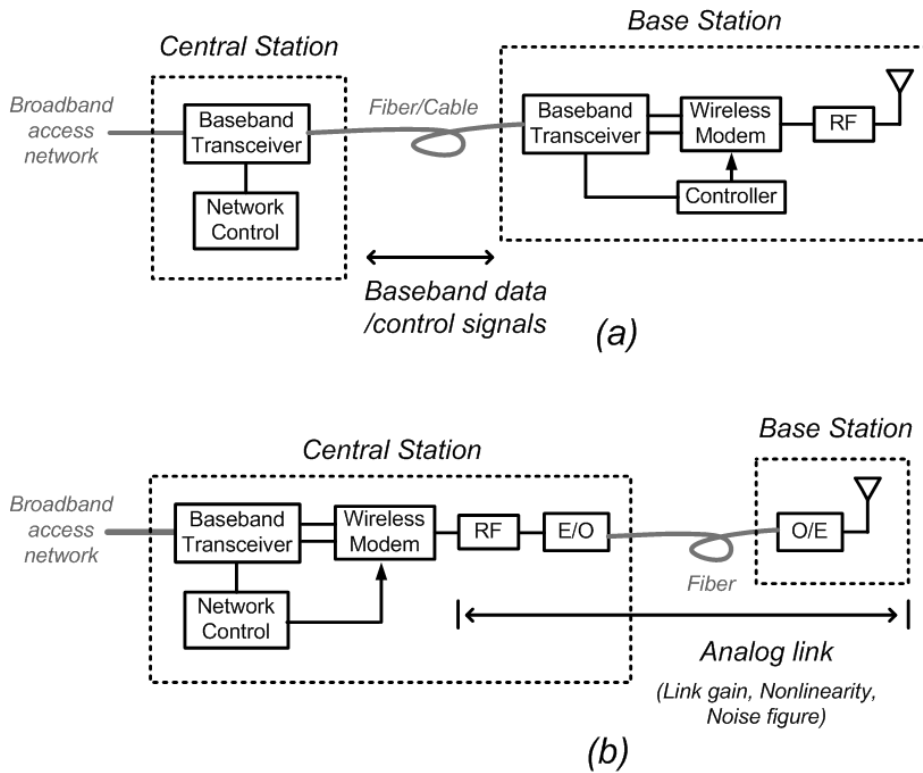
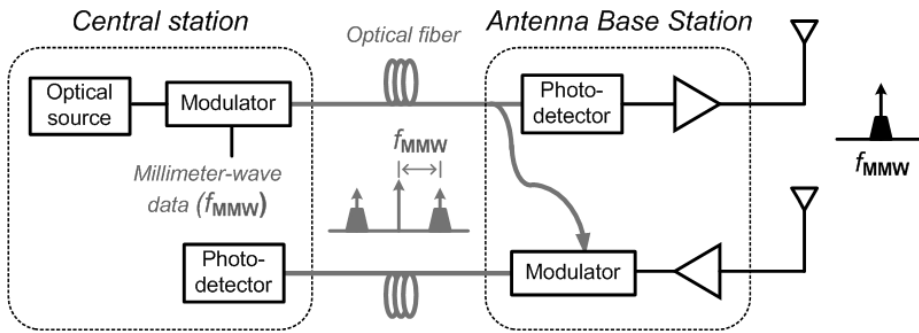


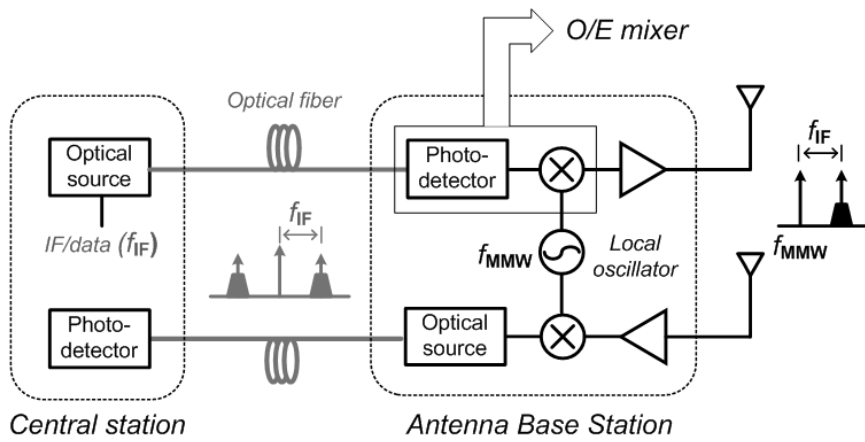
Fig. 1-3. A comparison of system configurations between (a) a conventional baseband-feeder wireless network, and (b) a fiber-fed wireless system.

1-2. Considerations for fiber-fed wireless schemes

Fig. 1-4 shows the two different fiber-fed wireless schemes that have been chiefly investigated. In the first scheme, called optical millimeter-wave transmission [13-16] shown in Fig 1-4 (a), the millimeter-wave signals are optically generated in the central station for downlink transmission. After the optical transmission through a fiber, the optical signals are converted back to electrical millimeter-wave in the antenna base station for radiation. For uplink, the downlink optical carrier can be reused to simplify the antenna base station by eliminating the lightwave source [13, 15]. Although this scheme can provide the simplest antenna base station architecture with just a photo-detector, an optical modulator, amplifiers and an antenna, the photo-detector and modulator operating in millimeter-wave band are expensive. Additionally, the optical millimeter-wave transmission scheme suffers from the dispersion-induced carrier suppression effect [19]. Because the two sidebands of intensity modulated optical signals experience different phase shifts within the fiber due to chromatic dispersion, especially in high frequency modulation, the detected electrical signal power in the photo-detector is periodically suppressed. The optical single sideband modulation or optical heterodyning methods can solve this problem with the cost of system complexity [20-21].



(a)



(b)

Fig. 1-4. Simplified configurations of millimeter-wave fiber-fed wireless systems based on (a) optical millimeter-wave transmission scheme, and (b) remote frequency conversion scheme.

The other approach for the fiber-fed wireless system is the remote frequency conversion scheme [17-18] shown in Fig 1-4 (b). In this scheme, the downlink and uplink data are transmitted through the optical fiber in the immediate frequency (IF) band. The narrow spacing between the two sidebands of the optical signal in the IF modulation can mitigate the chromatic dispersion problem. In this scheme, the antenna base station should support the frequency conversion functionality between IF and RF bands. Consequently, the antenna base station becomes complex because the millimeter-wave local oscillation (LO) source and mixers are necessary. Instead, this scheme no longer requires the expensive optoelectronic components such as photo-detectors and modulators operating in millimeter-wave band. Also, the lower speed optoelectronic devices are relatively easy to be monolithically integrated with transistor fabricated technologies such as MMIC (monolithic microwave integrated circuit) and Si CMOS (complementary metal-oxide-semiconductor) processes.

In the remote conversion scheme, the antenna base station can be simplified with the optoelectronic (O/E) mixers that utilize the nonlinear photo-detection characteristics of photodiodes [22-23] or photo-transistors [24-29]. When electrical LO signals are supplied to the O/E mixer, the optically injected IF signals are simultaneously

photo-detected and modulated by the LO signals for frequency conversion as shown in Fig. 1-5. Also, the electrical LO for the O/E mixer can be replaced with optically supplied LO. Fig. 1-6 shows the remote frequency conversion architecture utilizing the optical LO distribution scheme, in which the millimeter-wave LO signals are generated in the central station and then optically distributed to the antenna base stations [30-32]. Because the numerous number of antenna base station can share the optical LO, the overall system cost can be greatly reduced by replacing the individual phase-locked electrical LO source.

The photo-detection and conversion efficiencies of an O/E mixer can directly affect the overall gain and noise figure of the optoelectronic analog link between the central and antenna base stations. This dissertation mainly deals with the optoelectronic mixers for the remote frequency conversion schemes with electrical and optical LO. For both schemes, the conversion efficiency enhancement techniques for the O/E mixers are investigated with the feasibility study.

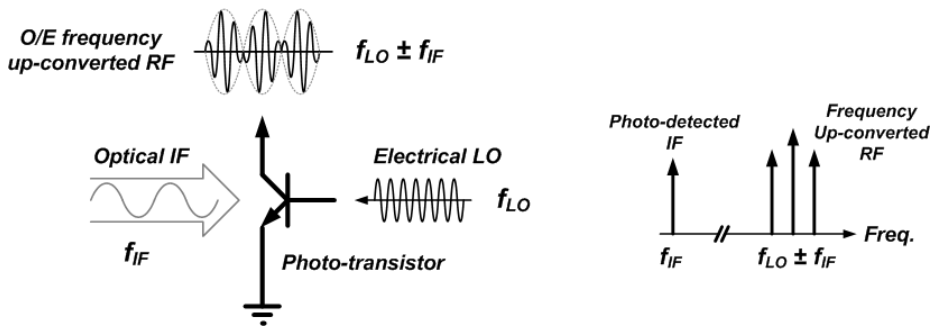


Fig. 1-5. Operation principle of an O/E mixer based on photo-transistor with electrical LO supply.

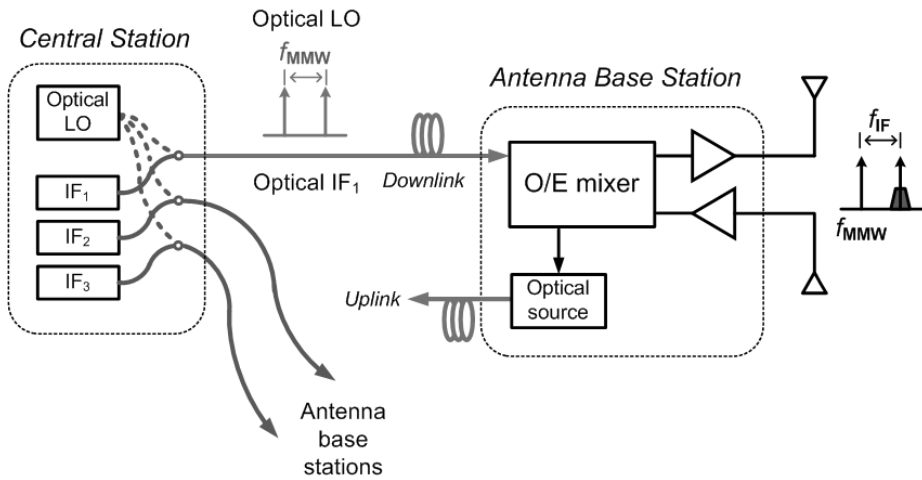


Fig. 1-6. Fiber-fed wireless configuration utilizing optical LO distribution.

1-3. Optoelectronic mixers for antenna base station

The fiber-fed wireless system can be implemented with one of the optical links using either long-wavelength (1.3 or 1.55 μm) lightwave or short-wavelength (850 nm) lightwave. The long-wavelength optical link has been widely used for long-range and high-speed optical communication, and there are mature technologies for high-speed optical components. Additionally, the high-speed optoelectronic device technologies based on InP-InGaAs materials can be utilized for implementation of a high efficiency fiber-fed wireless link.

Short-wavelength optical links have recently been receiving much interest for short-range optical interconnections and access networks. By utilizing vertical-cavity surface-emitting laser (VCSEL) and multi-mode fiber (MMF), cost-reduction of the optical link can be accomplished. Furthermore, the lightwave of the 850-nm wavelength enables photo-detectors based on complementary metal-oxide-semiconductor (CMOS) technology for optoelectronic integrated circuit (OEIC) approaches [33-36]. Fig. 1-7 shows a low-cost fiber-fed wireless configuration utilizing the short-wavelength lightwave.

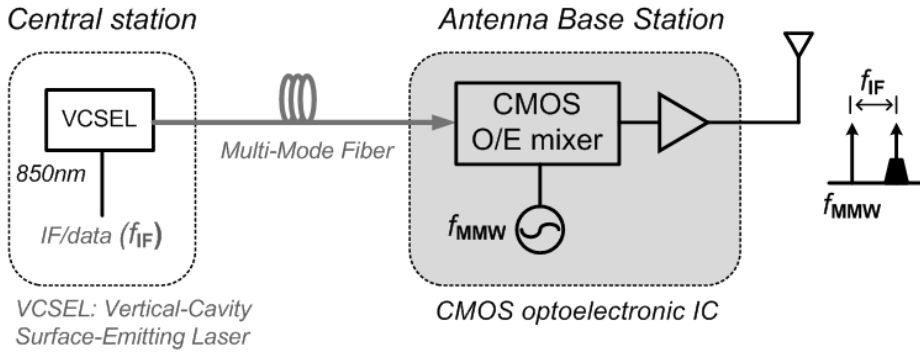


Fig. 1-7. A low cost fiber-fed wireless configuration utilizing short-wavelength (850 nm) lightwave, multi-mode fiber and CMOS-based OEIC antenna base station including O/E mixer.

1-3-1. InP-based O/E mixer for long-wavelength (1.3 or 1.55 μm) optical link

For the fiber-fed wireless application using the long wavelength lightwave, several types of O/E mixers have been reported based on InP high electron-mobility transistor (HEMT) [24-25] and heterojunction bipolar transistor (HBT) [26-29]. These InP-based photo-transistors can be beneficial for O/E mixer implementation [37-40]. Firstly, the optical signals of long wavelength can be detected in the InGaAs layer. Because the input signal frequency to the O/E mixer is under few gigahertz, the photo-transistors can provide large photo-detection gain.

Secondly, the photo-detection gain of photo-transistors can be modulated by supplied LO through the base or gate terminal so that the O/E mixing is possible. Lastly, the InP HEMT and HBT are fully compatible to the MMIC fabrication process [40-41].

The InP HEMT has a large photo-detection gain and excellent microwave performances. However, the low optical responsivity due to the shallow InGaAs absorption layer (~few tens nanometer) [42], and the narrow photo-detection bandwidth due to the photo-voltaic gain mechanism [42-44] degrades the performance merit of InP HEMT O/E mixers.

The InP HBT is a bipolar transistor in which the base-collector junction acts as a photodiode. Thus, the photo-detection bandwidth follows the electrical speed of the HBT. Also, the thicker absorption layer between the base and the collector junction compared to the HEMT enables higher quantum efficiency and optical responsivity. With these structural advantages, the reported 60-GHz-band InP HBT O/E mixer exhibits frequency up-converted RF power of about -30 dBm from optical IF power of 0 dBm [45].

The high-speed photo-detection capability of InP HBT enables the utilization of the optical LO supplied through optical fiber as shown in Fig. 1-8 [46]. By replacing the electrical LO with optical LO, the base

terminal of the HBT can be used as the input port for uplink RF signals. Hence, the InP HBT O/E mixer can simultaneously perform O/E frequency up- and down-conversion for bi-directional operation. Using this type of O/E mixer, the bi-directional 60-GHz fiber-fed wireless data transmission was demonstrated in [46]. However, a disadvantage of this scheme is that the required optical LO power for sufficiently high frequency up-conversion must be considerably elevated. Also, the variation of delivered optical LO power due to differences in the distance between the central and base stations may seriously degrade system performance.

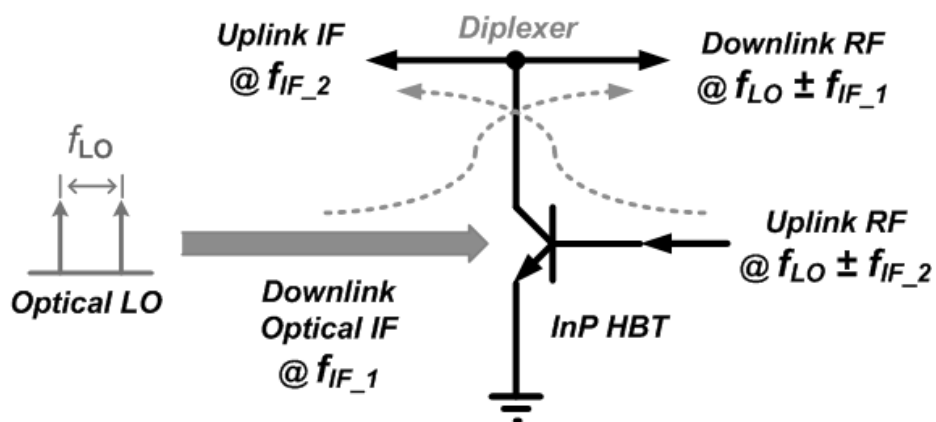


Fig. 1-8. Bi-directional operation of InP HBT O/E mixer with optical LO supply.

1-3-2. CMOS-based O/E mixer for short-wavelength (850 nm) optical link

Because CMOS technology is the most wide-spread and the lowest cost semiconductor process, CMOS-based photo-detectors have received significant attention [33-36]. However, there are several drawbacks of the standard CMOS process for photo-detector implementation [47-48]. Firstly, the 850-nm lightwave has a long penetration depth in silicon compared to the narrow depletion width of a highly doped *N-well/P+* or *P-well/N+* junction. Thus, it is hard to obtain high quantum efficiency in CMOS-based photo-detectors. Secondly, the large diffusion current in the neutral region seriously reduces the photo-detection bandwidth.

To overcome these disadvantages, the CMOS-based avalanche photodiode (APD) using the *P+/N-well* junction was proposed [49-51]. Fig. 1-9 shows the simplified cross section of the CMOS-based APD. Using the shallow *P+/N-well* junction for photo-detection, the diffusion current is rejected for photo-detection bandwidth enhancement. Instead, the quantum efficiency of the APD is relatively lower than other photodiodes utilizing the *N-well/P-substrate* junction. To increase the photo-detection efficiency, the APD operates around avalanche breakdown voltage and obtains avalanche multiplication gain for

enhanced optical responsivity as is schematically illustrated in Fig. 1-9.

For a CMOS-based O/E mixer, the APD is a very promising optoelectronic device because the avalanche gain of APD has a nonlinear relationship to the reverse bias voltage. The electrical LO that is applied in the p-n junction modulates the photo-detection gain and generates O/E frequency conversion as shown in Fig. 1-10 [22-23]. Also, the CMOS-based APD has a wide photo-detection bandwidth. It can be utilized for optical IF detection. A 60-GHz CMOS-based APD sub-harmonic O/E mixer using a 30-GHz LO was reported in [23]. However, in this result, 60-GHz RF power is less than -50 dBm when 0-dBm optical IF and 21-dBm electrical LO pumping are injected.

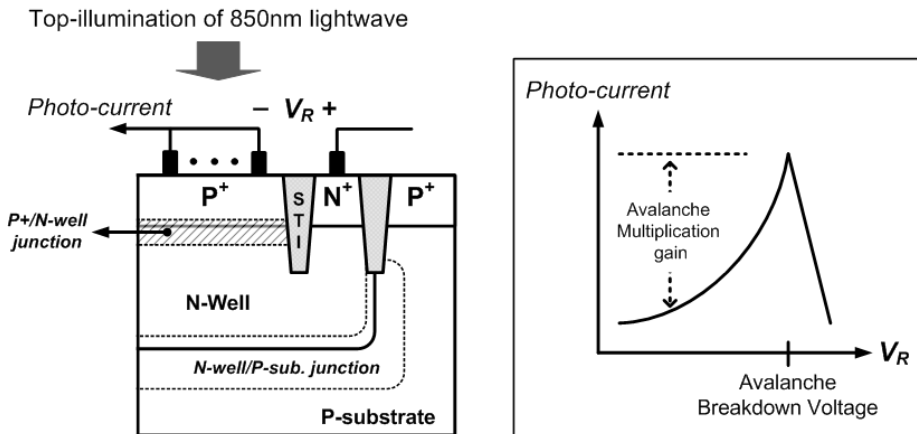


Fig. 1-9. Simplified cross-section of a CMOS-based APD using P+/N-well junction and DC avalanche multiplication characteristics of APD.

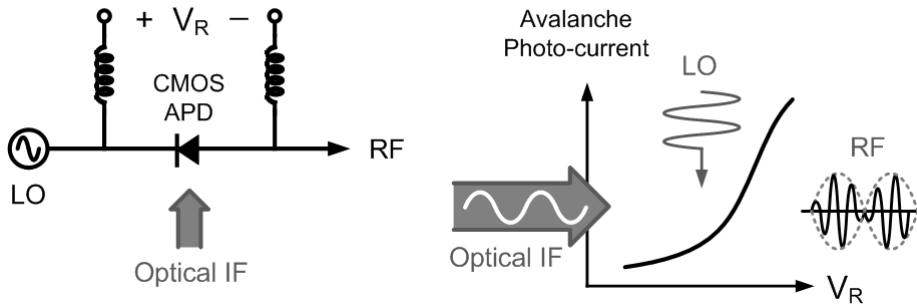


Fig. 1-10. Operation principle of CMOS-based APD O/E mixer.

1-4. Objective of dissertation

In the antenna base station of a fiber-fed wireless system, the optical IF signals are photo-detected and frequency up-converted to RF as shown in Fig. 1-11. If the frequency up-converted RF power is not high enough, the millimeter-wave amplifier should have a large gain, which may further increase the complexity of the antenna base station. As summarized in Table 1-1, the output RF powers of the reported O/E mixers are relatively low for wireless radiation. The large conversion loss of the InP HBT O/E mixer with optical LO and the CMOS-based APD O/E mixer can compromise the merits of a low-cost and simple fiber-fed wireless architectures based on these components due to large link loss and signal-to-noise ratio (SNR) degradation.

The objective of this dissertation is the conversion efficiency enhancement techniques for millimeter-wave O/E mixers with optical LO and electrical LO supply schemes. For a long-wavelength fiber-fed wireless system with optical LO distribution, the InP HBT-based optically injection-locked self-oscillating O/E mixer (OIL-SOM) scheme is investigated [52-54]. By utilizing the self-oscillating mixer, the large LO power can be generated by itself so that high conversion efficiency can be accomplished. For a short-wavelength fiber-fed wireless system with electrical LO supply, the CMOS-based APD O/E mixers are investigated. By utilizing the balanced APD pair structure, an APD O/E mixer is optimized for sub-harmonic operation.

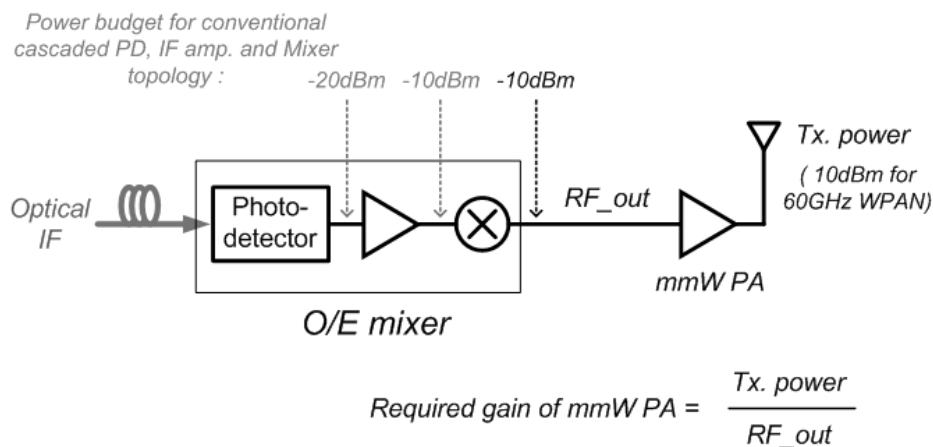


Fig. 1-11. Power budget for antenna base station based on O/E mixer or conventional cascaded photo-detector, IF amp. and mixer topology.

O/E mixer type	InP HBT with optical LO [46]	InP HBT with electrical LO [45]	CMOS-based APD with electrical LO [23]
Optical wavelength	1550 nm	1550 nm	850 nm
Conversion efficiency	Poor	Moderate	Poor
IF detection power (0dBm optical IF)	-15dBm with photo-Tr. gain	-15 dBm with photo-Tr. gain	-25 dBm with avalanche gain
Output RF power (60GHz)	< -40 dBm (Depends on optical LO power)	-30 dBm	-50 dBm
Limiting factor on O/E mixing	Insufficient LO power	Structure & parasitic loss	Structure & parasitic loss
Remarks	Simple ABS architecture	Moderate complexity (LO source in ABS)	Low-cost solution for optical link and ABS

Table 1-1. Summarized performances of conventional O/E mixers.

1-5. Outline of dissertation

This dissertation will focus on the conversion efficiency enhancement of the O/E mixers and the feasibility demonstration in terms of fiber-fed data transmission. An InP HBT-based O/E mixer and a CMOS-based APD O/E mixer will be presented in chapters 2 and 3, respectively. Details of the dissertation outline are as follows.

In chapter 2, the operation principle and characteristics of InP HBT-based OIL-SOM will be discussed. Section 2-2 shows the characteristics of MMIC HBT self-oscillating O/E mixer including the conversion efficiencies, the noise, and the nonlinearities. In section 2-3, the 30-GHz-band bi-directional fiber-fed link will be demonstrated using 3rd harmonic operation of MMIC HBT OIL-SOM. Also, in section 2-4, 60-GHz fiber-fed downlink will be demonstrated using 2nd harmonic operation of 30-GHz hybrid OIL-SOM.

Chapter 3 describes the CMOS-based APD O/E mixer with enhanced conversion efficiency. In section 3-2, the large-signal equivalent circuit model of the CMOS-based APD and parameter extraction will be presented. Using the established equivalent circuit model, the device optimization of the CMOS-based APD for O/E mixer will be discussed in section 3-3. This section also includes the measurement results of the CMOS-based APD O/E mixers in different geometric structures for

verification. Section 3-4 will present the 60-GHz-band balanced sub-harmonic APD O/E mixer with its operation principle, prototype design, and measurement results.

Finally, this dissertation will be summarized in chapter 4.

2. InP HBT-based self-oscillating O/E mixers

2-1. Introduction

This chapter describes the optically injection-locked self-oscillating O/E mixer (OIL-SOM) based on InP HBT oscillator. Fig. 2-1 shows the operation principle of the OIL-SOM. The OIL-SOM oscillates by itself and generates a LO signal for the frequency up/down conversion process. Thus, the LO power is higher than the optically provided LO and can be constant over the optical power variation. Through direct optical injection-locking [55], the oscillation frequency and phase noise of OIL-SOM follow those of the optically provided LO.

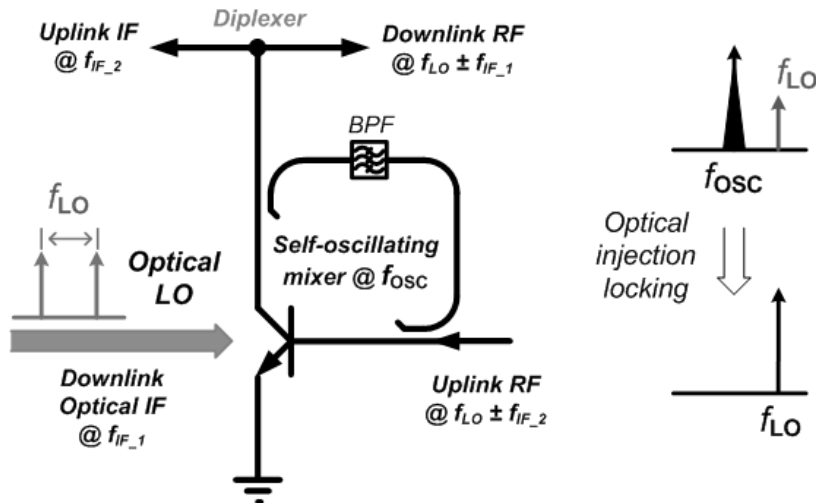


Fig. 2-1. The operation principle of optically injection-locked self-oscillating O/E mixer based on InP HBT.

The InP–InGaAs HBT [56-57]¹ used in this work has a 70-nm thick undoped InP emitter, a 50-nm carbon-doped InGaAs base, and a 300-nm-thick InGaAs collector as shown in Fig. 2-2. The optical illumination is performed through the optical window with a 5- μ m diameter on the top layer. The DC optical responsivity of the HBT is of 0.2 A/W at the photodiode (PD)-mode when the base-emitter is shorted. The electrical current gain cutoff frequency (f_T) and the maximum frequency of oscillation (f_{max}) of this device are 153 and 94 GHz, respectively.

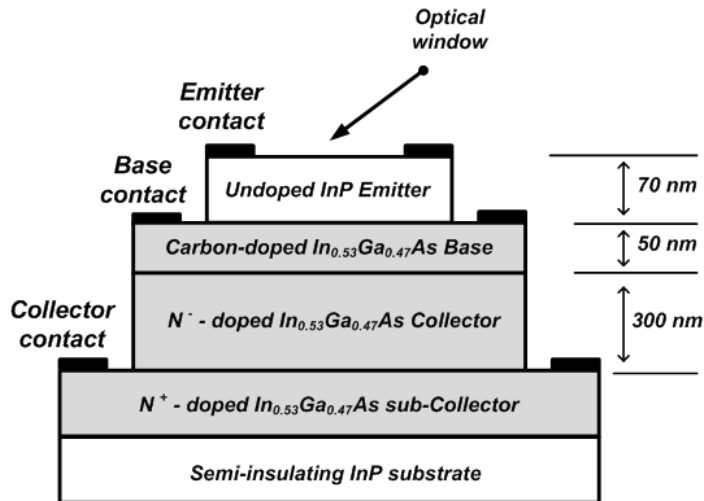


Fig. 2-2. Cross-sectional layer structure of the undoped-emitter InP/In_{0.53}Ga_{0.47}As HBT used in this work.

¹ The InP/InGaAs HBT used in this dissertation is provided by NTT Photonics Laboratories, Japan

In section 2-2, the 10-GHz-band OIL-SOM is realized using a 10-GHz MMIC HBT oscillator that is based on the InP/InGaAs HBT [55]. For evaluation of the proposed OIL-SOM topology, the optoelectronic frequency conversion efficiency and spurious-free dynamic range of the OIL-SOM are experimentally investigated and compared with that of the discrete HBT O/E mixer. In section 2-3, the feasibility of bi-directional fiber-fed wireless link is demonstrated in 30-GHz-band using the MMIC HBT OIL-SOM as a 3rd harmonic frequency up- and down-converter.

For the fiber-fed wireless system in higher frequency band such as 60 GHz, the higher frequency OIL-SOM is needed. Also, for high efficiency conversion, fundamental or sub-harmonic mixers are more preferred than higher-order mixers. Fortunately, the 60-GHz-band direct optical injection-locked oscillator can be implemented with InP HBT MMIC [58-59], so the 60-GHz MMIC OIL-SOM is also possible for the 60-GHz-band bi-directional fiber-fed wireless system. In this work, the 60-GHz hybrid-type sub-harmonic OIL-SOM is implemented using the discrete InP/InGaAs HBT [56-57]. The characteristics of the hybrid OIL-SOM and the 60-GHz fiber-fed downlink will be described in section 2-4.

2-2. Characteristics of self-oscillating O/E mixer

This section describes the characteristics of OIL-SOM which is realized with a 10-GHz InP HBT MMIC oscillator [55]². Fig. 2-3 shows the circuit diagram of the MMIC oscillator. This oscillator has common-emitter series feedback configuration, so the base terminal of the photo-transistor can be utilized as RF input port for frequency down-mixing operation. Also, the free-running oscillation frequency can be controlled with a variable resistor implemented with a HBT in feedback loop. The optical injection-locking characteristic of this MMIC oscillator can be found in [55] and Appendix.

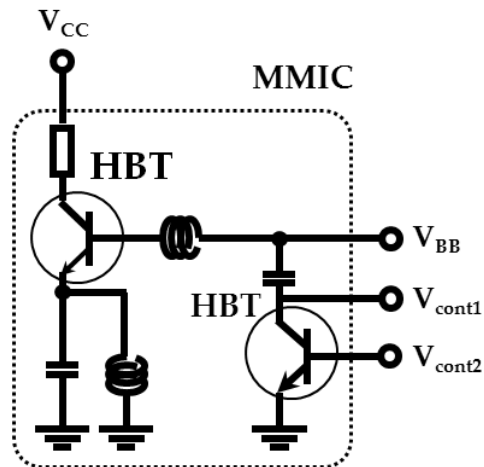


Fig. 2-3. Circuit diagram of 10-GHz InP HBT MMIC oscillator.

² The 10-GHz InP HBT MMIC oscillator used in this dissertation is provided by NTT Photonics Laboratories, Japan

2-2-1. Conversion efficiency of self-oscillating O/E mixer

The major advantage of self-oscillating O/E mixer is higher conversion efficiency by providing higher LO power. To validate this, conversion efficiency of the self-oscillating mixer was directly compared with that of the discrete HBT O/E mixer with the same measurement setup. Fig. 2-4 (a) and (b) are experimental setups for measurement of O/E frequency up- and down-conversion, respectively.

10.8-GHz optical LO was generated with the double-sideband suppressed-carrier method (DSB-SC) [60], in which two optical modes separated by 10.8 GHz were generated with a Mach-Zehnder modulator (MZM) biased at $V\pi$ and modulation with 5.04-GHz RF signal. For O/E frequency up-conversion, optical IF signals were generated by direct modulation of a distributed-feedback laser diode (DFB-LD) with 0.8-GHz IF signals. The optical IF signal with 0-dBm power was injected to the O/E mixers with the 10.8-GHz optical LO.

The resulting RF powers of 10-GHz lower sideband signals from the OIL-SOM and discrete HBT O/E mixer were measured with change of optical LO power and compared in Fig. 2-5. The spectrum in Fig. 2-5 is the frequency up-converted RF output of the OIL-SOM when optical LO power is -6 dBm. For frequency down-conversion, the 10-GHz RF signal with -10 dBm power was injected into the base port of the OIL-

SOM and discrete HBT O/E mixer while the optical LO signals are also injected. The 10-GHz input RF signals are frequency down-converted to 0.8-GHz IF band and measured with RF spectrum analyzer (RF-SA). Fig. 2-6 shows the resulting IF power as a function of optical LO power. Also, the spectrum of Fig. 2-6 is the frequency down-converted IF signal from the OIL-SOM when optical LO power is -6 dBm.

These results show that the OIL-SOM has higher conversion efficiency and less dependence on optical LO power than the discrete HBT O/E mixer. The resulting O/E frequency up-converted RF power from the OIL-SOM is about -30 dBm when the input optical IF power is 0 dBm. Also, the frequency down-converted IF power from the OIL-SOM is about -30 dBm when the input RF power is -10 dBm.

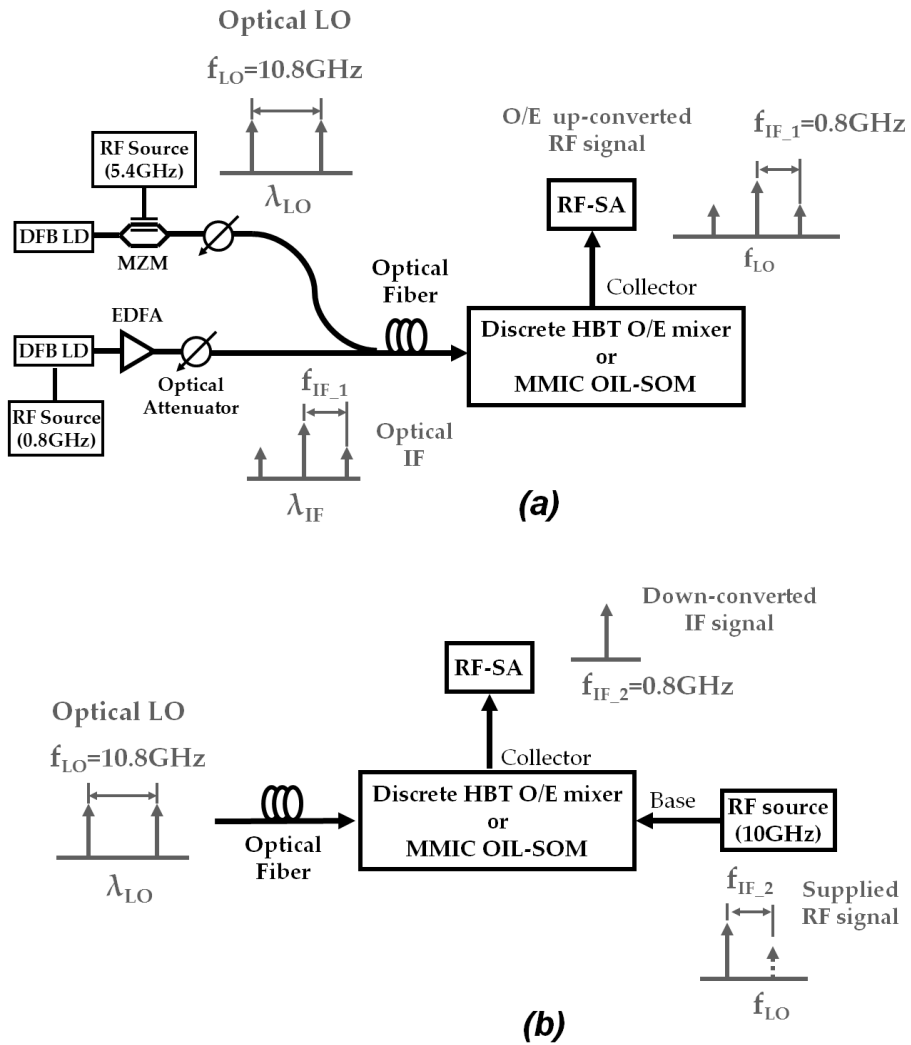


Fig. 2-4. Experimental setup for measurement and comparison of O/E mixing efficiencies. (a) O/E frequency up-conversion (b) frequency down-conversion

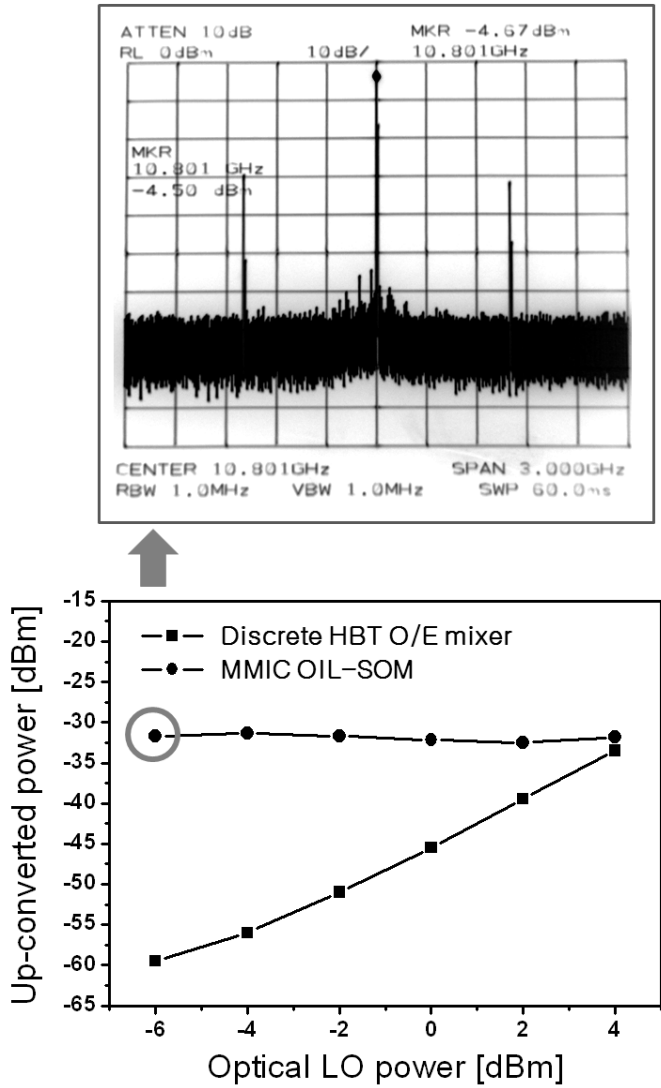


Fig. 2-5. O/E frequency up-conversion efficiencies of OIL-SOM and discrete HBT O/E mixer with change of optical LO power. Spectrum is RF signal of OIL-SOM when optical LO power is -6 dBm.

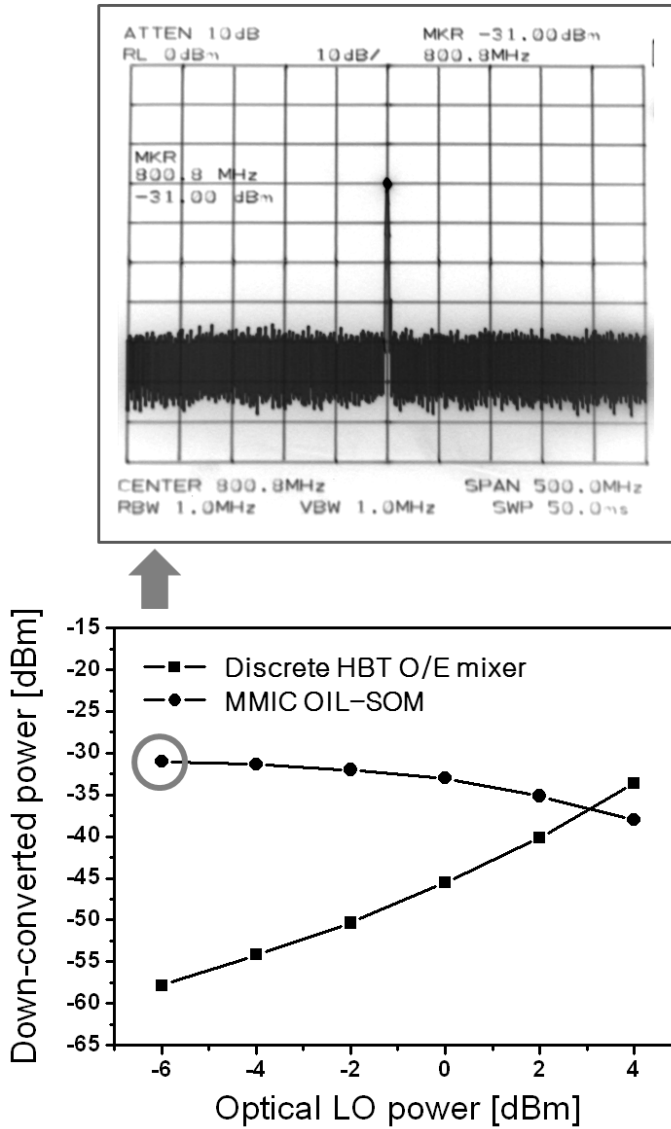


Fig. 2-6. Frequency down-conversion efficiencies of OIL-SOM and discrete HBT O/E mixer with change of optical LO power. Spectrum is output IF signals of OIL-SOM when optical LO power is -6 dBm.

2-2-2. Spurious-free dynamic range of self-oscillating O/E mixer

In RF applications, front-end RF components such as LNA and mixers should have lower noise level or higher conversion efficiency to meet required SNR. In addition, if the device handles high power signals, the nonlinear properties are also important because the IMD3 (third-order inter-modulation distortion) signals are located in adjacent channel and seriously degrade the signal performance.

The OIL-SOM is a sort of front-end device in fiber-fed wireless system because this device firstly detects the input optical signals. Also, the frequency conversion processes originate from the highly nonlinear property of the OIL-SOM so that the generation of IMD3 components is inevitable. The noise and nonlinear characteristics of a device can be expressed as a term of spurious-free dynamic range (SFDR). The MMIC OIL-SOM can be used as an O/E frequency up-converter and down-converter, and the SFDRs in up-conversion and down-conversion may be different. So, the SFDR of OIL-SOM was measured when it is used as an O/E up-converter or down-converter, separately.

Fig. 2-7 shows experimental setup for SFDR measurement of O/E frequency up-converter. To avoid nonlinearity of DFB-LD, the two-tone optical IF signals were generated by direct modulation of two DFB-LDs with 0.46-GHz and 0.459-GHz RF sources, respectively. The

10.7-GHz optical LO signal is optically injected into the free-running oscillator. The up-converted fundamental and IMD3 frequencies were measured with RF-SA after passing through BPF and LNA. For measurement of the IMD3 of which power is low, the BPF was used for rejection of high power LO signal, and the LNA with 32-dB gain and 2.2-dB noise figure was used for signal amplification over the noise floor level of RF-SA. The saturation power of the LNA is high enough for the nonlinearity measurement. The noise floor was also measured in the same measurement setup without the optical IF and LO illumination to reject optical noise influence. From the averaged noise power level displayed in RF-SA, the gain of LNA and noise figure were subtracted for calculation of noise floor [61]. Fig. 2-8 shows the measurement results. The measured SFDR of OIL-SOM in O/E frequency up-conversion is about $94.7\text{-dB/Hz}^{2/3}$ which is similar value with previously reported SFDR of discrete HBT O/E mixer [62].

Fig. 2-9 shows the experimental setup for SFDR measurement of frequency down-converter. The two-tone RF signals in 9.5-GHz band with 10-MHz separation were generated by different RF sources and injected to the OIL-SOM through base port of HBT of the oscillator. Because the high power input RF signals are injected, the spurious signal level is relatively high so that the amplification was not required.

For measurement of noise floor, the baseband amplifier with gain of 28 dB and noise figure of 8 dB was used at the output port of the OIL-SOM. As shown in Fig. 2-10, the measured SFDR of OIL-SOM in frequency down-conversion is about $83.6\text{-dB/Hz}^{2/3}$ which is smaller than that of O/E frequency up-conversion.

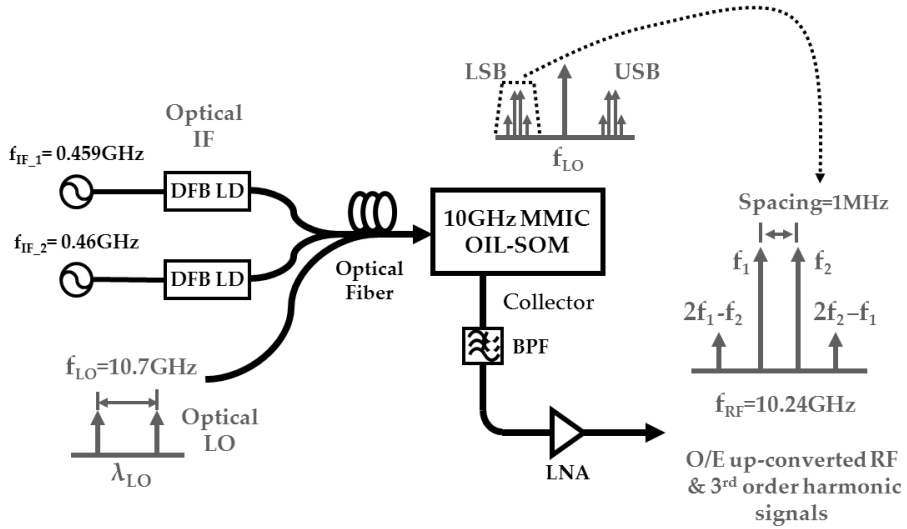


Fig. 2-7. Experimental setup for measurement of SFDR of O/E frequency up-conversion in MMIC OIL-SOM.

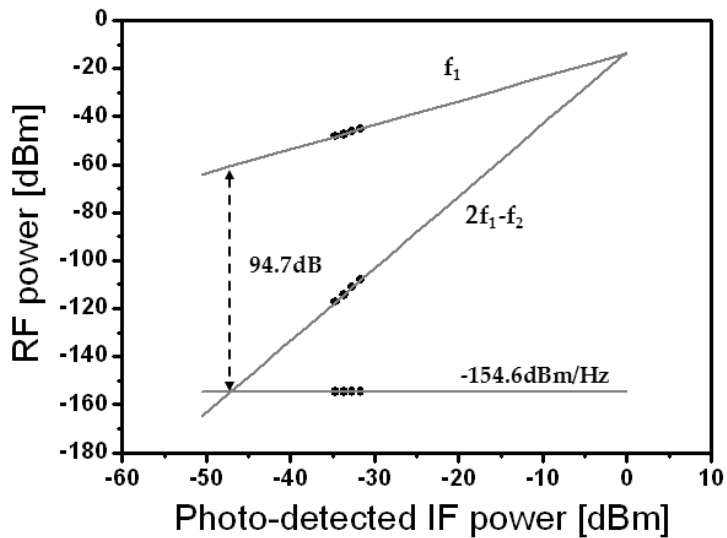


Fig. 2-8. Measurement of SFDR of O/E frequency up-conversion in MMIC OIL-SOM.

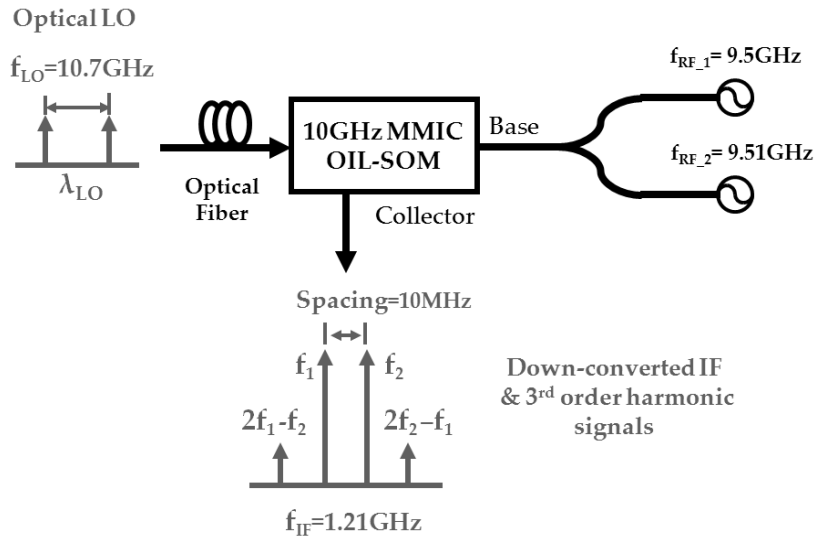


Fig. 2-9. Experimental setup for measurement of SFDR of frequency down-conversion in MMIC OIL-SOM.

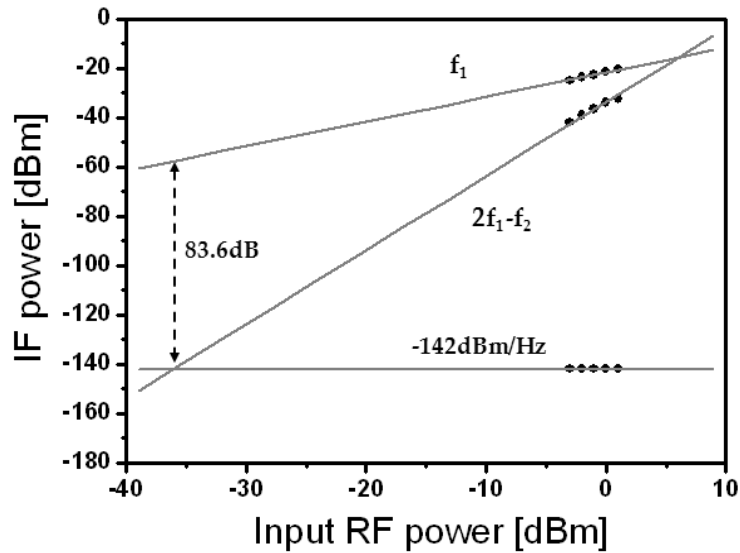


Fig. 2-10. Measurement of SFDR of O/E frequency up-conversion in MMIC OIL-SOM.

2-3. 30-GHz-band Bi-directional fiber-fed wireless link demonstration

2-3-1. Bi-directional fiber-fed wireless system

As evaluated in previous section, the MMIC-based OIL-SOM has simultaneous frequency up/down conversion ability. In this section, the 3rd harmonic operation of the OIL-SOM is utilized for 30-GHz-band bi-directional fiber-fed wireless link demonstration. Fig. 2-11 schematically shows the 30-GHz bi-directional fiber-fed wireless scheme using the 10-GHz MMIC OIL-SOM as a 3rd harmonic frequency up/down converter in antenna base station. Firstly, the third harmonic frequency conversion characteristics and phase noise of the OIL-SOM are evaluated. Based on these results, bi-directional transmission of 32-QAM (quadrature amplitude modulation) format data is demonstrated in 30-GHz band.

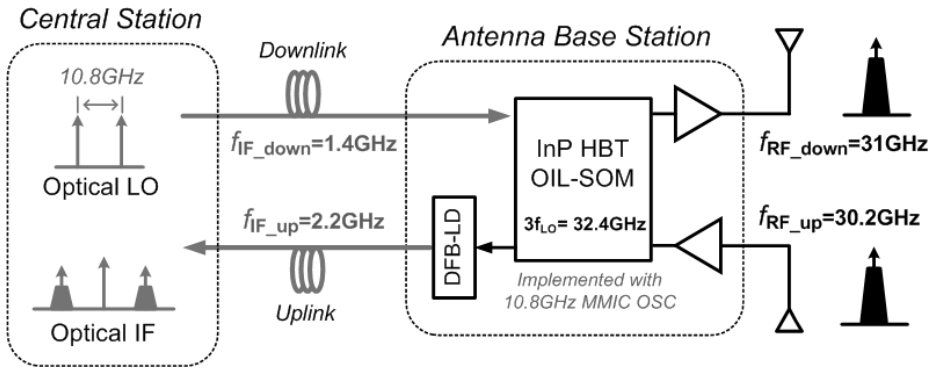


Fig. 2-11. Schematic diagram of 30GHz bi-directional fiber-fed wireless system utilizing 3rd harmonic operation of 10GHz MMIC OIL-SOM.

2-3-2. Experimental setup and results for 30-GHz downlink

Fig. 2-12 shows the experimental setup for measurement of 3rd harmonic O/E frequency up-conversion characteristics and downlink data transmission. 10.8-GHz optical LO was generated with the DSB-SC method and injected into the free-running oscillator. The injection-locked oscillator generates 3rd harmonic LO signals at 32.4 GHz. The 30-GHz-band output signal from the OIL-SOM was measured with a spectrum analyzer after passing through a broadband attenuator and a 30-GHz amplifier. A broadband attenuator with a 10-dB loss was used,

because without it, the 30-GHz amplifier was not impedance-matched to $50\ \Omega$ in 10-GHz-band, which would result in unstable oscillation.

Fig. 2-13 (a) shows the spectrum of optically injection-locked 32.4-GHz LO signals of the OIL-SOM when injected optical LO power is 0 dBm. The reduction of phase noise by optical injection-locking is observed from single-sideband phase noise measurement results shown in Fig. 2-13 (b).

Optical IF signals were generated by direct modulation of a distributed-feedback laser diode with 1.4-GHz IF signals and injected into the MMIC oscillator through a lensed fiber. The harmonically frequency up-converted 30-GHz-band RF output is shown in Fig. 2-14. Also, Fig. 2-14 shows the power of frequency up-converted RF signals as a function of delivered optical LO power when the input optical IF power was 0 dBm. The internal conversion gain is defined as the power ratio of frequency up-converted RF signal to photo-detected IF signal. Because the photo-detected IF power is -40 dBm in PD-mode, the internal conversion loss of the harmonic frequency up-conversion using the OIL-SOM is about 4 dB. The measured conversion efficiency is nearly independent of optical LO power. However, when the optical LO power is larger than 4 dBm, the conversion efficiency decreases because the saturation effect of HBT oscillator under high optical

illumination made the oscillation power and the conversion efficiency low.

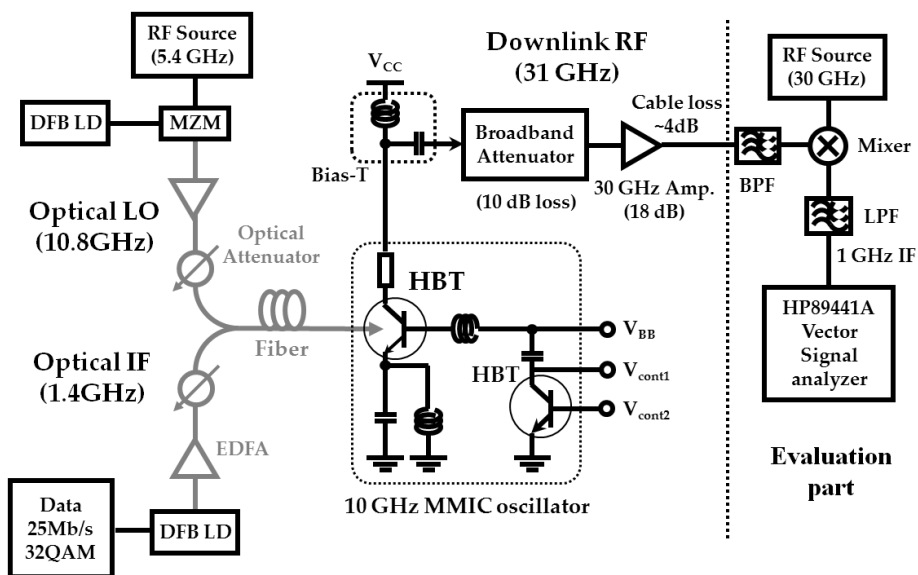
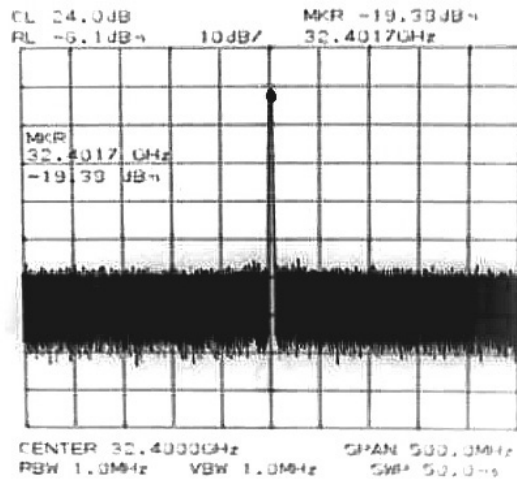
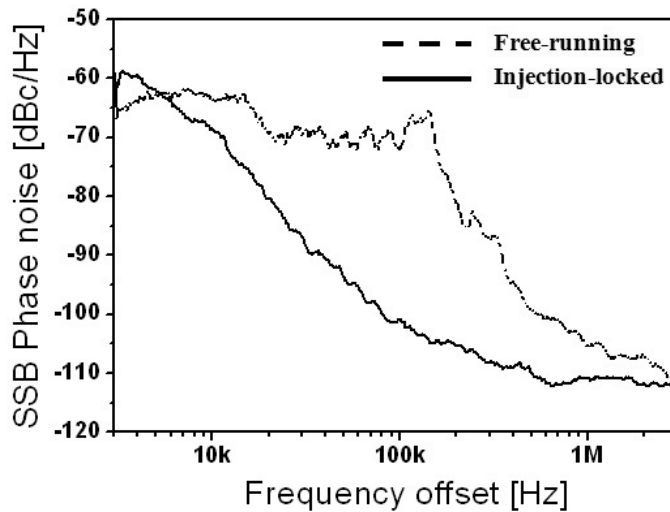


Fig. 2-12. Experimental setup for 30-GHz downlink data transmission.



(a)



(b)

Fig. 2-13. (a) Spectrum of optically injection-locked 32.4-GHz 3rd harmonic LO (b) Measured phase noise of 32.4-GHz 3rd harmonic LO in free-running and optically injection-locked conditions.

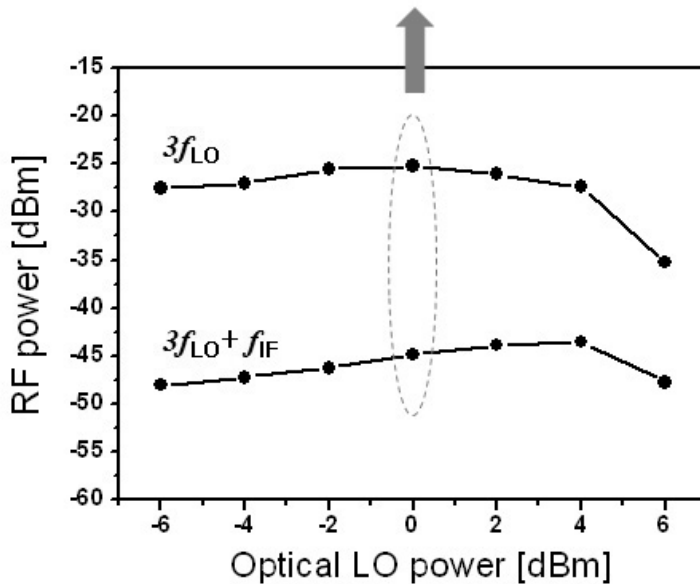
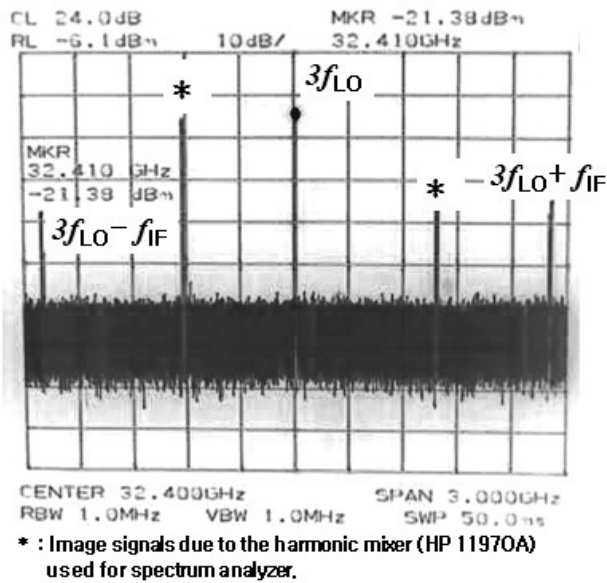
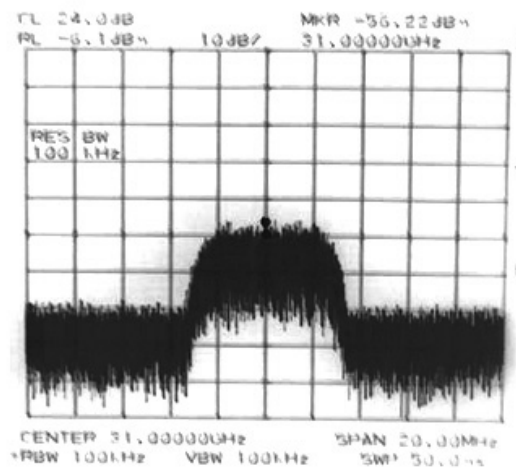


Fig. 2-14. 3rd harmonic LO and harmonically frequency up-converted RF signal power with change of optical LO power and measured spectrum when optical LO power is 0 dBm.

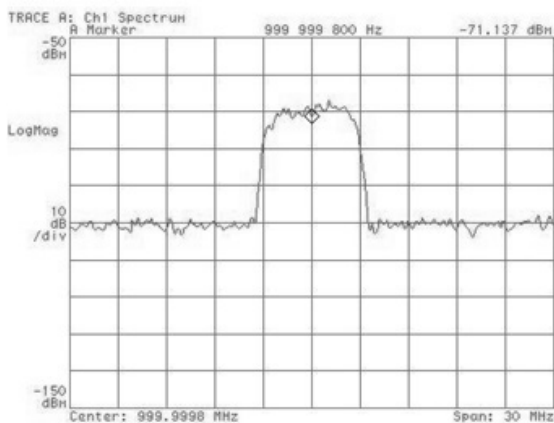
For downlink data transmission, optical IF signals were generated by direct modulation of the DFB-LD with 25-Mbps 32-QAM signals at 1.4-GHz IF. The optical IF signals were injected into the OIL-SOM and frequency up-converted to 30-GHz band as shown in Fig. 2-15 (a). In practical systems, they would radiate to mobile terminals through an antenna. For evaluation of the signal quality, up-converted 30-GHz RF signals were down-converted to 1-GHz IF-band using an electrical mixer and a bandpass filter, and then demodulated by a vector signal analyzer. Fig. 2-15 (b) shows the spectrum of down-converted 1-GHz IF signals.

When both optical LO and IF powers were 0 dBm, the measured error vector magnitude (EVM) of the demodulated signal was 4.34 %, which is sufficient for many wireless applications. For example, the IEEE 802.15.3 standard specifies the transmitter EVM to be less than 4.8 % for 32QAM [63]. The inset of Fig. 2-16 shows the constellation of demodulated 32-QAM signal. The EVMs were measured as a function of incident optical LO powers and the results are shown in Fig. 2-16. They show that there is an optimum range of optical LO power from 0 to 4 dBm. When the optical LO power is less than 0 dBm, the EVM increases due to phase error increase. On the other hand, when the optical LO power is larger than 4 dBm, the EVM increases due to

degradation of conversion efficiency caused by the saturation effect of the oscillator under high power optical illumination.



(a)



(b)

Fig. 2-15. Spectrum of (a) 3rd harmonically frequency up-converted downlink RF signal (b) frequency down-converted downlink IF and data signal.

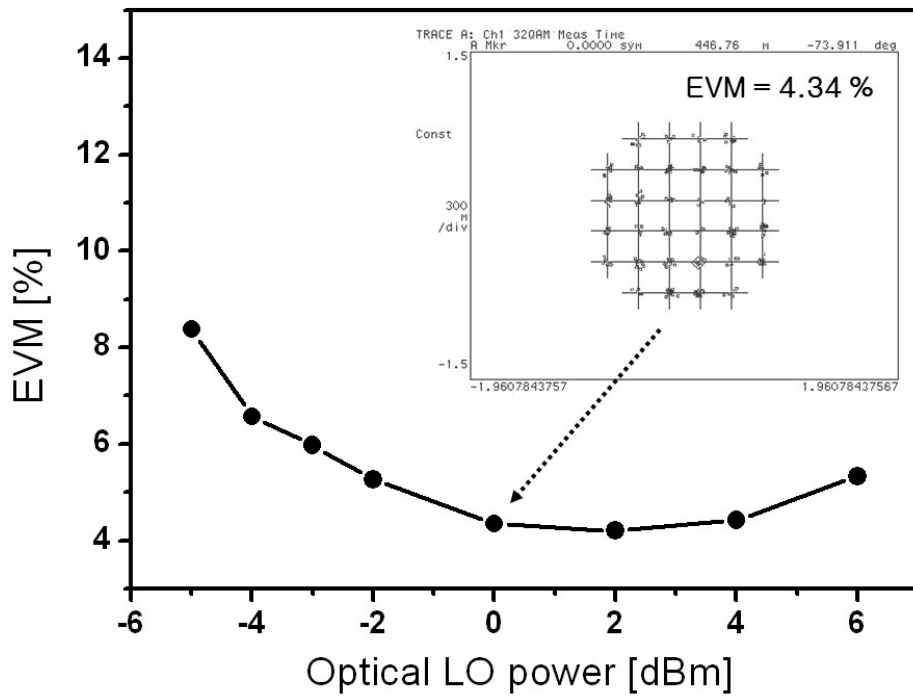


Fig. 2-16. Measured error vector magnitudes (EVMs) as a function of optical LO power when the optical IF power is 0 dBm. Inset is constellation of 32-QAM data demodulated by vector signal analyzer.

2-3-3. Experimental setup and results for 30-GHz uplink

The experimental setup for 30-GHz-band 3rd harmonic frequency down conversion and uplink data transmission is shown in Fig. 2-17. While the optical LO with 10.8-GHz frequency is injected to the OIL-SOM, the 30-GHz RF signals were injected to the base terminal of the HBT and harmonically frequency down-converted to 2.2-GHz IF. The down converted signals were measured with a spectrum analyzer after a broadband attenuator and a baseband amplifier. The broadband attenuator was connected to the collector and base terminals of the HBT for impedance matching in 10-GHz-band. Fig. 2-18 shows the power of down-converted IF signals as function of injected optical LO power when the input RF power at base terminal was -2 dBm. The measured down-conversion efficiency is nearly independent of optical LO power, which is similar to the case of frequency up-conversion.

For uplink data transmission, the 30-GHz-band uplink RF signals were generated by frequency up-converting of 25-Mbps 32-QAM signals with 1.3-GHz IF using an electrical mixer and 31.5-GHz electrical LO source. After passing through a bandpass filter, an amplifier, and a broadband attenuator, 30.2-GHz RF signals were injected into the OIL-SOM for harmonic frequency down-conversion to 2.2-GHz IF-band. The spectrum of uplink RF and down-converted IF

signal is shown in Fig. 2-19. For optical uplink transmission from antenna base station to central station, frequency down-converted signals directly modulated a DFB-LD and the optical uplink signals were detected by a photo-detector. The link loss of the optical uplink transmission was about 10 dB.

After optical uplink transmission, IF signals were demodulated by a vector signal analyzer for evaluation. Fig. 2-20 shows the measured EVMs as a function of optical LO power. There is an optimum range of optical LO power from -1 to 3 dBm. The inset of Fig. 2-25 shows the constellation of demodulated 32-QAM signal when the injected optical LO and electrical RF powers were 0 dBm and -2 dBm, respectively, in which the EVM was 5.47 %. The EVM values from uplink transmission are relatively larger than those from the downlink transmission shown in Fig. 2-16. This may be because the lower down-conversion efficiency of the OIL-SOM compare to the up-conversion efficiency degrades the SNR of uplink signals more seriously than the downlink signals.

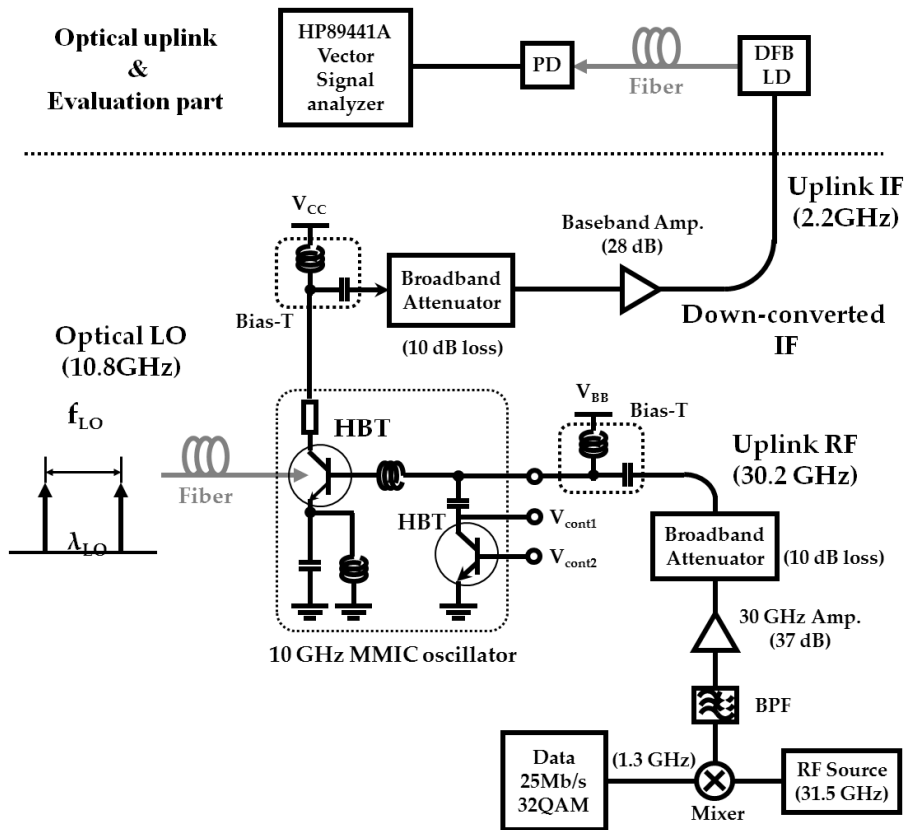


Fig. 2-17. Experimental setup for 30-GHz uplink data transmission.

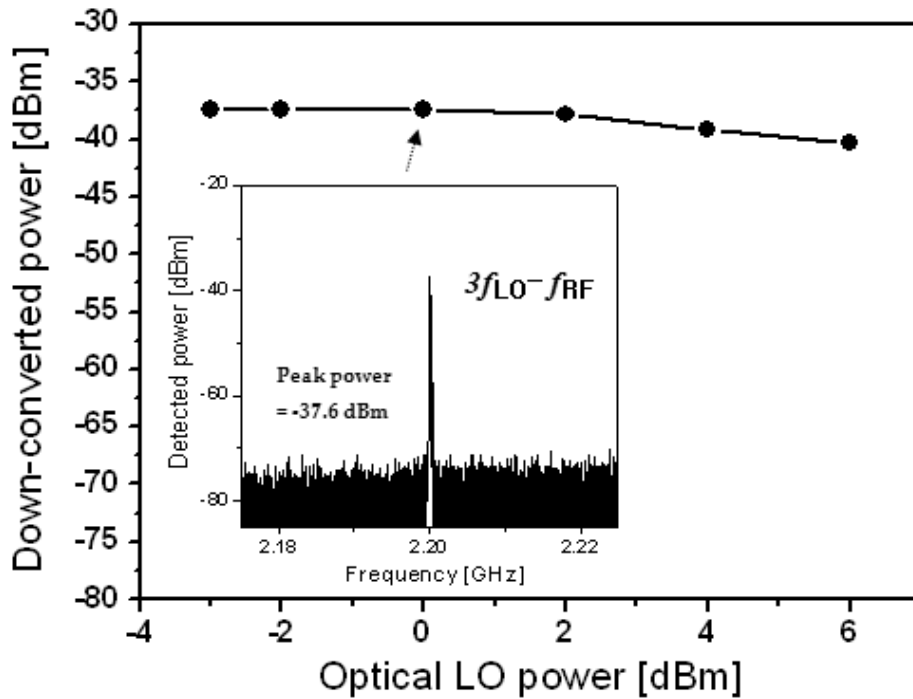
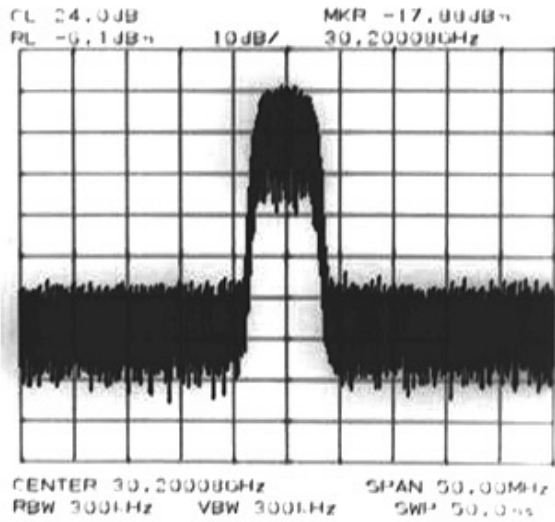
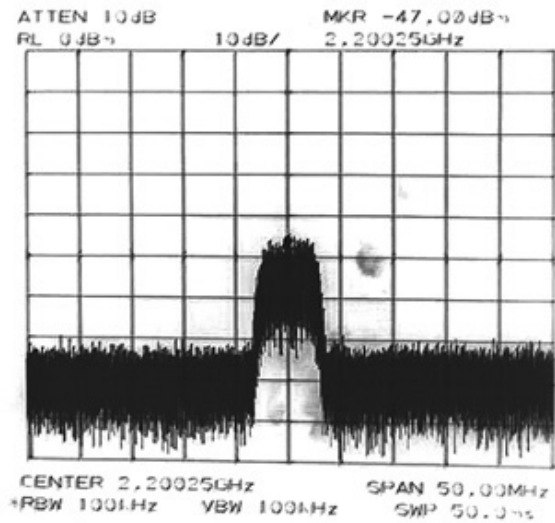


Fig. 2-18. Harmonically frequency down-converted IF signal power with change of optical LO power. Inset is measured IF spectrum when optical LO power is 0 dBm.



(a)



(b)

Fig. 2-19. Spectrum of (a) 30.2-GHz input uplink RF signal (b) harmonically frequency down-converted uplink IF signal.

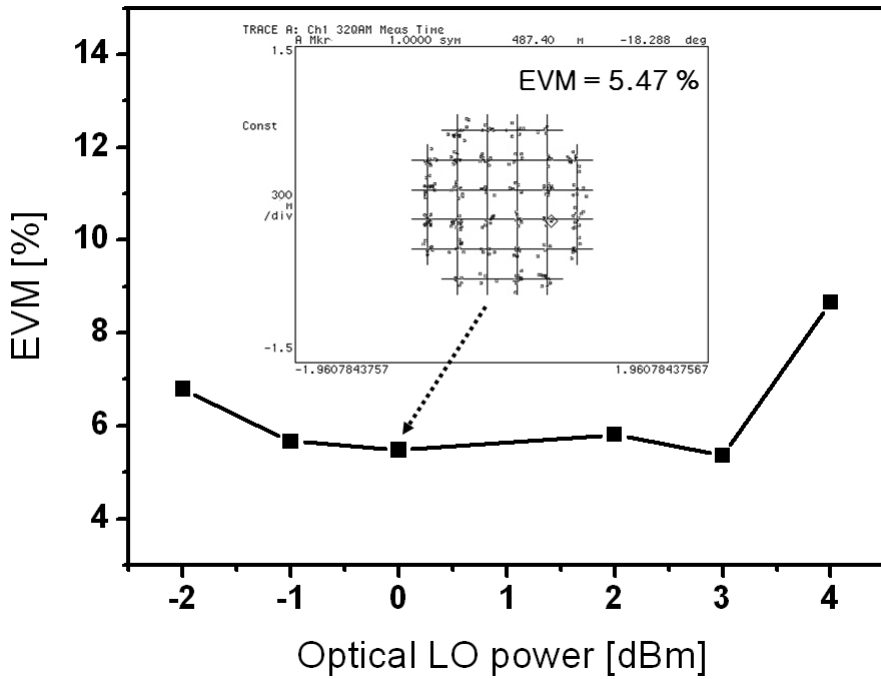


Fig. 2-20. Measured error vector magnitudes (EVMs) as a function of optical LO power when the uplink RF power is -2 dBm. Inset is constellation of 32-QAM data demodulated by vector signal analyzer.

2-4. 60GHz-band fiber-fed downlink demonstration

2-4-1. 60-GHz sub-harmonic O/E frequency up-converter

In this section, 60-GHz sub-harmonic OIL-SOM is realized using a hybrid-type 30-GHz HBT oscillator and utilized for 60-GHz fiber-fed downlink demonstration. The 30-GHz hybrid-type HBT oscillator was implemented using a discrete HBT [56-57] and external feedback loop composed of amplifier and bandpass filter as shown in Fig. 2-21. Because the HBT has sufficient gain of 14 dB at 30 GHz, a free-running HBT oscillator can be implemented with a simple feedback loop connecting the collector and base ports through a 30-GHz bandpass filter with a quality factor of 100.

This OIL-SOM can be directly injection-locked by 30-GHz optical LO and can generate sub-harmonic 60-GHz LO signal. The inset of Fig. 2-21 shows the 60-GHz sub-harmonic oscillation output of the hybrid oscillator in optically injection-locked condition. The inset in Fig. 2-22 shows the single-sideband phase noise characteristics of the 60-GHz LO in free-running and injection-locked. Fig. 2-22 also shows the phase noise at 10-kHz and 100-kHz offset frequencies measured with change of optical LO power. When the optical LO power is higher than -10 dBm, low phase-noise characteristics are maintained. However,

when the optical LO power is lower than -10 dBm, the HBT oscillator becomes unlocked and the phase noise increases sharply.

The locking range of the hybrid oscillator is shown in Fig. 2-23. The locking range increases as the optical LO power increase. However, the locking range of the hybrid oscillator is less than 1 MHz which is much smaller than that of the MMIC oscillator (shown in Fig. A-3) due to the high quality factor (~ 100) of the bandpass filter. Instead, this high quality factor has an advantage that the low phase noise of the injection-locked oscillator can be maintained to quite low power LO injection as shown in Fig. 2-22.

By injecting the optical IF to the OIL-SOM, sub-harmonic O/E mixing can be obtained. However, because the base terminal of the used HBT was occupied for connection of the feedback loop, the bi-directional operation is not possible. In this work, the hybrid OIL-SOM is used for sub-harmonic O/E frequency up-converter for 60-GHz application. Fig. 2-24 shows the sub-harmonically frequency up-converted 60-GHz-band spectrum and internal conversion gain of OIL-SOM as a function of incident optical LO power when the input optical IF power is -6 dBm. The measured conversion gain is independent of optical LO power, however, when the optical LO power becomes larger than 1 dBm, the conversion efficiency decreases. This is because the

saturation effect of the HBT under high-power optical illumination lowers the oscillation power of the HBT oscillator.

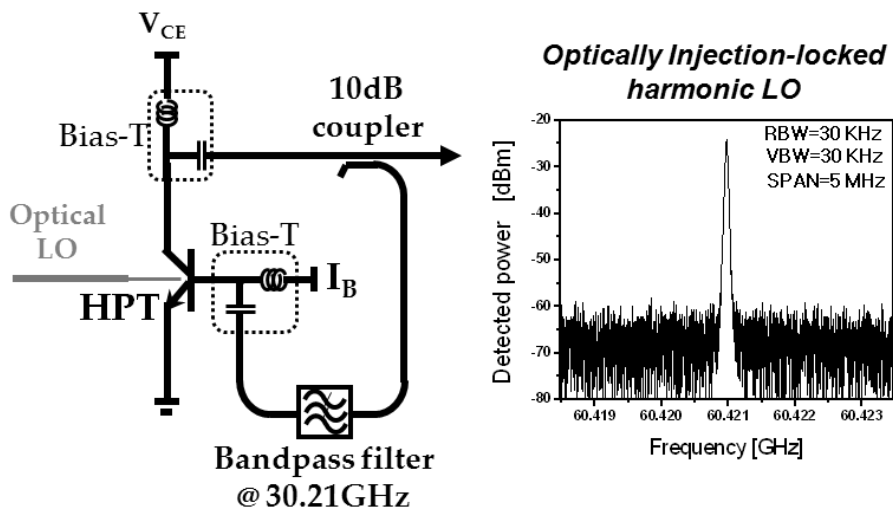


Fig. 2-21. Schematic diagram of 30-GHz hybrid OIL-SOM and spectrum of optically injection locked 60-GHz sub-harmonic LO.

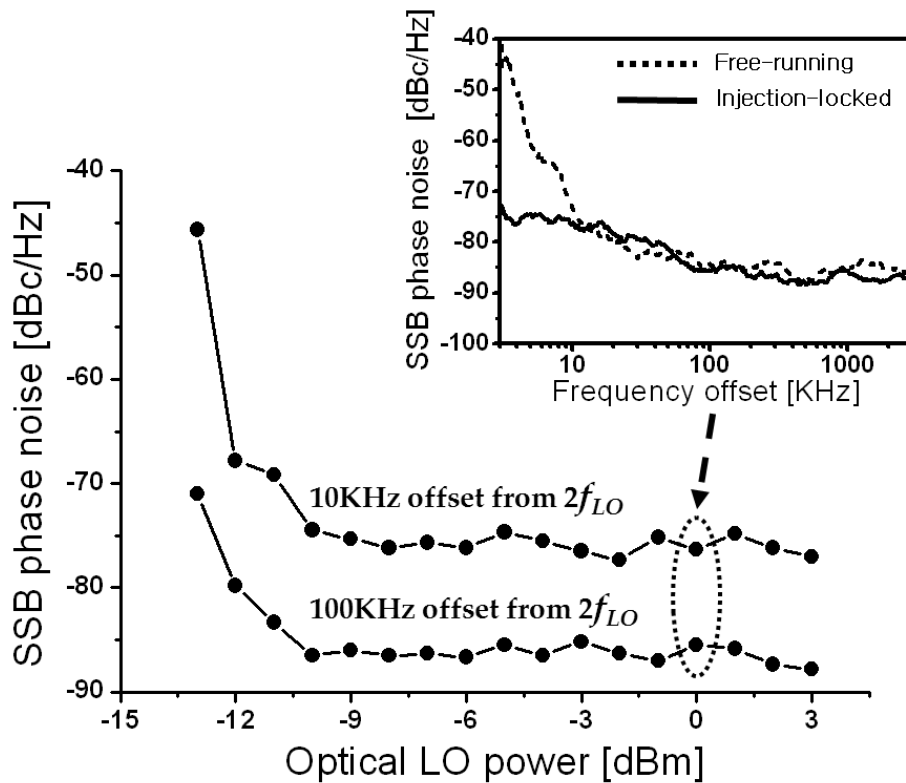


Fig. 2-22. Measured phase noise of 60-GHz injection-locked LO at 10-kHz and 100-kHz frequency offset with change of incident optical LO power. Inset is measured phase noise in free-running and injection-locked conditions.

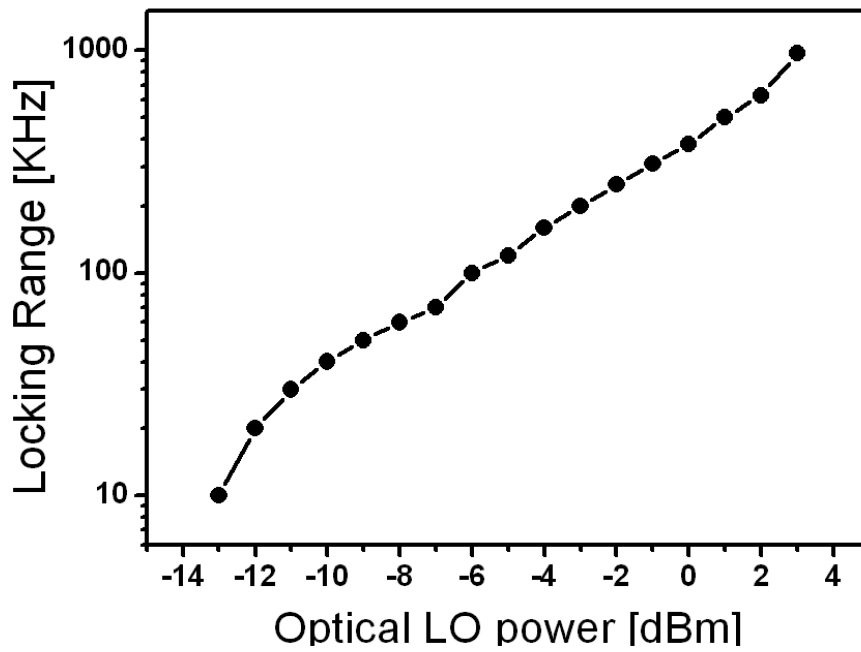


Fig. 2-23. Measured locking range of hybrid HBT oscillator with change of incident optical LO power.

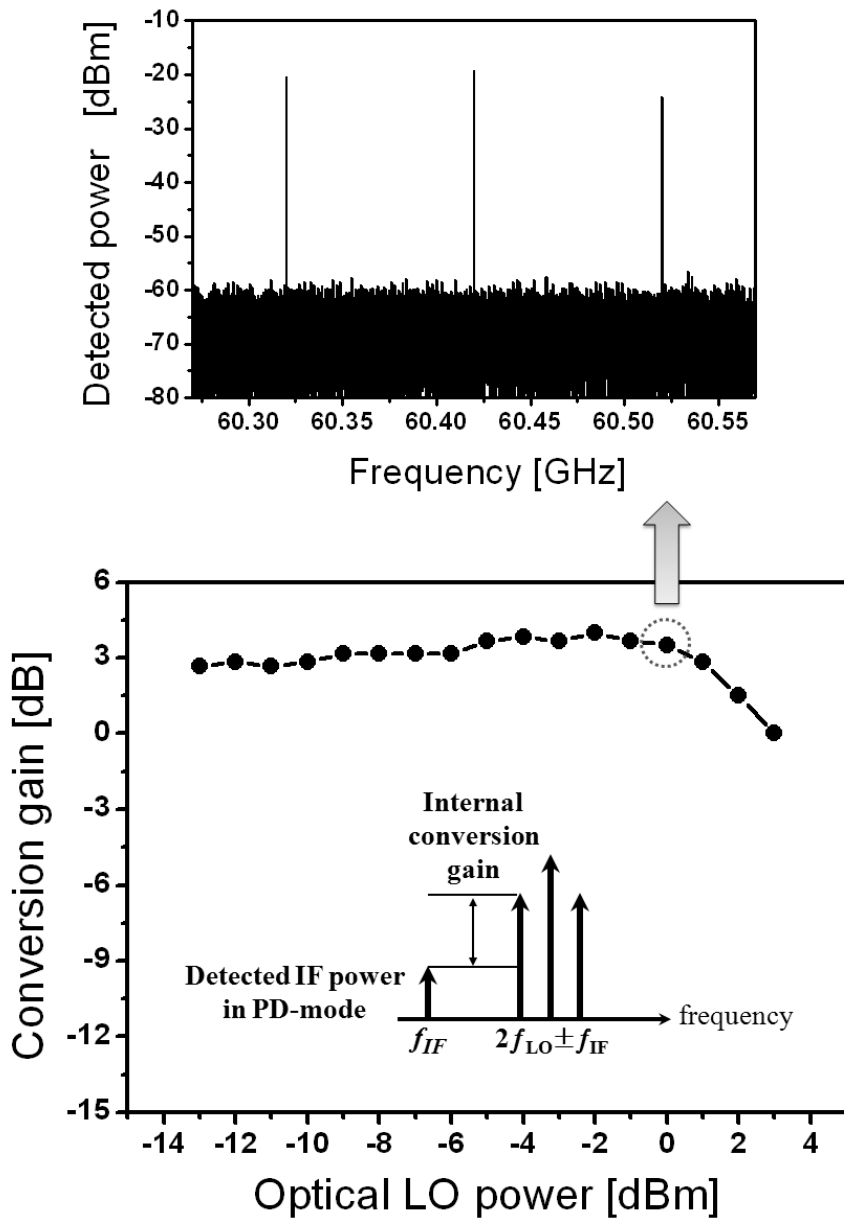


Fig. 2-24. Internal conversion gain of 60-GHz harmonic O/E frequency up-conversion with change of optical LO power. Spectrum was measured with 0-dBm optical LO and -6 dBm optical IF powers.

2-4-2. Experimental setup and results for 60-GHz downlink

Utilizing the OIL-SOM as a harmonic O/E frequency up-converter, 60-GHz-band downlink transmission was demonstrated. Fig. 2-25 shows the experimental setup. Optical IF signals are generated by direct modulation of a DFB-LD with 20-Mb/s 16-QAM data signal in 100-MHz IF. Then, the optical IF signals were injected to the OIL-SOM after 10-km transmission in a single-mode fiber. The 30.21-GHz optical LO generated by the DSB-SC method was also injected to the OIL-SOM for injection-locking. The resulting 60GHz-band RF spectrum is shown in Fig. 2-26. The resulting RF signals were frequency down-converted to IF band. As shown in Fig. 2-27, the EVMs were measured as a function of input optical LO power with fixed optical IF power of -6 dBm. The optimum range of optical LO power is from -11 to 0 dBm in which the EVMs are maintained in low values. The lower boundary of this range is caused by the phase noise degradation due to unlocking of OIL-SOM. On the other hand, the upper boundary is caused by the conversion efficiency degradation effect in high power optical illumination shown in Fig. 2-24.

The demonstrated 60-GHz OIL-SOM provides uniform link performance over optical LO power range of about 11 dB (-11 ~ 0 dBm), which corresponds to substantial margin in system design to

accommodate fiber length and other variations.

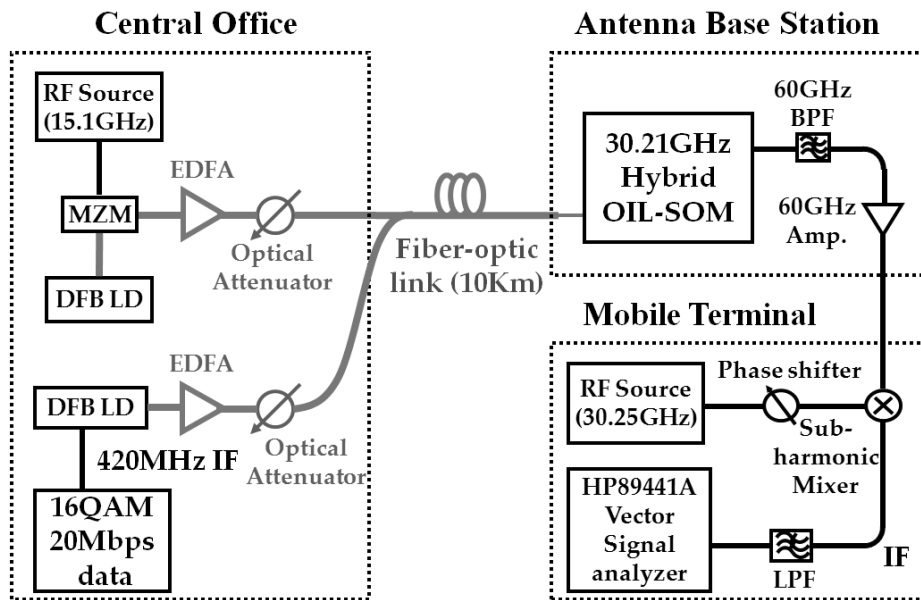


Fig. 2-25. Experimental setup for 60-GHz downlink data transmission.

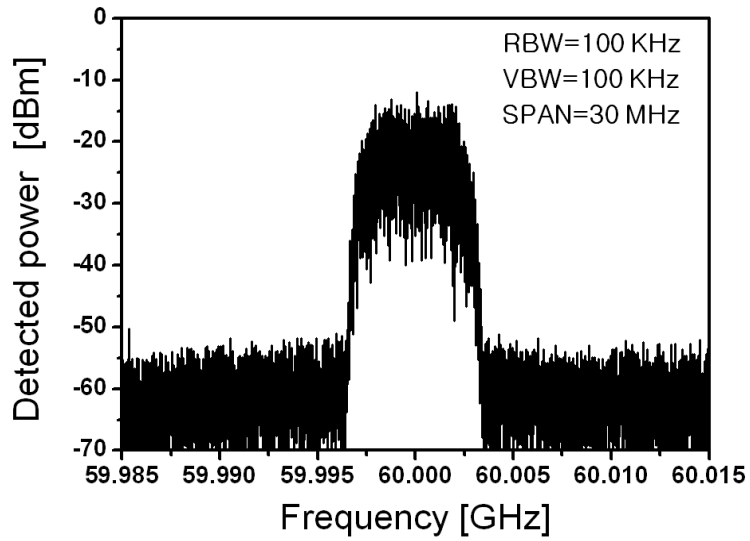


Fig. 2-26. Spectrum of 60-GHz downlink signal.

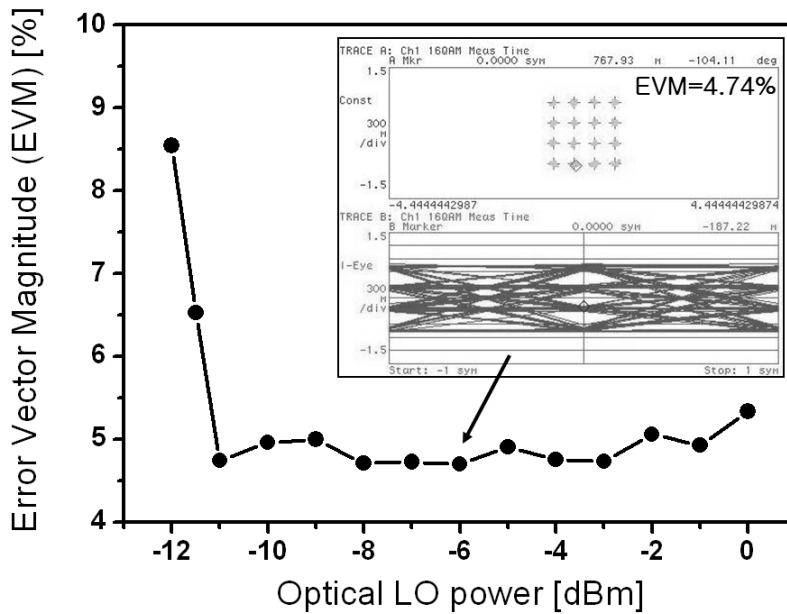


Fig. 2-27. Measured EVM as a function of optical LO power when the optical IF power is -6 dBm. Inset is constellation of 16-QAM data.

2-5. Summary

The InP HBT-based O/E mixer utilizing the optical LO is a promising approach for the realization of a simple and low-cost antenna base station. However, the utilization of the optical LO with a discrete HBT O/E mixer can induce the disadvantage of yielding low conversion efficiency due to insufficient LO power.

In this study, the optically injection-locked self-oscillating O/E mixer (OIL-SOM) based on an InP HBT oscillator was proposed. As summarized in Table 2-1, the realized MMIC and hybrid OIL-SOMs show higher conversion efficiency than the discrete HBT O/E mixer with little dependence on LO power [46]. Also, the conversion efficiency of the OIL-SOM is not largely different from that of the HBT O/E mixer which utilizes the electrical LO [45].

For the feasibility study of the OIL-SOM utilization in fiber-fed wireless system, the 30-GHz-band bi-directional link using the 10-GHz MMIC HBT oscillator and the 60-GHz data transmission using the 30-GHz hybrid HBT oscillator were demonstrated.

	[45]	[46]	This work	
O/E mixer type	Discrete O/E mixer with Electrical LO	Discrete O/E mixer with Optical LO	MMIC HBT OIL-SOM	Hybrid HBT OIL-SOM
IF detection	-15 dBm with photo-Tr. gain (for 0dBm optical IF)			
10GHz Output RF power	-	-60 ~ -35 dBm (fundamental)	-32dBm (fundamental)	-
60GHz Output RF power	-30 dBm (fundamental)	< -40 dBm (fundamental)	-	-35 dBm (sub-harmonic)
Conversion efficiency	Moderate	Poor	Moderate	Moderate
Remarks	Electrical LO source required in ABS	Depends on optical LO power	Insensitive on optical LO power	

Table 2-1. Performance comparison of InP HBT-based conventional O/E mixers and OIL-SOMs.

3. CMOS-based APD optoelectronic mixers

3-1. Introduction

This chapter describes a CMOS-based APD O/E mixer with enhanced conversion efficiency. For simulation of the APD O/E mixer, the large-signal equivalent circuit model of the CMOS APD is established by expanding the previously reported small-signal model [64] in section 3-2. In section 3-3, the CMOS-based APD O/E mixer is simulated using the established large-signal model and the CMOS-based APD is redesigned at device level for conversion efficiency enhancement of the O/E mixer. Section 3-4 describes the 60-GHz-band balanced APD O/E mixer that is designed for the improvement of the sub-harmonic frequency conversion efficiency. The sub-harmonic O/E mixer utilizes an LO input at half of the desired mixing frequency, so the complexity of LO source implementation can be reduced.

3-2. Large-signal equivalent circuit modeling of CMOS-based APD

3-2-1. CMOS-based APD used in the modeling

Fig. 3-1 schematically shows the cross-sectional layer structure of P^+/N -well junction APD used in this work [49]. The APD is fabricated in 0.18- μm standard CMOS process and the lateral dimension is $30 \times 30 \mu\text{m}^2$. Fig. 3-2 shows measured I-V curve of the APD. The DC photo-detection current in low bias voltage is about $2.5 \mu\text{A}$ for 1-mW optical illumination and the optical responsivity is 0.0025 A/W. As the reverse bias voltage approaches to the avalanche breakdown voltage (V_{BR}) of 10.1 V, the photo-current increases due to the avalanche multiplication process. The peak optical responsivity of the APD is about 0.4 A/W at the reverse bias voltage of 10.1 V, in which the avalanche multiplication gain is about 160. When the reverse bias voltage increases over the breakdown voltage, the electrical noise current overcomes the photo-current so that the APD cannot be properly used as a photo-detector. The avalanche gain of APD, $M(V_R)$, is defined as the ratio of photo-current in avalanche region to the photo-current in reverse bias of 1 V.

Hence, the photo-current of APDs can be expressed as

$$I_{Av} = I_{ph} \cdot M(V_R) \quad (3-1)$$

where I_{Av} is an avalanche photo-current, I_{ph} is a photo-current without avalanche gain, $M(V_R)$ is an avalanche multiplication gain that depends on the reverse bias voltage.

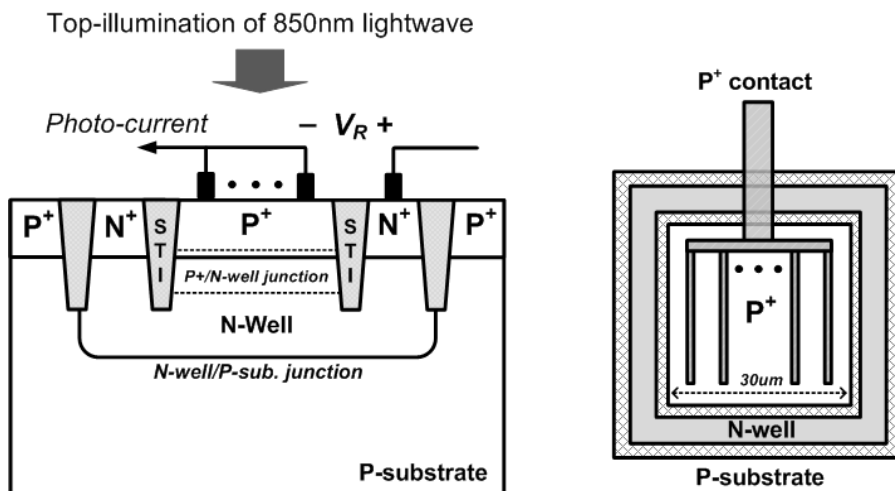


Fig. 3-1. Schematic cross-section and layout of CMOS-based APD using P+/N-well junction surrounded by swallow trench isolation (STI).

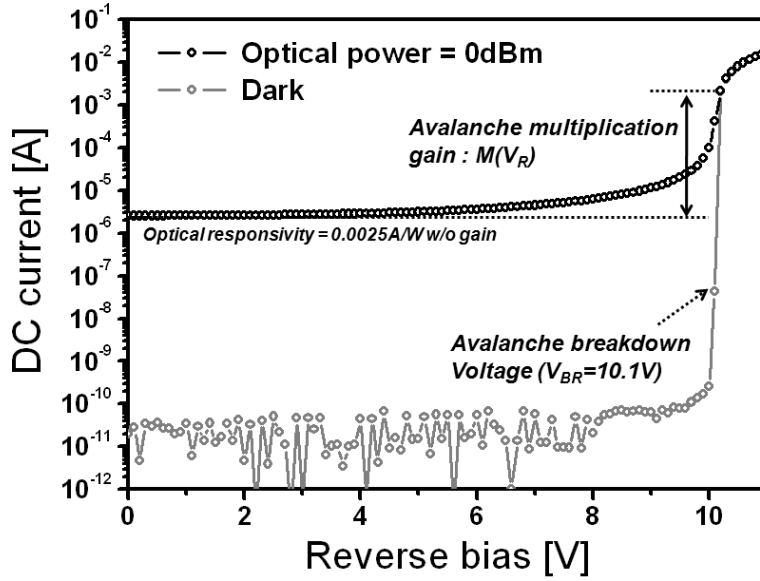


Fig. 3-2. Measured I-V characteristics of CMOS-based APD in dark and 0-dBm optical illumination.

3-2-2. Equivalent circuit model for the CMOS-based APD

Fig. 3-3 shows the equivalent circuit model of the CMOS-based APD. The avalanche photo-current I_{Av} was modeled with a current source which depends on both of the photo-current I_{ph} and the avalanche multiplication gain $M(V_R)$, following equation (3.1). An inductive component L_a was inserted in series with the current source to describe the avalanche transit time in avalanche region [65]. C_j and R_j are junction capacitance and drift region resistance. The N-well

resistance is represented with R_{S1} and R_{S2} . The N-well/P-substrate junction capacitance is C_{P1} . Also, the parasitic capacitance and resistance of substrate was modeled with C_{P2} and R_p .

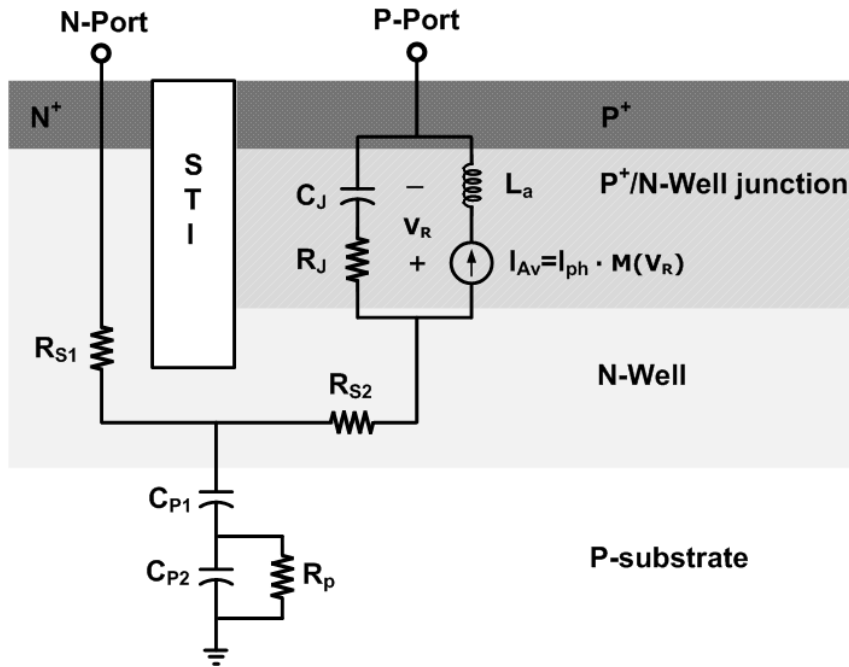


Fig. 3-3. Large-signal equivalent circuit model of CMOS-based APD.

3-2-3. Parameter extraction process and fitting results

Using the equivalent circuit model, the circuit parameters were extracted for the CMOS-based APD described in section 3-2-1. For parameter extraction, two-port S-parameter sets were measured with various reverse bias voltages. The parasitic effect of pads and metal

interconnections were de-embedded from the measured S-parameters using pad, open, short method [66].

In the measured DC curve shown in Fig. 3-4, the output current of the APD has a linear relationship to reverse bias voltage over the avalanche breakdown voltage. From this result, the parasitic series N-well resistance of $R_{S1} + R_{S2}$ was initially set as the slope of this I-V curve. The initial values of capacitances and inductances were set as the pre-established small-signal model parameters in [64]. Then, by empirical fitting of measured S-parameters with changing of reverse bias, the model parameters were extracted.

Table 3-1 shows the extracted parameters at the reverse bias voltages from 9.8 V to 10.5 V with 0.1-V step. The values of junction capacitance C_J and avalanche inductance L_a changes with a reverse bias voltage in the avalanche breakdown region over 10.1V. Under the avalanche breakdown region, C_J is determined at the constant value of 350 fF and L_a doesn't exist. Except for these two components, the other circuit parameters are fixed all over the bias conditions.

The avalanche photo-current model was numerically fitted with an equation which describes the avalanche gain as a function of reverse bias across the intrinsic *P+/N-well* junction as shown in Fig. 3-4. To obtain the intrinsic I-V relationship, the voltage drop across the series

N-well resistance was subtracted from the external bias voltage across the APD. For simplification, the dark current was ignored so that the established model is not accurate in photo-detection characteristics in avalanche breakdown region over 10.1 V.

Fig. 3-5 shows the DC curve fitting results with 0-dBm optical illumination both in log and linear scales. Fig. 3-6 ~ Fig. 3-9 shows the measured two-port S-parameters and fitting results with reverse bias voltage of 9.9, 10.0, 10.1 and 10.2 V. The fitting results are well matched to measured data over change of bias conditions.

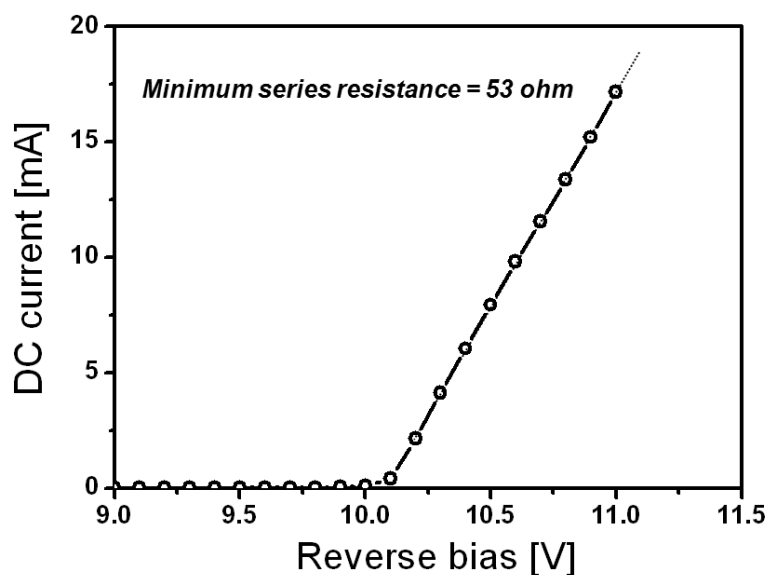


Fig. 3-4. Measured DC characteristics of CMOS-based APD with 0-dBm optical illumination in linear scale.

Parameters	Values
R_{S1}	5Ω
R_{S2}	35Ω
R_J	30Ω
R_P	120Ω
C_{P1}	220 fF
C_{P2}	100 fF

Reverse Bias	C_J	L_a
9.8V	350fF	-
9.9V		
10.0V		
10.1V		
10.2V	250fF	2.6nH
10.3V	200fF	1.4nH
10.4V	160fF	1.0nH
10.5V	120fF	0.8nH

Table 3-1. Extracted circuit parameters.

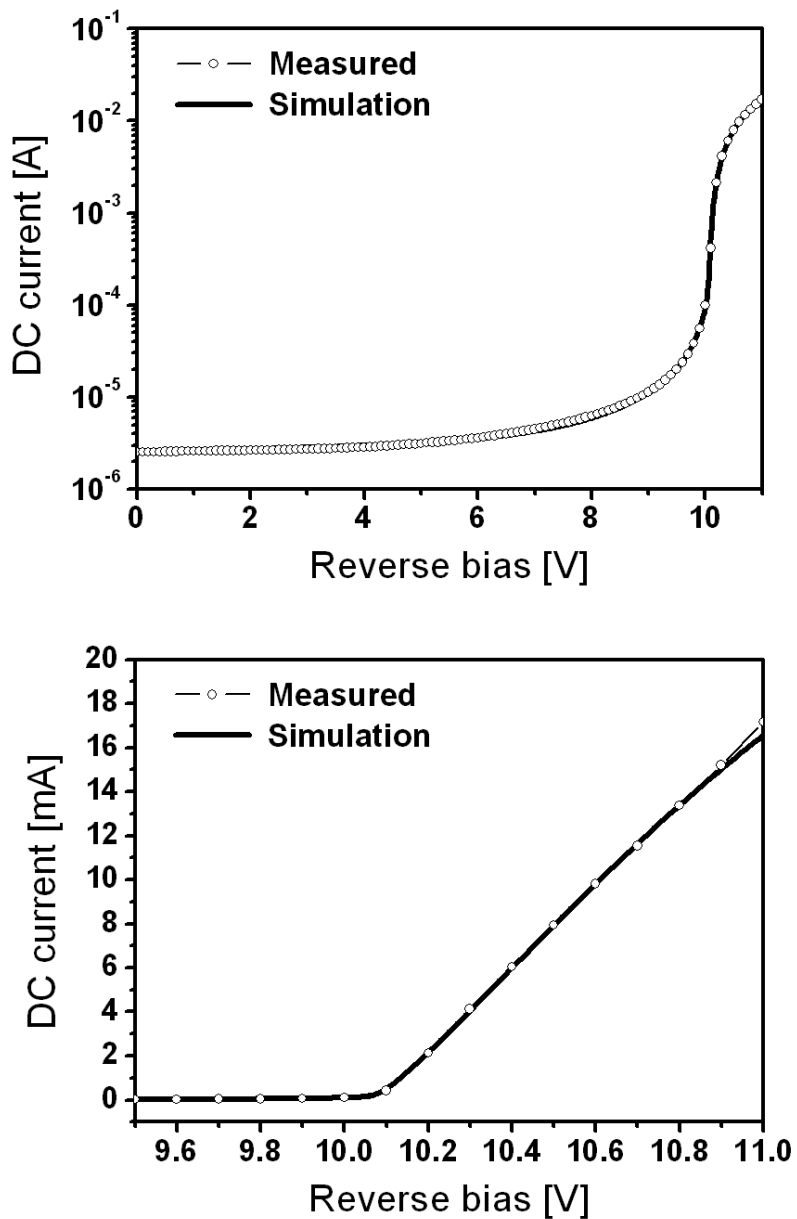


Fig. 3-5. Measured DC characteristics and simulation results with 0-dBm optical illumination in log and linear scale.

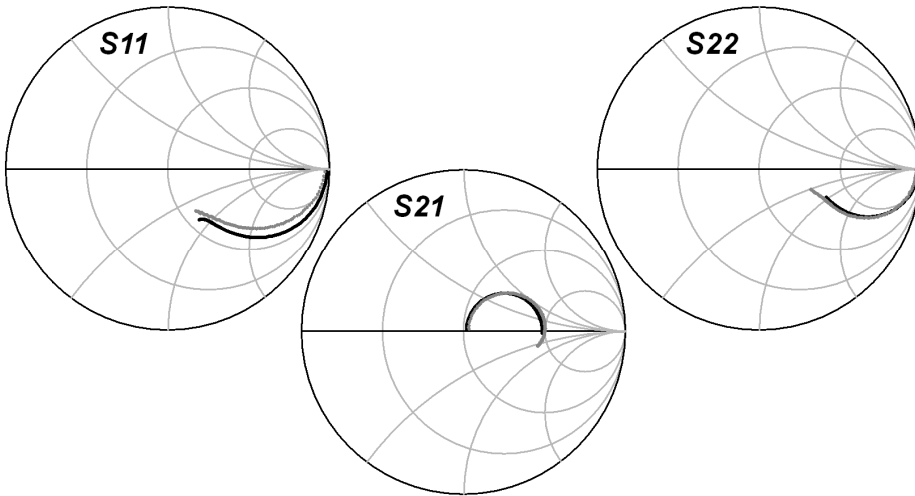


Fig. 3-6. Measured S-parameters and simulation results with 0-dBm optical illumination and 9.9 V reverse bias voltage.

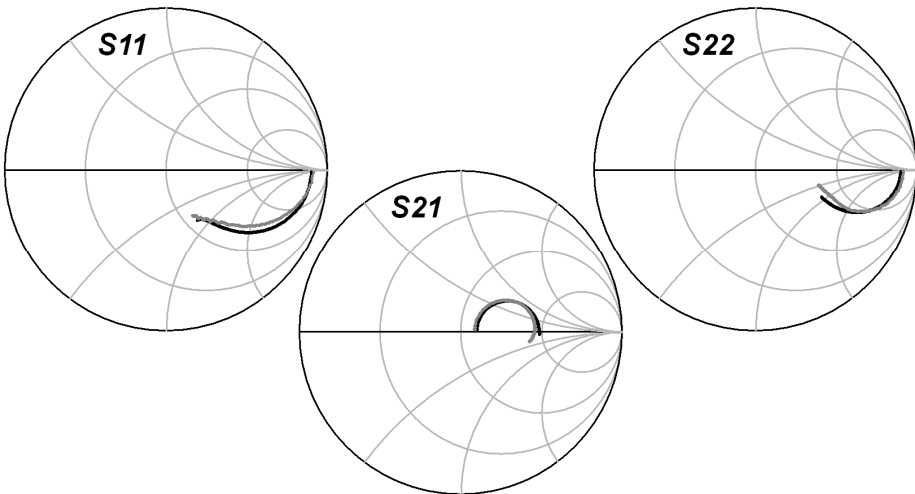


Fig. 3-7. Measured S-parameters and simulation results with 0-dBm optical illumination and 10.0 V reverse bias voltage.

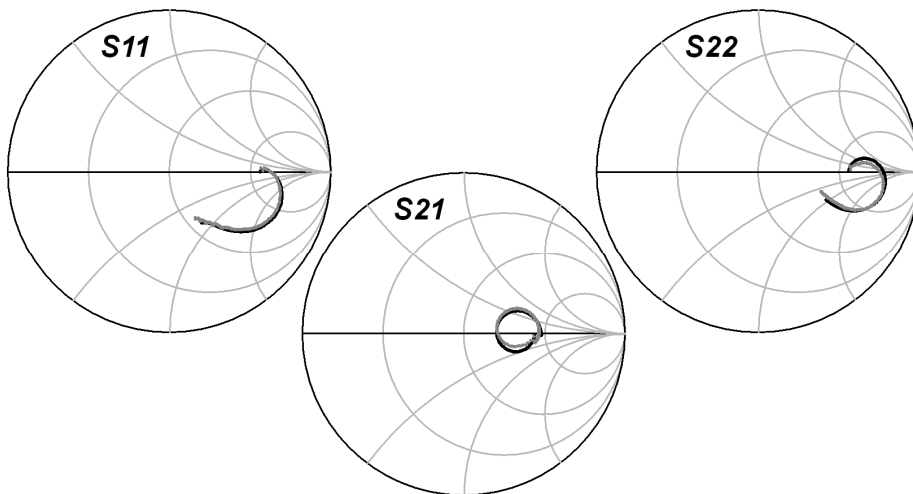


Fig. 3-8. Measured S-parameters and simulation results with 0-dBm optical illumination and 10.1 V reverse bias voltage.

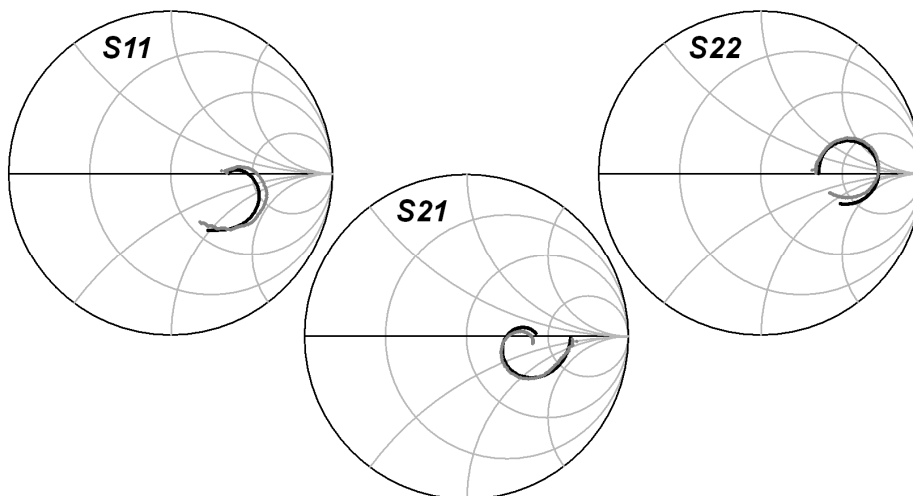


Fig. 3-9. Measured S-parameters and simulation results with 0-dBm optical illumination and 10.2 V reverse bias voltage.

3-3. Optimization of CMOS-based APD for 60-GHz O/E mixer

3-3-1. Considerations for RF loss of APD O/E mixer

Fig. 3-10 shows 60-GHz sub-harmonic O/E mixer operation of the CMOS-based APD, in which the APD is described in detail based on the equivalent circuit model. For O/E mixing operation, 30-GHz LO applied to *N-well* of the APD modulates the reverse bias voltage across the APD. Because the supplied LO power partially contributes on the voltage swing across the intrinsic *P+/N-well* junction, the small impedance across the *P+/N-well* junction can seriously reduce the avalanche gain modulation and mixing efficiency. Consequently, the large parasitic capacitance of *N-well* to *P-substrate* junction also can degrade the mixing efficiency by LO power loss. In high frequencies such as 30 GHz, the junction capacitance (C_j) of about 350 fF corresponds to the impedance of about 15 Ω , which is much smaller than the other parasitic impedances such as series *N-well* resistances.

Fig. 3-11 shows the 60-GHz sub-harmonic O/E mixing simulation results using the equivalent circuit model established in section 3-2. The optical IF and electrical LO powers were set to 0 and 10 dBm, respectively. The simulated 60.1-GHz frequency up-converted RF

powers are plotted as a function of reverse bias voltage with change of the junction capacitance. The simulation result shows that the dependence of conversion efficiency on the reverse bias voltage and the junction capacitance. The small junction capacitance is expected to significantly enhance the conversion efficiency.

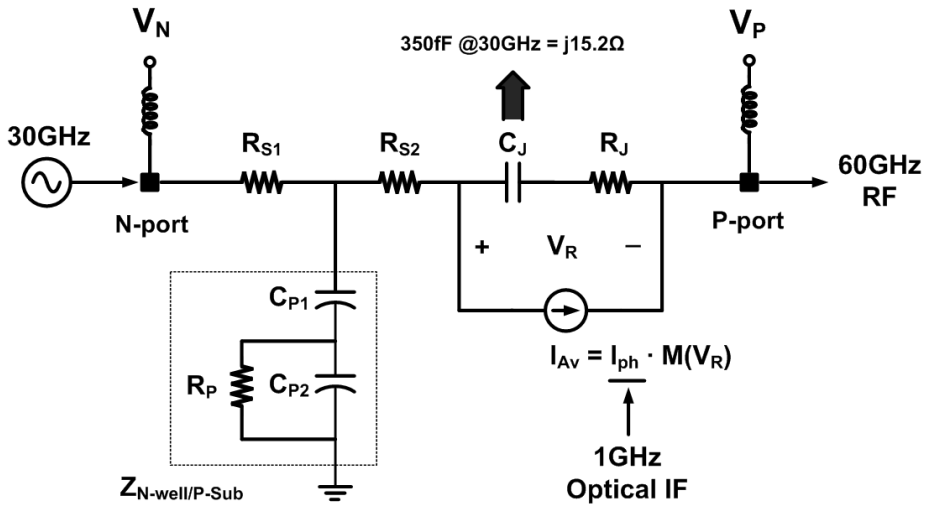


Fig. 3-10. 60-GHz sub-harmonic O/E mixer operation described with equivalent circuit model.

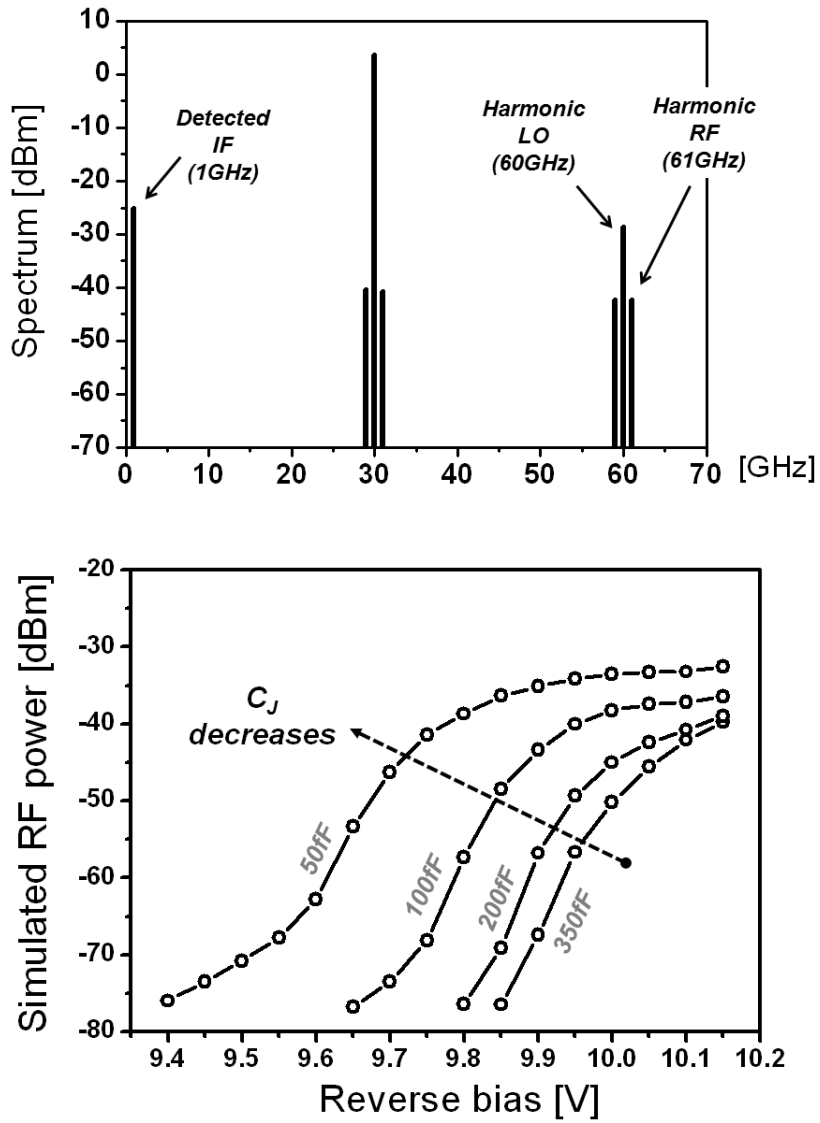


Fig. 3-11. 60-GHz sub-harmonic O/E mixer simulation results with a plot of the 61-GHz RF power as a function of reverse bias voltage with change of junction capacitance.

3-3-2. Design optimization and experimental verification

The junction capacitance and parasitic capacitance strongly depend on the lateral size of APD. To evaluate the size dependence of CMOS-based APD O/E mixer, the APDs with different active areas of $10 \times 10 \mu\text{m}^2$ and $30 \times 30 \mu\text{m}^2$ were fabricated in 0.13- μm standard CMOS process.

Fig. 3-12 shows the DC characteristic of the fabricated APDs in dark and 0-dBm optical illumination conditions. The optical power of 0 dBm was injected to the APDs through lensed fiber of 10- μm spot diameter. The measured dc optical responsivities of the APDs with $10 \times 10 \mu\text{m}^2$ and $30 \times 30 \mu\text{m}^2$ devices are 0.0093 A/W and 0.0124 A/W, respectively without avalanche gain. The peak avalanche gain for $10 \times 10 \mu\text{m}^2$ and $30 \times 30 \mu\text{m}^2$ devices are 112 and 121, respectively, at reverse bias voltage of 10.3 V. This means that both of the photo-detection efficiency and avalanche gain are not significantly affected by the device size when the optical coupling efficiency is the same.

Fig. 3-13 shows the measured photo-detection frequency response at the reverse bias voltage of 10.25 V where the optical responsivity is maximum. The incident optical power is 0 dBm. As can be seen, $10 \times 10 \mu\text{m}^2$ APD has much larger bandwidth ($\text{BW}_{-3\text{dB}} = 5.75 \text{ GHz}$) than $30 \times 30 \mu\text{m}^2$ APD ($\text{BW}_{-3\text{dB}} = 2.1 \text{ GHz}$). This is mainly due to the reduced

RC time constant of the smaller device with smaller junction capacitance.

For measurement of 60-GHz sub-harmonic mixing efficiency, 30-GHz LO and 100-MHz optical IF were applied on the APDs. Fig. 3-14 shows the measured powers of 60-GHz harmonic LO and 60.1-GHz frequency up-converted signals from the two kinds of APDs. The $10 \times 10 \mu\text{m}^2$ APD has over 20-dB larger conversion efficiency than the $30 \times 30 \mu\text{m}^2$ device. Also, there is a saturation effect of frequency up-converted RF power which was also observed in simulation results.

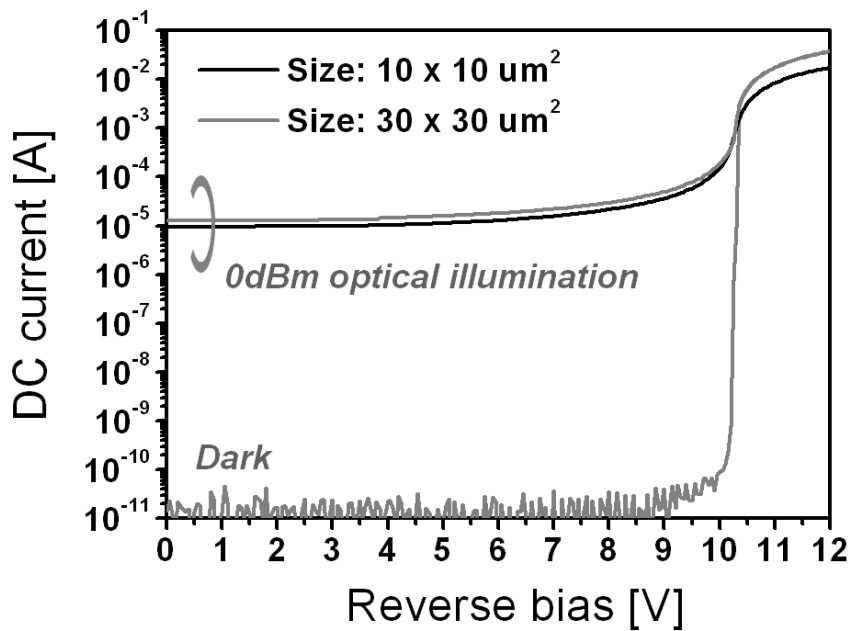


Fig. 3-12. Measured DC optical response of APDs with different device size.

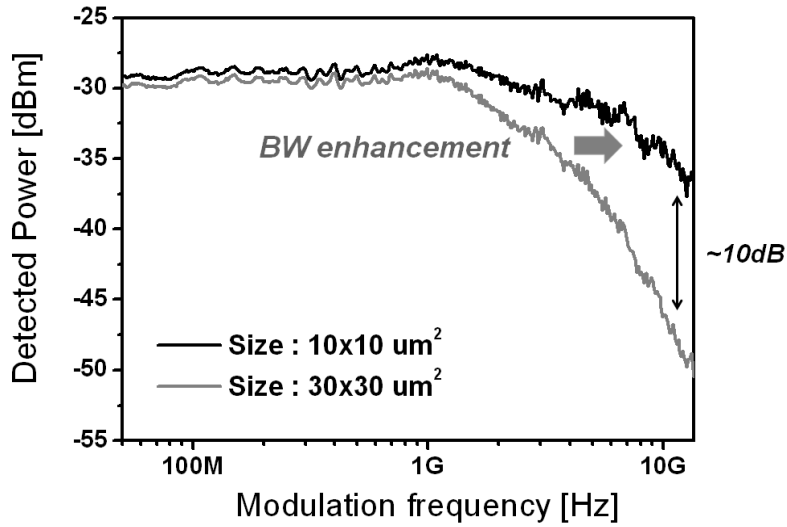


Fig. 3-13. Measured AC photo-response of APDs with different device size under 0-dBm optical illumination.

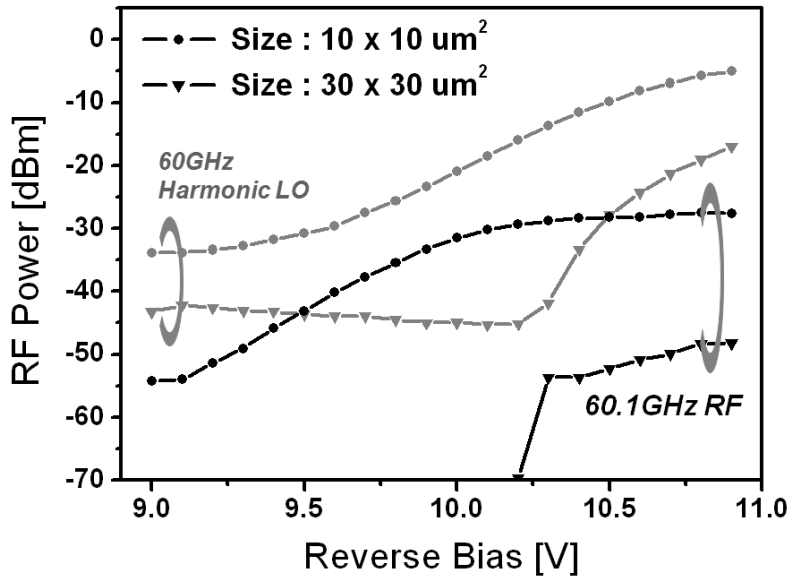


Fig. 3-14. Measured 60-GHz LO and 60.1-GHz RF signal powers with 0-dBm optical IF power and APDs with different size.

In the smaller APD, the conversion efficiency of O/E mixer can be greatly enhanced. However, the APD with reduced size and small junction capacitance can suffer from the other parasitic effects. These effects are significant in the small APD. Firstly, the LO power loss by the *N-well/P-substrate* junction capacitance can be highlighted. Secondly, the smaller lateral area of *P+* region can increase the contact resistance. These parasitic effects were also investigated.

For applying DC reverse bias on the APD, two kinds of configuration are possible. First one is to bias on *N-well* ($V_N = V_R$) when *P+* is grounded ($V_P = 0$). Second method is to bias on *P+* ($V_P = -V_R$) when *N-well* is grounded ($V_N = 0$). These two bias configurations make no significant difference in DC and AC photo-detection characteristics. However, in O/E mixing operation especially in high frequency, the bias configuration can affect on the conversion efficiency because the *N-well/P-substrate* junction capacitance (C_{PI}) can be changed by voltage across the junction.

Fig. 3-15 shows the measured conversion efficiencies of the CMOS-base APD O/E mixers with the two types of bias configuration. In this result, the biasing on *N-well* shows higher conversion efficiency than *P+* biasing. If the *N-well* is biased in high voltage, the *N-well/P-substrate* junction is also highly reverse-biased so that the junction

capacitance C_{p1} is reduced. On the other hand, the $P+$ biasing remains the N -well to ground and the voltage across the N -well/ P -substrate junction is 0 V in which the junction capacitance C_{p1} is much larger than former case (see Fig. 3-3).

The parasitic resistances of $P+$ contact also can degrade the conversion efficiency. In a CMOS process, the silicide layer is required to form a low resistance metal contact. However, in optical illumination, the silicide layer blocks the incident lightwave. Although the silicide layer does not significantly affect on the photo-detection performance in the low frequency operation, the O/E mixing performance can be seriously affected as shown in Fig. 3-16. The contact resistances estimated from the process documents are about 0 Ω and 10 Ω with and without the silicide layer, respectively. So, for the millimeter-wave CMOS-based APD O/E mixer design, the amount of metal contact and layout should be carefully controlled for both of low contact resistance and low optical coupling loss.

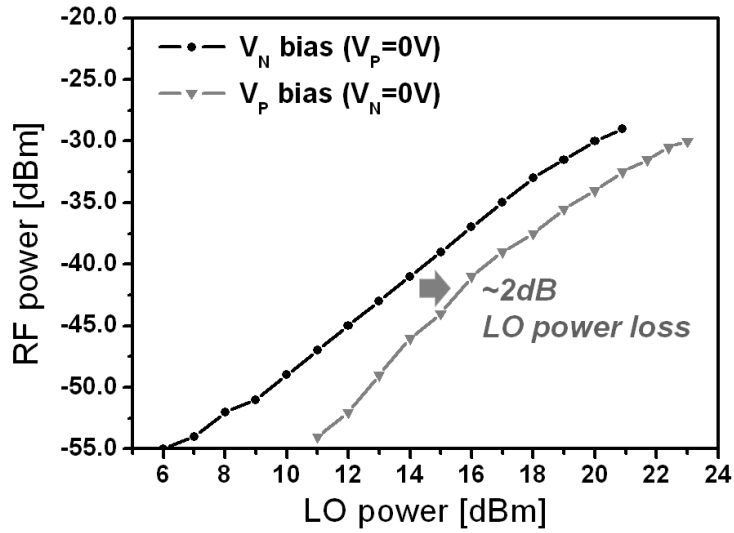


Fig. 3-15. Measured 60.1-GHz RF signal powers with different bias configurations.

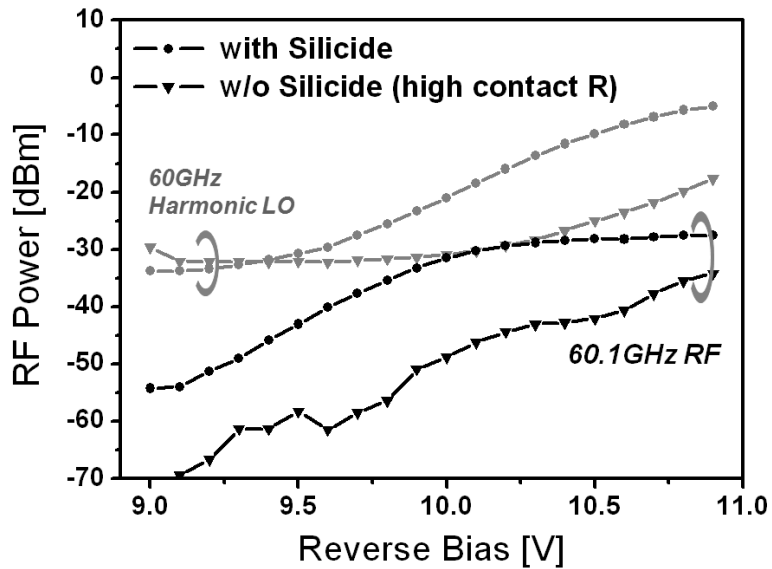


Fig. 3-16. Measured 60-GHz LO and 60.1-GHz RF signal powers with and without silicide layer under P+ model contact.

3-4. 60-GHz-band sub-harmonic balanced O/E mixer

3-4-1. Operation principle of balanced sub-harmonic O/E mixer

In RF systems, the sub-harmonic mixers have been widely used due to the several advantages such as easy RF/LO matching and low frequency LO source requirement [67-68]. Especially in millimeter-wave circuits, the utilization of a low frequency LO source is highly efficient for cost reduction. The electrical sub-harmonic mixer can be implemented with an anti-parallel diode pair as shown in Fig. 3-17 (a). Because the anti-parallel diode pair offers higher odd-mode nonlinear coefficient, high sub-harmonic mixing can be obtained from the 3rd harmonic nonlinear component.

The nonlinear DC curve of the CMOS-based APD in avalanche region is very similar with the electrical diode. One different thing is that the IF signals are optically injected to the APD and linearly contribute to the output current of the APD. So, the sub-harmonic mixing can be obtained from the 2nd harmonic nonlinearity. The antipodal diode pair structure with differential LO can be used for the sub-harmonic APD O/E mixer design as shown in Fig. 3-17 (b). This type of 2nd harmonic enhancement can be found in push-push oscillators [69-70].

Fig. 3-18 shows the simulation comparison of 60-GHz sub-harmonic APD O/E mixers with single-ended and balanced structures using the equivalent circuit model established in section 3-2. The balanced O/E mixer shows enhanced conversion efficiency from 7 to 15 dB in this simulation. The utilization of the differential LO in balanced O/E mixer should not be a serious drawback in an integrated antenna base station because LO circuits are usually implemented with a balanced structure [71-72].

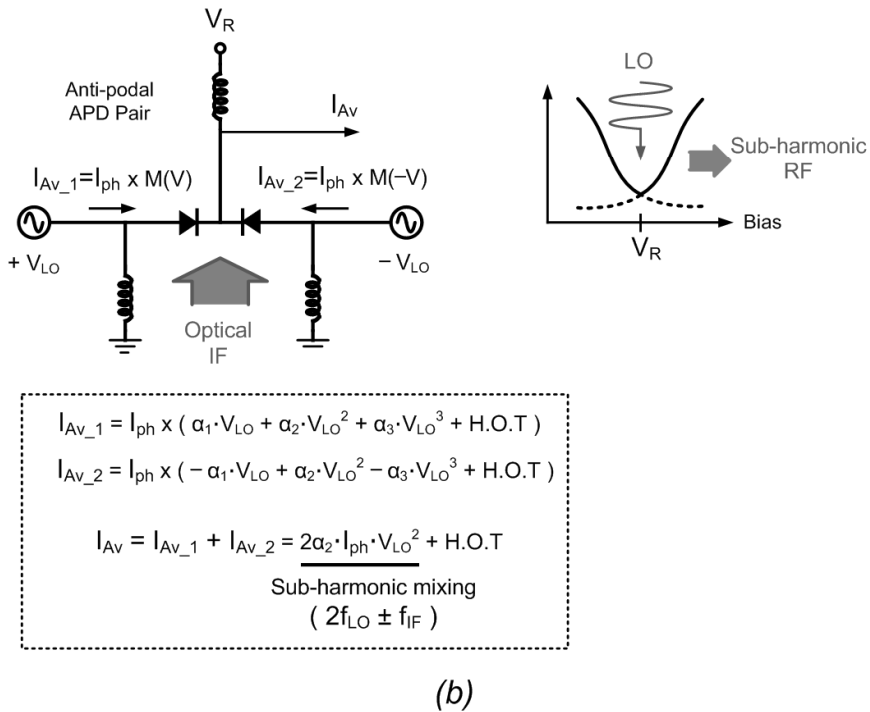
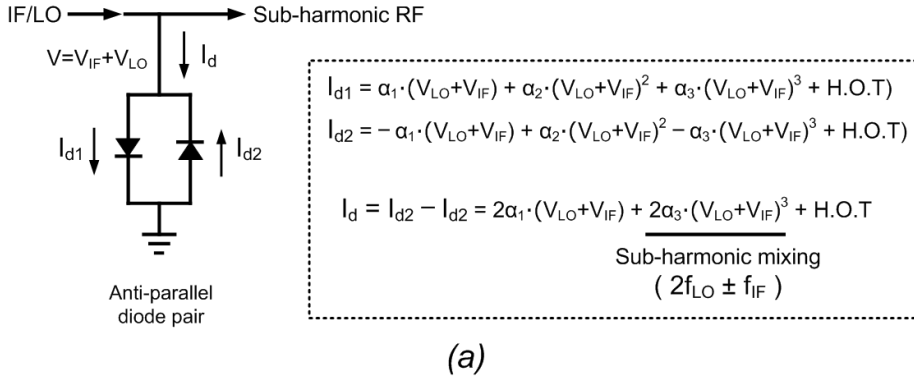


Fig. 3-17. Operation principles of (a) electrical sub-harmonic mixer using anti-parallel diode pair (b) balanced APD O/E mixer in anti-podal APD pair structure.

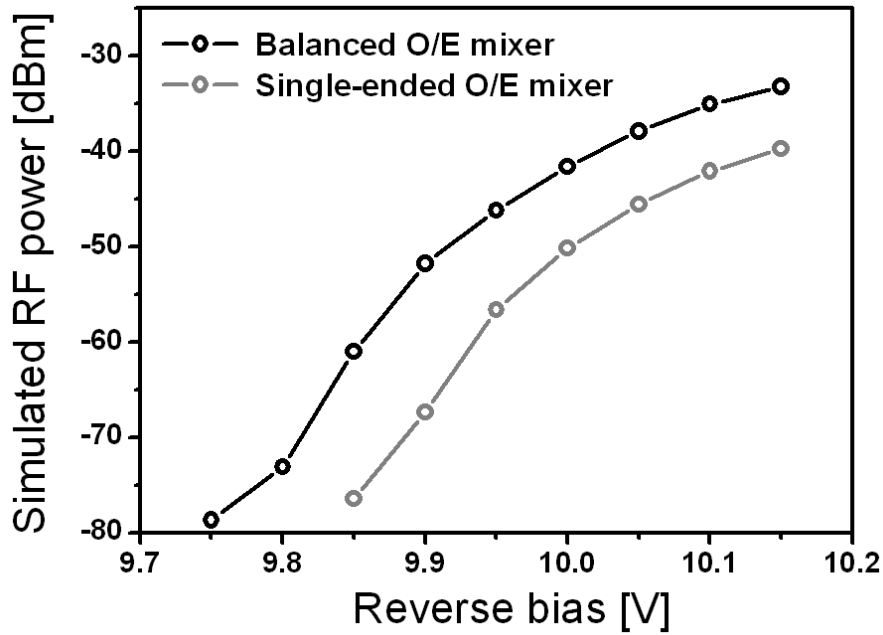
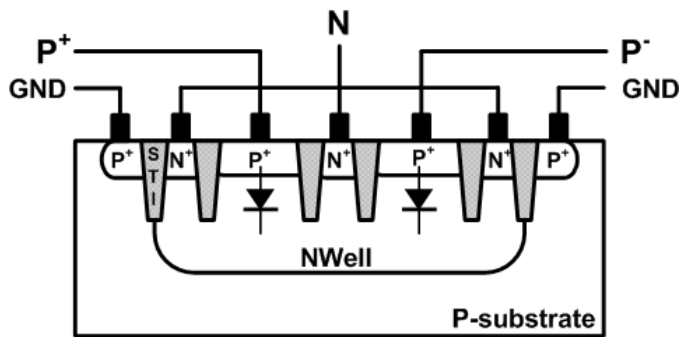


Fig. 3-18. Simulated 60-GHz sub-harmonic O/E mixing efficiencies based on balanced and single-ended structures.

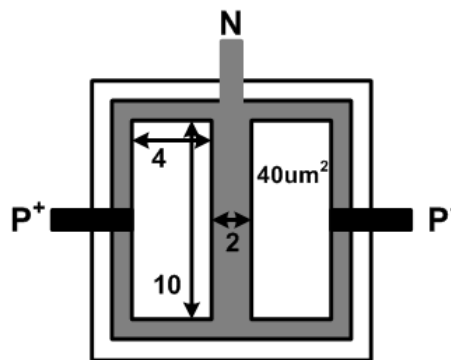
3-4-2. Design of balanced APD O/E mixers

Utilizing the balanced APD pair structure, 60-GHz CMOS-based APD O/E mixer was designed and fabricated. Fig. 3-19 shows the cross-section and top-view of the balanced APD O/E mixer fabricated with CMOS layers provided by 0.25- μm SiGe BiCMOS foundry. Two separated $P+$ active regions make vertical p-n junctions in contacts with the N -well region. By implementing the p-n junctions in a single

N-well, the cathodes of two p-n diodes are combined as a single node to make the antipodal diode pair. The two anode electrodes are separately formed on P^+ regions for differential LO injection. Each APD is $4 \times 10 \mu\text{m}^2$ with lateral spacing of $2 \mu\text{m}$ within a $10 \times 10 \mu\text{m}^2$ square. To evaluate the performance enhancement by the proposed balanced O/E mixer, a single $10 \times 10 \mu\text{m}^2$ APD O/E mixer was also fabricated within the same chip.



(a)



(b)

Fig. 3-19. (a) cross-section and (b) top-view schematic diagram of fabricated balanced APD pair.

3-4-3. Measurement results

Fig. 3-20 shows the DC and IF photo-detection characteristics measured with a single CMOS-based APD. The fabricated balanced mixer and single-ended mixer were designed to have total optical window size of about $10 \times 10 \mu\text{m}^2$ so that the same lensed fiber with $10\text{-}\mu\text{m}$ spot diameter was used for optical coupling. When 0-dBm optical power is applied to the CMOS-based APD, the peak optical responsivity is about 0.32 A/W with avalanche gain of about 34 at the reverse bias voltage of 11.1 V which is slightly below the avalanche breakdown voltage of 11.2 V. The peak IF detection power is about -31 dBm at the reverse bias voltage of 11.1 V. With reverse bias voltages over 11.2 V, dark currents rapidly increase and the DC and IF photo-detection efficiency are suppressed.

The DC and IF photo-detection characteristics of balanced APD pair are also measured in the same experimental condition. The lateral photo-detection area of the balanced APD pair is $80 \mu\text{m}^2$ which is 20 % smaller than $10 \times 10 \mu\text{m}^2$ single APD due to $2\text{-}\mu\text{m}$ spacing between two separated APDs. However, the small difference in the area does not significantly affect the optical coupling efficiencies. In addition, the measured DC and IF photo-detection characteristics of the balanced APD pair are nearly the same as those of the single APD.

Fig. 3-21 shows the measurement setup for 60-GHz band sub-harmonic O/E mixing characteristics. For optical IF generation, 850-nm lightwave from VCSEL was modulated in MZM with 100-MHz IF signals. 30-GHz differential LO signals are generated with a RF synthesizer and a 180° hybrid divider, and injected into the APD pair. The inset of Fig. 3-21 shows the measured RF spectrum when the 30-GHz LO power is 22 dBm and the reverse bias voltage is 11 V.

Fig. 3-22 shows the measured 60-GHz sub-harmonic LO and 60.1-GHz frequency up-converted RF powers obtained from the balanced and single-ended APD O/E mixers. Supplied LO power was 19 dBm and the reverse bias voltage is swept from 9.5 to 11 V.

Fig. 3-23 also shows the resulting 60.1-GHz RF powers as a function of supplied LO power when the reverse bias voltage is fixed at 11 V. The LO saturation power for balanced APD O/E mixer is about 20 dBm and the peak frequency up-converted power is about -24 dBm which is 7-dB higher than the peak IF photo-detection power. As can be seen in the figure, the balanced APD O/E mixer exhibits about 11-dB conversion efficiency enhancement compared to the signal APD O/E mixer.

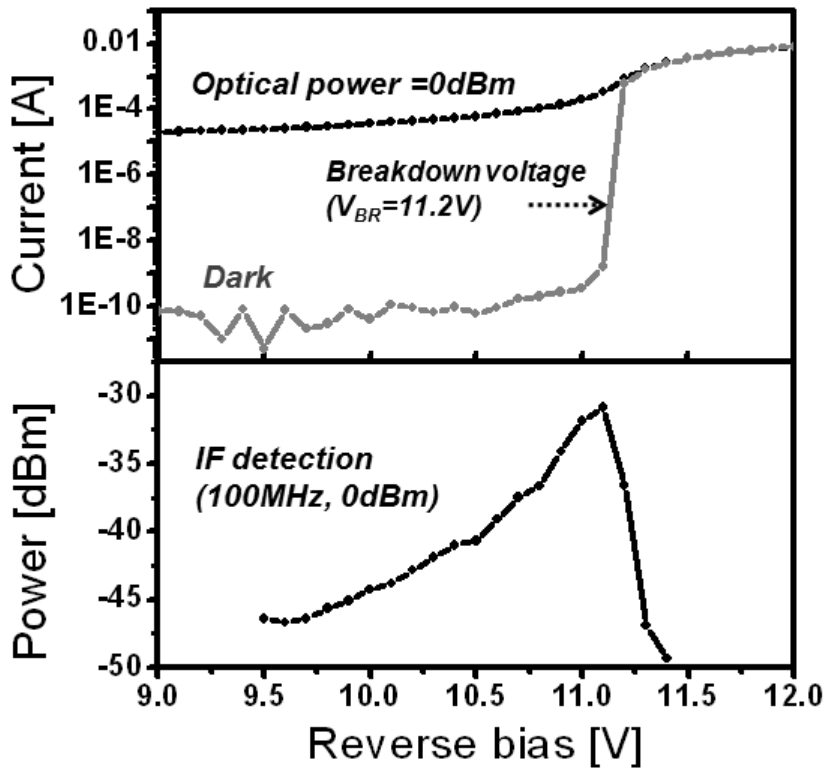


Fig. 3-20. Measured DC and IF photo-detection characteristics of a single CMOS-based APD with lateral dimension of $10 \times 10 \mu\text{m}^2$ as a function of reverse bias voltage.

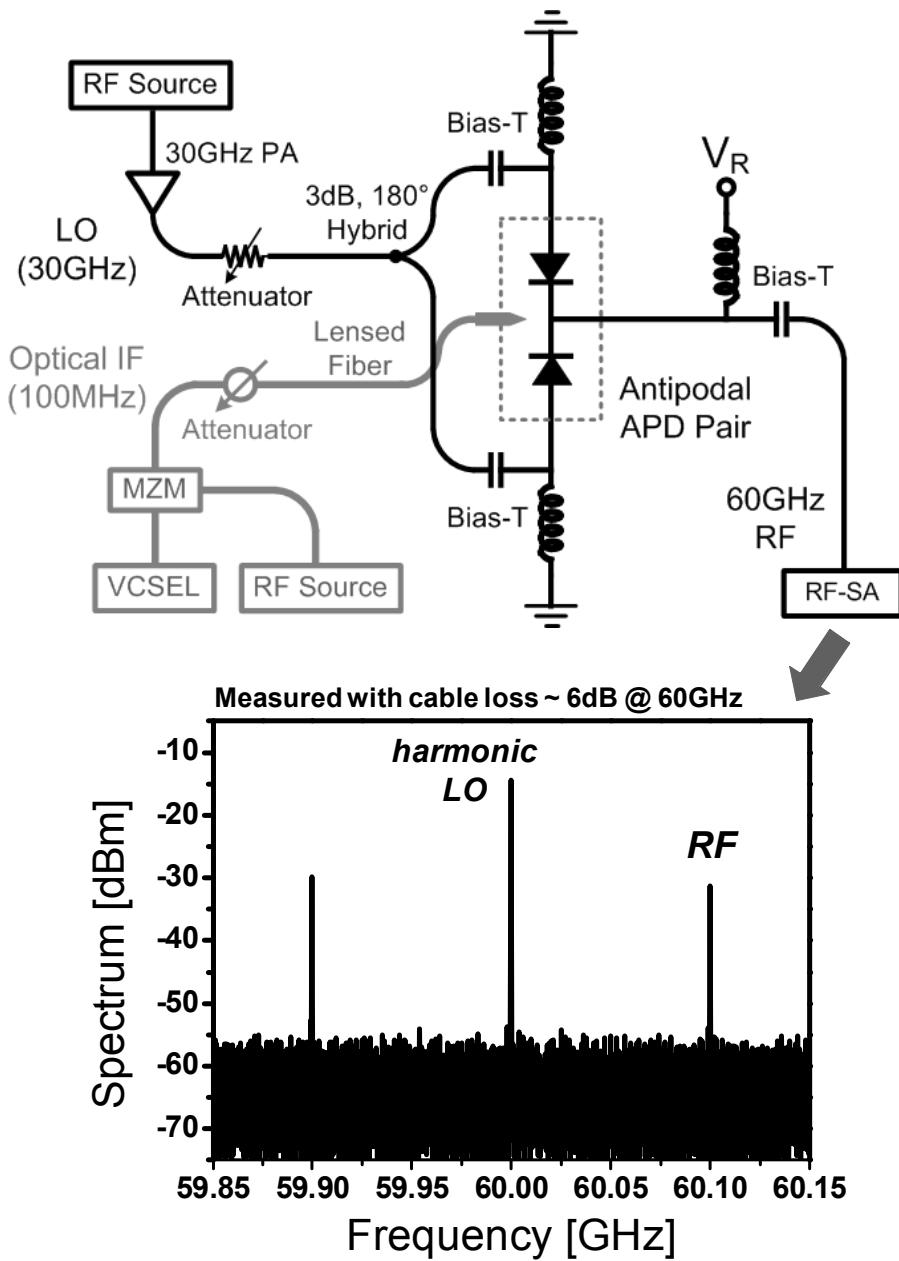


Fig. 3-21. Measurement setup for 60-GHz band sub-harmonic O/E mixing characteristics using the fabricated balanced APD O/E mixer.

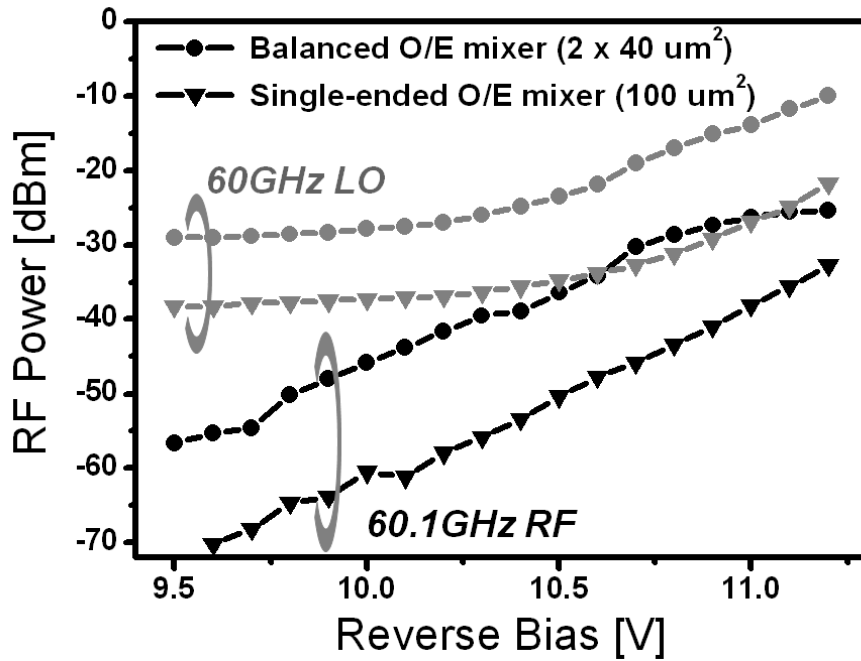


Fig. 3-22. Measured 60-GHz-band sub-harmonic LO and 60.1-GHz RF power from the balanced APD O/E mixer and single APD O/E mixer with 0-dBm optical IF and 19-dBm LO powers.

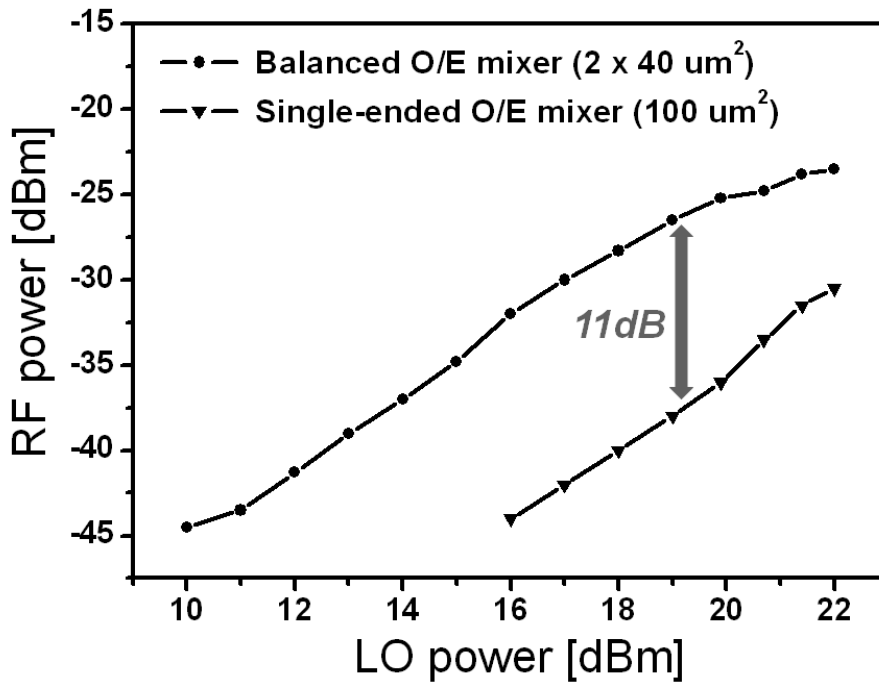


Fig. 3-23. Measured 60.1-GHz harmonic RF power from the balanced APD O/E mixer and single APD O/E mixer as a function of LO power in reverse bias voltage of 11 V.

3-5. Summary

The CMOS-based APD O/E mixer has a significant potential for implementation into the low cost integrated antenna base station and short-wavelength fiber-fed wireless system. In this work, based on the large-signal equivalent circuit model, the CMOS-based APD was optimized for 60-GHz operation and was used for the implementation of the balanced sub-harmonic APD O/E mixer. As summarized in Table 3-2, the 60-GHz-band balanced APD O/E mixer in this work has largely enhanced conversion efficiency compared to the previously reported APD O/E mixer [23].

	[23]	This work
O/E mixer type	Single-ended sub-harmonic O/E mixer	Balanced sub-harmonic O/E mixer
IF detection	-25 dBm with avalanche gain (for 0dBm optical IF)	-30 dBm with avalanche gain (for 0dBm optical IF)
60GHz Output RF power	-50 dBm	-24 dBm
30GHz LO power	20 dBm	20 dBm
Conversion efficiency	Poor	Good
Remarks	Large parasitic loss	Balanced sub-harmonic mixer based on optimized APD

Table 3-2. Performance comparison of CMOS-based APD O/E mixers.

4. Conclusion

Wireless communication technologies have rapidly evolved in speed and coverage and have become ubiquitous in our daily lives. Consequently, the growth of our network usage has created a demand for higher data rate in wireless systems beyond the gigabit per second throughput. To meet the requirements, a wireless communication system should use a wide bandwidth surrounding a high-frequency carrier. Also, the cell coverage is reduced within a dense network topology. Thus, the network that is designed with simple antenna base station architecture is critical for cost reduction. For a low-cost antenna base station design, the MMIC- or CMOS-compatible O/E mixers yield significant advantages.

This dissertation aimed at the implementation of cost-effective and simple O/E mixers based on InP and CMOS technologies.

The InP HBT is an excellent optoelectronic device with high optical responsivity, nonlinearity and high-speed photo-detection characteristics for optical LO utilization. However, the utilization of the optical LO with a conventional discrete HBT O/E mixer induced the disadvantage of having low conversion efficiency due to the insufficient LO power.

In Chapter 2, the optically injection-locked self-oscillating O/E

mixer (OIL-SOM) based on an InP HBT oscillator was proposed. The electrical LO generation of self-oscillating mixer provides high LO power for high conversion efficiency while the phase-locking is accomplished by injection locking by the optical LO. For evaluation of the proposed OIL-SOM, the conversion efficiency and spurious-free dynamic range of the OIL-SOM were experimentally investigated based on the 10-GHz MMIC HBT oscillator and compared with that of the discrete HBT O/E mixer. Also, the bi-directional fiber-fed wireless link was demonstrated in 30-GHz band using the MMIC HBT OIL-SOM as a 3rd harmonic frequency up- and down-converter. The 60-GHz OIL-SOM was realized with a 30-GHz hybrid HBT oscillator and utilized for 60-GHz fiber-fed downlink demonstration. The performance of the fiber-fed wireless link based on the OIL-SOM was insensitive to the optical LO power.

The CMOS-based APD O/E mixer has a significant potential for the low cost integrated antenna base station and short-wavelength fiber-fed wireless system based on VCSEL and MMF. Although the photo-detection efficiency and speed of CMOS APD is not adaptive for optical LO utilization, the integration ability of the CMOS process is a merit of the CMOS APD O/E mixer.

In chapter 3, the CMOS APD O/E mixer was investigated. This study

has focused on the device optimization and the application of RF circuit technologies. Based on the large-signal equivalent circuit model, the CMOS-based APD was optimized at device level for operation at 60-GHz. The balanced APD O/E mixer was proposed for the enhancement of sub-harmonic conversion efficiency. Also, the prototype of the 60-GHz-band balanced APD O/E mixer was implemented with the down-scaled CMOS-based APDs. The implemented balanced APD O/E mixer has largely enhanced conversion efficiency compare to the previously reported APD O/E mixers, and offers conversion gain of about 7 dB in a 60-GHz band.

The OIL-SOM and balanced O/E mixer should be very effective O/E frequency conversion techniques for the realization of the compact and cost-effective future broadband wireless communication systems. The OIL-SOM allows us to effectively utilize the optically distributed LO for simple antenna base station architecture. Also, the balanced O/E mixer structure can be widely used in long- and short-wavelength fiber-fed wireless systems for effective sub-harmonic O/E frequency conversion.

Appendix

A-1. Optical injection-locking of MMIC HBT oscillator

In applications environment, many factors can vary self-oscillating frequency of OIL-SOM. So, if the frequency difference between the free-running oscillator and injected optical LO is too large, the oscillator cannot be locked by the injected optical LO. Consequently, obtaining a large locking range is an important feature of OIL-SOM for stable operation. The locking range is defined as the frequency deviation which allows injection-locking.

Fig. A-1 shows the experimental setup for optical LO generation and measurement of optical injection locking range of the MMIC oscillator. When the 10.8-GHz optical LO was injected into the free-running oscillator, the oscillator was injection-locked by the optical LO. Fig. A-2 shows the measured spectrum of the 10-GHz oscillation output signal in free-running and optically injection-locked conditions. By optical injection-locking, the phase noise of the MMIC oscillator is suppressed and follows to that of injection source.

The locking range of injection-locked oscillator depends on the incident optical LO power. Fig. A-3 shows the measured locking range of the oscillator in which the locking range increases as the power of

optical LO increases. Due to the moderate Q-factor and high photo-detection efficiency, the MMIC oscillator has a wide locking range of about 1.5-GHz with 6-dBm optical LO injection [73].

The variance of the free-running oscillation frequency over change of temperature was measured as shown in Fig. A-4. The frequency change was about 18 MHz with 94-degree change in temperature. Because the locking range of the MMIC oscillator is much larger than the frequency drift with temperature change, the stable operation of OIL-SOM is possible over the temperature variation of the antenna base station.

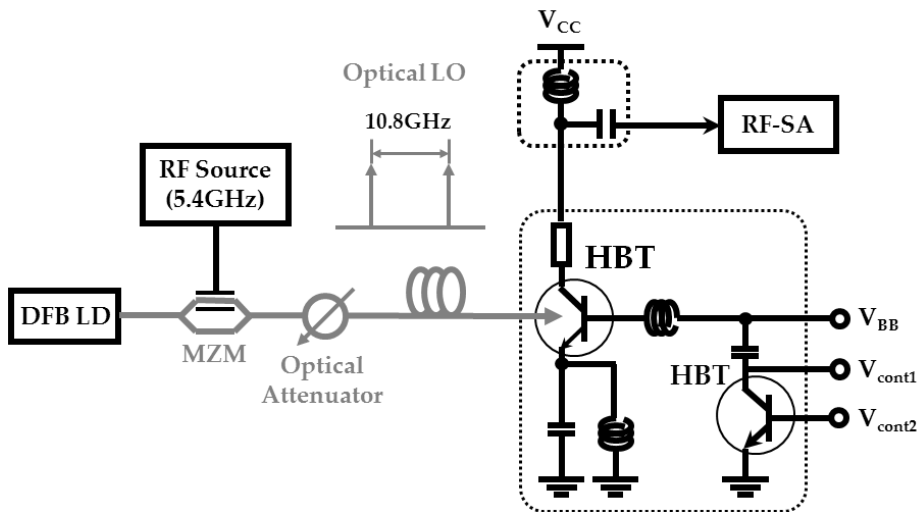
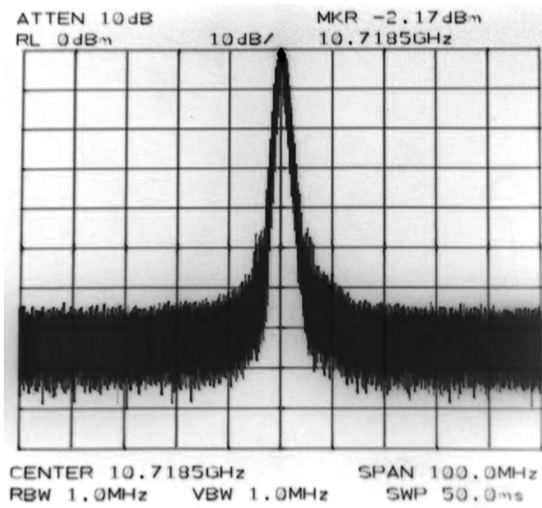
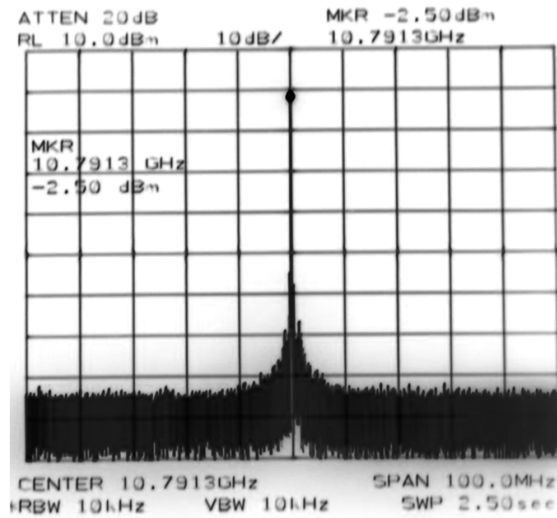


Fig. A-1. Experimental setup for optical injection-locking of MMIC oscillator.



(a)



(b)

Fig. A-2. Measured output spectrum of oscillator in (a) free-running and (b) optically injection-locked by optical LO of 0-dBm power.

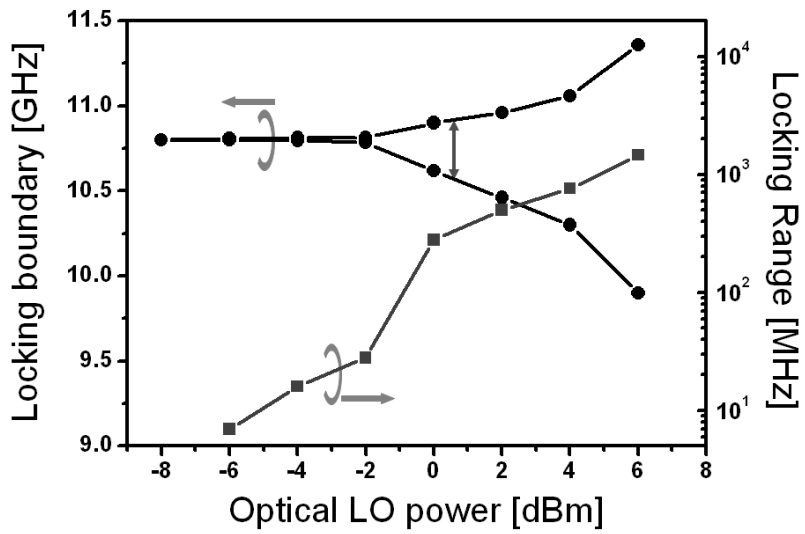


Fig. A-3. Measured locking range of MMIC oscillator with change of incident optical LO power.

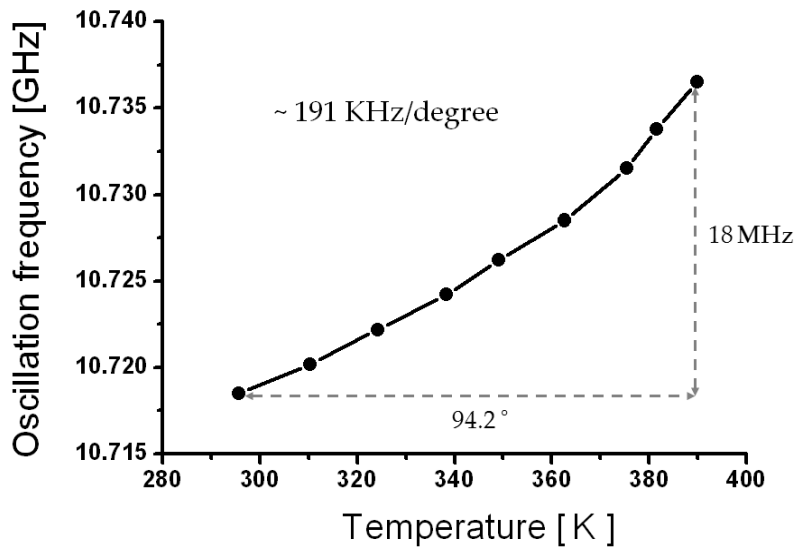


Fig. A-4. Free-running oscillation frequency of MMIC oscillator with change of operating temperature.

Bibliography

- [1] B. Bosco, R. Emrick, S. Franson, J. Holmes and S. Rockwell, "Emerging Commercial Applications Using the 60 GHz Unlicensed Band: Opportunities and Challenges," *IEEE Wireless and Microw. Tech. Conference*, pp, 1-4, Dec. 2006.
- [2] A. Bourdoux, J. Nsenga, W. V. Thillo, F. Horlin and L. Van der Perre, "Air Interface and Physical Layer techniques for 60 GHz WPANs," *Symposium on Commun. and Vehicular Tech.*, pp-1-6, Nov. 2006.
- [3] P. Smulders, "Exploiting the 60 GHz band for local wireless multimedia access Prospects and future directions," *IEEE Commun. Mag.*, pp. 140-147, Jan. 2002.
- [4] E. Grass, F. Herzel, M. Piz, Y. Sun and R. Kraemer," Implementation Aspects of Gbits Communication System for 60 GHz Band," *Proceedings of the 14th Wireless World Research Forum*, pp. 1-8, Jul. 2005.
- [5] C. H. Doan, S. Emami, D. A. Sobel, A. M. Niknejad, and R. W. Brodersen," Design Considerations for 60GHz CMOS Radios," *IEEE Commun. Mag.*, pp. 132-140, Dec. 2004.
- [6] C. H. Doan, S. Emami, A. M. Niknejad and R. W. Brodersen," Millimeter-Wave CMOS Design," *IEEE J. Solid-State Circuits*, vol. 40, no. 1, pp. 144-155, Jan. 2005.
- [7] S. K. Reynolds, B. A. Floyd, U. R. Pfeiffer, T. Beukema, J. Grzyb, C. Haymes, B. Gaucher and M. Soyuer, "A Silicon 60-GHz Receiver and Transmitter Chipset for Broadband

- Communications,” *IEEE J. Solid-State Circuits*, vol. 41, no. 12, pp. 2820-2831, Dec. 2006.
- [8] Al. M. Niknejad,” Siliconization of 60GHz,” *IEEE Commun. Mag.*, pp. 78-85, Feb. 2010.
- [9] <http://www.ieee802.org/15/pub/TG3c.html>
- [10] http://www.ieee802.org/11/Reports/tgad_update.htm
- [11] M. Marcus, and W. P. Shillue, “Millimeter wave propagation: spectrum management implications,” *IEEE Microw. Mag.*, pp. 54-62, Jun. 2005.
- [12] A. J. Seeds, “Microwave photonics,” *IEEE Trans. Microw. Theory Tech.*, vol. 50, no. 3, pp. 877–887, Mar. 2002.
- [13] K.-I. Kitayama, A. Stöhr, T. Kuri, R. Heinzelmann, D. Jäger and Y. Takahashi, “An approach to single optical component antenna base stations for broad-band millimeter-wave fiber-radio access systems,” *IEEE Trans. Microw. Theory Tech.*, vol. 48, no. 12, pp. 2588-2595, Dec. 2000.
- [14] W. W. Hu, K. Inagaki and T. Ohira, “Radio-on-fiber techniques using two-mode injection-locked lasers for broadband millimeter-wave communications,” *Int. Conf. on Microw. and Millimeter Wave Tech.*, pp. 7-10, Aug. 2002.
- [15] A. Stöhr, C. miesner and D. Jäger. ”All-optical radio-independent millimeter-wave radio-on-fiber system with lean antenna base stations,” *Int. Topical Meeting on Microw. Photon.*, pp.213-216, Nov. 2002.
- [16] T. Kuri, K.-I. Kitayama, A. Stohr, and Y. Ogawa, “Fiber-Optic Millimeter-Wave Downlink System Using 60 GHz-Band External

- Modulation,” *IEEE J. Lightwave Technol.*, vol. 17, no. 5, pp. 799-806, May 1999.
- [17] G. H. Smith and D. Novak, “Broadband millimeter-wave fiber-radio network incorporating remote up-down conversion,” *IEEE MTT-S Int. Microw. Symp. Dig.*, pp. 1509-1512, Jun. 1998.
- [18] H. Ogawa, d. Polifko and S. Banda, “Millimeter-wave fiber optics systems for personal radio communication,” *IEEE Trans. Microw. Theory Tech.*, vol. 40, no. 12, pp. 2285-2293, Dec. 1992.
- [19] J. M. Fuster, J. Marti and J. L. Corral, “Chromatic dispersion effects in electro-optical upconverted millimetre-wave fibre optic links,” *Electron. Lett.*, vol. 33, no. 23, pp. 1969-1970, Nov. 1997.
- [20] H.-S. Ryu, Y.-K. Seo and W.-Y. Choi, “Dispersion-Tolerant Transmission of 155-Mb/s Data at 17GHz Using a 2.5Gb/s-Grade DFB Laser With Wavelength-Selective Gain From an FP Laser Diode,” *IEEE Photon. Technol. Lett.*, vol. 16, no. 8, pp.1942-1944, Aug. 2004.
- [21] Y. J. Wen, H. F. Liu and D. Novak, “Optical signal generation in millimeter-wave repetition rates using semiconductor lasers with pulsed subharmonic optical injection,” *IEEE Trans. Microw. Theory Tech.*, vol. 37, no. 9, pp. 1183-1193, Sep. 2001.
- [22] W. K. Kulczyk and Q. V. Davis, “The avalanche photodiode as an electronic mixer in an optical receiver,” *IEEE Trans. Electron Devices*, vol. 19, no. 11, pp. 1181-1190, Nov. 1972.
- [23] H.-S. Kang and W.-Y. Choi, “Fibre-supported 60 GHz self-heterodyne systems based on CMOS-compatible harmonic optoelectronic mixers,” *Electron. Lett.*, vol. 43, no. 20, pp. 1101–

1103, Sep. 2007.

- [24] C.-S. Choi, H.-S. Kang, D.-H. Kim, K.-S. Seo and W.-Y. Choi, "60GHz Harmonic Optoelectronic Up-Conversion Using an InAlAs/InGaAs Metamorphic High-Electron-Mobility Transistor on a GaAs Substrate," *Jpn. J. Appl. Phys.*, vol.42, pp. L658-L659, Jun. 2003.
- [25] C.-S. Choi, H.-S. Kang, W.-Y. Choi, D.-H. Kim and K.-S. Seo, "Phototransistors based on InP HEMTs and their applications to millimeter-wave radio-on-fiber systems," *IEEE Trans. Microw. Theory Tech.*, vol. 53, no. 1, pp. 256-263, Jan. 2005.
- [26] E. Suematsu and N. Imai, "A fiber-optic/millimeter-wave radio transmission link using HBT as direct photodetector and an optoelectronic upconverter," *IEEE Trans. Microw. Theory Tech.*, vol. 44, no. 1, pp. 133-143, Jan. 1996.
- [27] C. P. Liu, A. J. Seeds and D. Wake, "Two-Terminal Edge-Coupled InP/InGaAs Heterojunction Phototransistor Optoelectronic Mixer," *IEEE Microw. Guided Wave Lett.*, vol. 7, no. 3, pp. 72-74, Mar. 1997.
- [28] Y. Betsler, D. Ritter, C. P. Liu, A. J. Seeds and A. Madjar, "A Single-Stage Three-Terminal Heterojunction Bipolar Transistor Optoelectronic Mixer," *IEEE J. Lightwave Technol.*, vol. 16, no. 4, pp. 605-609, Apr 1998.
- [29] Y. Betsler, J. Lasri, V. Sidorov, S. Cohen, D. Ritter, M. Orenstein, G. Eisenstein, A. J. Seeds and A. Madjar, "An Integrated Heterojunction Bipolar Transistor Cascode Opto-Electronic Mixer," *IEEE Trans. Microw. Theory Tech.*, vol. 47, no. 7, pp.

1358-1364, Jul. 1999.

- [30] G. H. Smith, D. Novak and C. Lim, "A millimeter-wave full-duplex fiber-radio star-tree architecture incorporating WDM and SCM," *IEEE Photon. Technol. Lett.*, vol. 10, no. 10, pp.1650-1652, Nov. 1998.
- [31] L. Noël, D. Wake, D. G. Moodie, D. D. Marcenac, L. D. Westbrook, and D. Nasset, "Novel Techniques for High-Capacity 60-GHz Fiber-Radio Transmission Systems," *IEEE Trans. Microw. Theory Tech.*, vol. 45, no. 8, pp. 1416-1423, Aug. 1997.
- [32] J.-H. Seo, C.-S. Choi, Y.-S. Kang, Y.-D. Chung, J. Kim, and W.-Y. Choi, "SOA-EAM Frequency Up/Down-Converters for 60-GHz Bi-Directional Radio-on-Fiber Systems," *IEEE Trans. Microw. Theory Tech.*, vol. 54, no. 2, pp. 959-966, Feb. 2006.
- [33] P. Bhadri, P. Mal, S. Konanki and F. R. Beyette, Jr., "Implementation of CMOS photodetectors in optoelectronic circuits," *15th annual meeting of IEEE Laser and Electro-optic Society*, vol. 2, pp. 683-684, Nov. 2002.
- [34] H. Zimmermann, T. Heide, and A. Ghazi, "A monolithically integrated 1-Gb/s optical receiver in 1 μ m CMOS technology," *IEEE Photon. Technol. Lett.*, vol. 13, pp. 711-713, Jul. 2001.
- [35] M. Jutzi, M. Grozing, E. Gaugler, W. Mazioschek and M Berroth, "2Gb/s CMOS optical integrated receiver with a spatially modulated photodetector," *IEEE Photon. Tech. Lett.*, vol. 17, no. 6, pp. 1268-1270, Jun. 2005.
- [36] S. Radovanovic, A. Johan and B. Nauta, "A 3Gb/s optical detector in standard CMOS for 850nm optical communication," *IEEE J.*

Solid-State Circuits, vol. 40, no. 8, pp. 1706-1717, Aug. 2005.

- [37] A. A. de Salles and M. A. Romero, "AlGaAs/GaAs HEMT's under optical illumination," *IEEE Trans. Microw. Theory Tech.*, vol. 39, no. 12, pp. 2010-2017, Dec. 1991.
- [38] C.-S. Choi, H.-S. Kang, W.-Y. Choi, H.-J. Kim, W.-J. Choi, D.-H. Kim, K.-C. Jang and K.-S. Seo, "High Optical Responsivity of InAlAs/InGaAs Metamorphic High-Electron Mobility Transistor on GaAs substrate with Composite Channels," *IEEE Photon. Technol. Lett.*, vol. 15, no. 6, pp.846-848, Jun. 2003.
- [39] D. Huber, R. Bauknecht, C. Bergamaschi, M. Bitter, A. Huber, T. Morf, A. Neiger, M. Rohner and I. Schnyder, "InP-InGaAs Single HBT Technology for Photoreceiver OEIC's at 40 Gb/s and Beyond," *IEEE J. Lightwave Technol.*, vol. 18, no. 7, pp. 992-1000, Jul. 2000.
- [40] H. Kamitsuna, Y. Matsuoka, S. Yamahata and N. Shigekawa, "Ultrahigh-Speed InP/InGaAs DHPTs for OEMMICs," *IEEE Trans. Microw. Theory Tech.*, vol. 49, no. 10, pp. 1921-1925, Oct. 2001
- [41] H. Kamitsuna and H. Ogawa, "Monolithic image-rejection optoelectronic up-converters that employ the MMIC process," *IEEE Trans. Microw. Theory Tech.*, vol. 41, no. 12, pp. 2323-2329, Dec. 1993.
- [42] H.-S. Kang, C.-S. Choi, W.-Y. Choi, D.-H. Kim, K.-S. Seo, "Characterization of phototransistor internal gain in metamorphic high-electron-mobility transistors," *Appl. Phys. Lett.*, vol. 84, no. 19, pp.3780-3782, May. 2004.

- [43] C.-S. Choi, "Photo-transistors based on InP HEMTs and HBTs, and their applications to fiber-optic/millimeter-wave data transmission system," (*Ph.D diss., Yonsei University, 2005*), 150-153.
- [44] L. M. de Barros, A. Paoletta, M. Y. Frankel, M. A. Romero and P. R. Herczfeld, "Photoresponse of microwave transistors to high-frequency modulated lightwave carrier signal," *IEEE Trans. Microw. Theory Tech.*, vol. 45, no. 8, pp. 1368-1374, Aug. 1997.
- [45] C.-S. Choi, J.-Y. Kim, H.-S. Kim, E.-S. Nam and W.-Y. Choi, "Gigabit data transmission in fiber-optic/60GHz-band links using InP Heterojunction phototransistors" *7th Topical Symposium on Millimeter-wave*, pp. 167-170, Feb. 2005.
- [46] C.-S. Choi, J.-Y. Kim, W.-Y. Choi, H. Kamitsuna, M. Ida and K. Kurishima, "60Ghz Bidirectional Radio-on-Fiber Links Based on InP-InGaAs HPT Optoelectronic Mixers," *IEEE Photon. Technol. Lett.*, vol. 17, no. 12, pp.2721-272, Dec. 2005.
- [47] W.-K. Huang, Y.-C. Liu, Y.-M Hsin, "A High-Speed and High-Responsivity photodiode in Standard CMOS Technology," *IEEE Photon. Tech. Lett.*, vol. 19, no. 4, pp. 197-199, Feb. 2007.
- [48] W.-K. Huang, Y.-C. Liu, Y.-M Hsin, "Bandwidth enhancement in Si Photodiode by eliminating slow diffusion photocarriers," *Electron. Lett.*, vol. 44, no. 1, pp. 52-53, Jan. 2008.
- [49] H. S. Kang, M. J. Lee and W. Y. Choi, "Si avalanche photodetectors fabricated in standard complementary metal-oxide-semiconductor process," *Appl. Phys. Lett.*, vol. 90, 151118, April 2007.

- [50] H. S. Kang, M. J. Lee and W. Y. Choi, "Low-Cost Multistandard Radio-Over-Fiber Downlinks Based on CMOS-Compatible Si Avalanche Photodetectors," *IEEE Photon. Technol. Lett.*, vol. 21, no. 7, pp. 463-464, Apr. 2009.
- [51] H.-S. Kang, M.-J. Lee and W.-Y. Choi, "6.25-Gb/s Optical Receiver Using a CMOS-Compatible Si Avalanche Photodetector," *J. Optic. Society Korea*, vol. 12, no. 4, pp. 217-220, Dec. 2008.
- [52] C.-S. Choi, J.-Y. Kim, W.-Y. Choi, H. Kamitsuna, M. Ida and K. Kurishima, "Optically Injection-Locked Self-Oscillating Optoelectronic Mixers Based on InP-InGaAs HPTs for Radio-on-Fiber Applications," *IEEE Photon. Technol. Lett.*, vol. 17, no. 11, pp.2415-2417, Nov. 2005.
- [53] J.-Y. Kim, C.-S. Choi, W.-Y. Choi, H. Kamitsuna, M. Ida and K. Kurishima, "Characteristics of InP/InGaAs HPT-based Optically Injection-Locked Self-oscillating Optoelectronic Mixers and Their Influence on RoF System Performance," *IEEE Photon. Technol. Lett.*, vol. 19, no. 3, pp.155-157, Feb. 2007.
- [54] J.-Y. Kim, C.-S. Choi, W.-Y. Choi, H. Kamitsuna, M. Ida and K. Kurishima, "Integrated Heterojunction Bipolar Transistor Optically Injection-locked Self-oscillating Optoelectronic Mixers for Bi-directional Fiber-fed Wireless Applications," *IEEE Trans. Microw. Theory Tech.*, vol. 55, no. 12, pp. 2734-2739, Dec. 2007.
- [55] H. Kamitsuna, T. Shibata, K. Kurishima and M. Ida, "Direct optical injection locking of InP/InGaAs HPT oscillator ICs for microwave photonics and 40-Gbit/s-class optoelectronic clock

- recovery,” *IEEE Trans. Microw. Theory Tech.*, vol. 50, no. 12, pp. 3002-3008, Dec. 2002.
- [56] M. Ida, K. Kurishima, H. Nakajima, N. Watanabe and S. Yamahata, “Undoped-Emitter InP/InGaAs HBTs for High-Speed and Low-Power Applications,” *IEEE Int. Electron Device Meeting*, pp.854-856, Dec. 2000.
- [57] H. Kamitsuna, K. Ishii, T. Shibata, K. Kurishima, and M. Ida, “A 43 Gbps clock and data recovery OEIC integrating an InP/InGaAs HPT oscillator with an HBT decision circuit,” *IEEE J. Sel. Topics Quantum Electron.*, vol. 10, no. 4, pp. 673–678, Jul./Aug. 2004.
- [58] H. Kamitsuna, M. Ida and K. Kurishima, “A 60-GHz-Band Optical Injection-Locked Oscillator Using a Top/Back-Illuminated InP/InGaAs HPT,” *IEEE Int. Conf. Indium Phosphide & Related Materials*, pp. 538-541, May 2007.
- [59] H. Kamitsuna, T. Shibata, K. Kurishima and M. Ida, “Direct Optical Injection Locking of a 52-GHz InP–InGaAs HPT Oscillator IC for Over-100-Gb/s Half- or Full-Rate Optoelectronic Clock Recovery,” *IEEE Photon. Technol. Lett.*, vol. 15, no. 1, pp. 108-110, Jan. 2003
- [60] R. Montgomery and R. DeSalvo, “A novel technique for double sideband suppressed carrier modulation of optical fields,” *IEEE Photon. Technol. Lett.*, vol. 7, no. 4, pp. 434-436, Apr. 1995.
- [61] “Three Methods of Noise Figure Measurement,” Maxim application note 2875, <http://pdfserv.maxim-ic.com/en/an/AN2875.pdf>
- [62] C.-S. Choi, “Photo-transistors based on InP HEMTs and HBTs,

- and their applications to fiber-optic/millimeter-wave data transmission system,” (*Ph.D diss., Yonsei University, 2005*), 84-85.
- [63] IEEE std. 802.15.3TM-2003, pp. 269.
- [64] M.-J. Lee, H.-S. Kang and W.-Y. Choi, “Equivalent Circuit Model for Si Avalanche Photodetectors Fabricated in Standard CMOS Process,” *IEEE Electron Device Lett.*, vol. 29, no. 10, pp. 1115-1117, Oct. 2008.
- [65] S. M. Sze and K. K. Ng, *Physics of Semiconductor Devices*, 3rd ed. Hoboken, NJ: Wiley, 2007.
- [66] R. Torres-Torres, R. Murphy-Arteaga and J. A. Reynoso-Hernández, “Analytical Model and Parameter Extraction to Account for the Pad Parasitics in RF-CMOS,” *IEEE Trans. Electron Devices*, vol. 52, no. 7, Jul. 2005.
- [67] M. Cohn, J. E. Degenford and B. A. Newman, “Harmonic Mixing with an Antiparallel Diode Pair,” *IEEE Trans. Microw. Theory Tech.*, vol. 23, no. 8, pp. 667-673, Aug. 1975.
- [68] S. Sarkar, P. Sen, S. Pinel, C. -H. Lee and J. Laskar, ” Si-based 60GHz 2X Subharmonic Mixer for Multi-Gigabit Wireless Personal Area Network Application,” *MTT-S Int. Microw. Symp.* pp. 1830-1833, Jun. 2006.
- [69] P.-C. Huang, M.-D. Tsai, G. D. Vendelin, H. Wang, C.-H. Chen and C.-S Chang, “A Low-Power 114-GHz Push-Push CMOS VCO Using LC Source Degeneration,” *IEEE J. Solid-State Circuits*, vol. 42, no. 6, pp. 1230-1239, Jun. 2007.
- [70] E. Seok, C. Cao, D. Shim, D. J. Arenas, D. B. Tanner, C.-M. Hung, K. K. O, “A 410GHz CMOS Push-Push Oscillator with an

- On- Chip Patch Antenna,” *Int. Solid-State Circuit Conf.* pp. 472, Feb. 2008.
- [71] C. Cao, Y. Ding and K. K. O, “A 50-GHz Phase-Locked Loop in 0.13- μm CMOS,” *IEEE J. Solid-State Circuit*, vol. 42, no. 8, pp. 1649-1656, Aug. 2007.
- [72] W. Winkler, J. Borngräber, B. Heinemann and F. Herzel, “A Fully Integrated BiCMOS PLL for 60 GHz Wireless Applications,” *IEEE Int. Conf. Solid-State Circuit*, pp. 406-407, Feb. 2005.
- [73] R. Adler, “A Study of Locking Phenomena in Oscillators,” *Proc. IEEE*, vol. 61, no. 10, pp. 1380-1385, Oct. 1973.

Publication Lists

International Journals

- [1] **Jae-Young Kim**, Myoung-Jae Lee, Holger Rucker and Woo-Young Choi, “60GHz-band Sub-harmonic Optoelectronic Mixer based on balanced CMOS Avalanche Photodiode Pair,” *submitted for publication in IEEE Microw. Wireless Compon. Lett.*
- [2] **Jae-Young Kim**, Woo-Young Choi and Hyuk-Kee Sung, “A Study on Modulation Configuration of Optoelectronic Oscillators Using Direct Modulation of Semiconductor Lasers,” *will be published in Jpn. J. Appl. Phys.*
- [3] **Jae-Young Kim** and Woo-Young Choi, “30 GHz CMOS Self-Oscillating Mixer for Self-Heterodyne Receiver Application,” *IEEE Microw. Wireless Compon. Lett.*, Vol. 20, No. 6, June 2010.
- [4] Kwang-Hyun Lee, **Jae-Young Kim** and Woo-Young Choi, “Injection-Locked Hybrid Optoelectronic Oscillators for Single-Mode Oscillation,” *IEEE Photon. Technol. Lett.*, Vol.20, No. 19, pp. 1645-1647, Oct. 2008.
- [5] Kwang-Hyun Lee, **Jae-Young Kim**, Woo-Young Choi, Hideki Kamitsuna, Minoru Ida, and Kenji Kurishima, “Low-Cost Optoelectronic Self-Injection-Locked Oscillators,” *IEEE Photon. Technol. Lett.*, Vol.20, No. 13, pp. 1151-1153, Jul. 2008.
- [6] **Jae-Young Kim**, Woo-Young Choi, Hideki Kamitsuna, Minoru Ida, and Kenji Kurishima, “Integrated Heterojunction Bipolar

Transistor Optically Injection-locked Self-oscillating Optoelectronic Mixers for Bi-directional Fiber-fed Wireless Applications,” *IEEE Trans. Microw. Theory Tech.*, Vol. 55, No. 12, pp.2734-2739, Dec. 2007.

- [7] Kwang-Hyun Lee, **Jae-Young Kim** and Woo-Young Choi, “A 30-GHz Self-Injection-Locked Oscillator Having a Long Optical Delay Line for Phase-Noise Reduction,” *IEEE Photon. Technol. Lett.*, Vol.19, No. 24, pp. 1982-1984, Dec. 2007.
- [8] **Jae-Young Kim**, Woo-Young Choi, Hideki Kamitsuna, Minoru Ida, and Kenji Kurishima, “Characteristics of InP/InGaAs HPT-based Optically Injection-Locked Self-oscillating Optoelectronic Mixers and Their Influence on RoF System Performance,” *IEEE Photon. Technol. Lett.*, Vol.19, No. 3, pp. 155-157, Feb. 2007.
- [9] Chang-Soon Choi, **Jae-Young Kim**, Woo-Young Choi, Hideki Kamitsuna, Minoru Ida, and Kenji Kurishima, “Optically Injection-Locked Self-Oscillating Optoelectronic Mixers Based on InP–InGaAs HPTs for Radio-on-Fiber Applications,” *IEEE Photon. Technol. Lett.*, Vol. 17, No. 5, pp.1073-1075, May 2005.

International Conferences

- [1] **Jae-Young Kim**, Myung-Jae Lee and Woo-Young Choi, “60GHz CMOS-APD Optoelectronic Mixers with Optimized Conversion Efficiency,” *IEEE International Topical Meeting on Microwave Photonics*, Montreal, Quebec, Canada, Oct. 05-09, 2010.

- [2] Woo-Young Choi, **Jae-Young Kim** and Myung-Jae Lee, “Optoelectronic Mixers for Fiber-fed 60-GHz Wireless Systems,” *Asia-Pacific Microwave Photonics Conference*, HongKong, China, Apr. 26-28, 2010 (Invited paper).
- [3] **Jae-Young Kim** and Woo-Young Choi, “Fiber-fed wireless systems based on remote up-conversion techniques,” *IEEE Radio and Wireless Symposium*, Orlando, FL, USA, Jan. 21, 2008 (Workshop on Radio over Fiber Technologies).
- [4] Kwang-Hyun Lee, **Jae-Young Kim**, and Woo-Young Choi, “Hybrid Dual-Loop Optoelectronic Oscillators,” *IEEE International Topical Meeting on Microwave Photonics*, pp. 74-77, The Empress, Victoria, Canada, Oct. 03-05, 2007.
- [5] **Jae-Young Kim**, Woo-Young Choi, Hideki Kamitsuna, Minoru Ida and Kenji Kurishima, “Optically Injection-locked Self-oscillating HBT MMIC Optoelectronic Mixer for Bi-directional Fiber-fed Wireless Links,” *IEEE MTT-S International Microwave Symposium*, pp. 237-240, Honolulu, HI, USA, Jun. 03-08, 2007.
- [6] **Jae-Young Kim**, Woo-Young Choi, Hideki Kamitsuna, Minoru Ida and Kenji Kurishima, “30GHz-band Radio-on-fiber downlink data transmission using InP HPT-based MMIC OIL-SOM,” *Asia-Pacific Microwave Photonics Conference*, pp 85-88, JeJu Island, Korea, Apr. 25-27, 2007.
- [7] Woo-Young Choi and **Jae-Young Kim**, “Technologies for Fiber-fed 60GHz Wireless Systems,” *OFC/NFOEC*, OWN1, Anaheim,

CA, USA, Mar. 25-29, 2007 (Invited paper).

- [8] **Jae-Young Kim**, Woo-Young Choi, Hideki Kamitsuna, Minoru Ida and Kenji Kurishima, “60GHz RoF Systems Using Remote Up-conversion Technique based on HBT Optoelectronic Mixers,” *Australian workshop on microwave photonics*, Melbourne, Australia, Dec. 08, 2006 (Invited paper).
- [9] **Jae-Young Kim**, Jun-Hyuk Seo, Woo-Young Choi, H. Kamitsuna, Minoru Ida and Kenji Kurishima, “60GHz Radio-on-Fiber systems using optically injection-locked self oscillating optoelectronic mixers based on InP/InGaAs HPTs,” *OFC/NFOEC, OWG6*, Anaheim, CA, USA, Mar. 05-10, 2006.
- [10] Chang-Soon Choi, **Jae-Young Kim**, Woo-Young Choi, Hideki Kamitsuna, Minoru Ida, and Kenji Kurishima, “Millimeter-wave InP/InGaAs HPT optoelectronic mixers and their application to 60GHz bi-directional radio-on-fiber systems,” *International Topical Meeting on Microwave Photonics*, pp. 333-336, Seoul, Korea, Oct. 12-14, 2005.
- [11] Chang-Soon Choi, **Jae-Young Kim**, Hong-Seung Kim, Eun-Soo Nam and Woo-Young Choi, “Gigabit data transmission in fiber-optic/60GHz-band links using InP Heterojunction phototransistors,” *The 7th Topical Symposium on Millimeter-wave*, pp. 167-170, Seoul, Korea, Feb. 2005.
- [12] **Jae-Young Kim**, Chang-Soon Choi, Hong-Seung Kim, Eun-Soo Nam and Woo-Young Choi, “Equivalent circuit models for

InP/InGaAs HPT,” *The 6th Korea-Japan Joint Workshop on Microwave and Millimeter-wave Photonics*, pp. 91-94, Gyeongju, Korea, Jan. 27-28, 2005.

Domestic Journals

- [1] 김재영, 최창순, 서준혁, 최우영, “고속 포토트랜지스터를 이용한 마이크로파 광전송 기술,” *광학과 기술*, Vol. 10, No. 1, pp.14-21, Jan. 2006.

Domestic Conferences

- [1] 김재영, 조준형, 최우영, 성혁기, “Optoelectronic Oscillators Using Optical SSB generation,” Conference on Optoelectronics and Optical Communications, 정선 하이원호텔, May 26-28, 2010.
- [2] 이광현, 김재영, 최우영, Hideki Kamitsuna, Minoru Ida, and Kenji Kurishima, “Optoelectronic Self-Injection-Locked Oscillators for Output Phase-Noise Reduction,” *Photonics conference*, FP-6, 제주 풍림 리조트, Nov. 14-16, 2007.
- [3] 고민수, 김재영, 최우영, “622-Mbps Transmission in 60 GHz Using a Novel CMOS BPSK Demodulator,” *추계 마이크로파 및 전파 학술대회*, pp. 741-744, 제주대학교, Sep. 13-14, 2007.
- [4] 김재영, 최우영, Hideki Kamitsuna, Minoru Ida, Kenji Kurishima, “양방향 Radio-over-Fiber 시스템을 위한 HBT OIL-

- SOM,” Conference on Optoelectronics and Optical Communications, pp. 196-197, 제주 한화리조트, May 16-18, 2007.
- [5] 한승찬, 남은수, 김재영, 최우영, “SFDR(Spurious-Free Dynamic Range) characteristics of InP/InGaAs HPT-based Optoelectronic Mixers,” *Photonics Conference*, pp. 190-191, 설악 대명리조트, Nov. 8-10, 2006.
- [6] 김재영, 최창순, 최우영, Hideki Kamitsuna, Minoru Ida, Kenji Kurishima, “InP HPT기반 O/E mixer와 OIL-SOM의 주파수 상-하향변환 효율,” *Photonics conference*, pp. 310-311, 설악 대명리조트, Nov. 8-10, 2006.
- [7] 김재영, 서준혁, 최우영, Hideki Kamitsuna, Minoru Ida, Kenji Kurishima, “InP HPT 기반 OIL-SOM의 광전 주파수 상향변환 특성,” *Photonic conference*, pp.15-16, 충무 마나 리조트, Nov. 02-04, 2005.
- [8] 최창순, 김재영, 김홍승, 남은수, 최우영, “A 1.25Gbps Radio-on-fiber Transmission in 60GHz band using an InP Heterojunction Phototransistor,” *Photonics Conference*, F1B2, 단양 대명리조트, Nov. 03-05, 2004.